Fall 2016

Computational fluid dynamic analysis in high permeability hydraulic fractured horizontal gas wells

Hrithu Vasudevan

Department:

COMPUTATIONAL FLUID DYNAMIC ANALYSIS IN HIGH PERMEABILITY HYDRAULIC FRACTURED HORIZONTAL GAS WELLS

by

HRITHU VASUDEVAN

A THESIS

Presented to the Faculty of the Graduate School of the

MISSOURI UNIVERSITY OF SCIENCE AND TECHNOLOGY

In Partial Fulfillment of the Requirements for the Degree

MASTER OF SCIENCE IN PETROLEUM ENGINEERING

2016

Approved by

Dr. Shari Dunn-Norman, Advisor
Dr. Baojun Bai
Dr. Ralph Flori

ABSTRACT

Hydraulic fracturing of horizontal wells in unconventional reservoirs has become the dominant type of well completion performed in the United States. In very low permeability reservoirs (~.00001-.0001 mD), the wellbore is aligned with the minimum horizontal stress, and the completion includes multiple transverse fractures. These fractures may be placed with either open hole sleeve type completion systems (OHMS), or cased hole plug and perf systems (P-n-P). In slightly higher permeability reservoirs (1 to 10 mD) multiple longitudinal fractures have been found to be preferred to completions with transverse fractures.

This study presents an evaluation of gas well productivity for both transverse and longitudinal fractured horizontal wells using CFD simulations. The first part of the work includes an evaluation of one and two transverse fractures, over reservoir permeability of 1, 10 and 100 mD. Results, given as fold of increase, are compared to the single transverse fracture model of Augustine (2011). The work includes a parametric study of fracture width, penetration ratio and vertical to horizontal permeability ratio on production rates.

The second part of the study includes CFD simulations for a single longitudinal fracture, and compares productivity results of this fracture orientation to transverse fractures in the 1, 10 and 100 mD cases.

Results of this study suggest OHMs completions outperform P-n-P completions. The results of the work also corroborate the findings of Yang (2015) and Kassim et al (2016) suggesting that longitudinal fractured wells perform better in the slightly higher permeability reservoirs (1-10 mD).

ACKNOWLEDGMENTS

I express my heartfelt gratitude and earnest appreciation:

To Dr. Shari Dunn-Norman, my guide and advisor, who was kind enough to provide me an opportunity to carry out this study, for her invaluable guidance and financial support which empowered me to this eventful outcome without any impediments.

To Dr. Baojun Bai and Dr. Ralph Flori, my committee members for their timely support and encouragement.

To Chatetha Chumkratoke, for his expert supervision and continuous advice at all junctures during the study which enabled me to accomplish this work to my level best.

I would also like to thank my friends and lab mates, Logeshwar Venkatesan, Samarth Gupte, Rashid Kassim and Vivek Rao, faculty and staff of the Department of Petroleum Engineering for their support, suggestions and constant appreciation. Words fail to convey my love and gratitude for the moral support extended by my family and their unconditional love which is priceless and inexpressible.

TABLE OF CONTENTS

LIST OF ILLUSTRATIONS

LIST OF TABLES

1. INTRODUCTION

There are numerous methods for completing horizontal wells, the earliest of which were simply open lateral holes. With the application of fracturing in horizontal wells, industry has developed and has been applying both openhole multi-stage systems (OHMS) and Plug-n-Perf systems (P-n-P). These systems are shown in Figures 1.1 and 1.2.

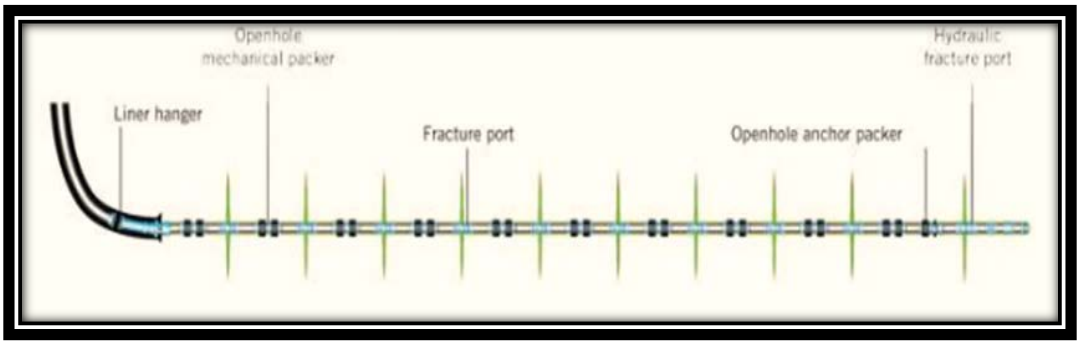

Figure 1.1. OHMS system (ogj.com/articles)

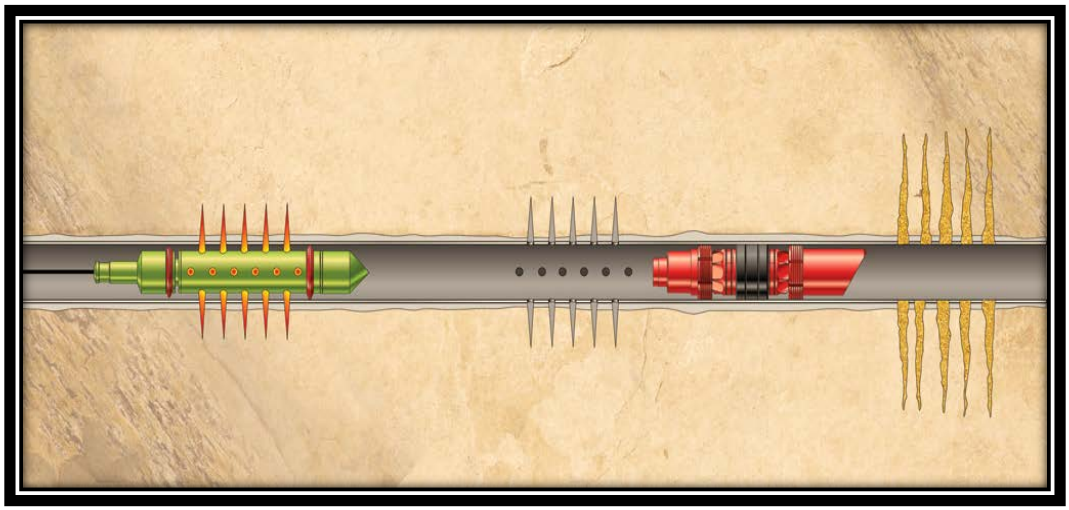

Figure 1.2. P-n-P system (drillingcontractor.org)

.

In a horizontal well Open Hole Multi-stage System (OHMS) completion, the producing formation is uncased and uncemented along the length of the horizontal wellbore. An open-hole packer system with fracturing ports in a sleeve is located between each packer, throughout the length of the lateral. Each sleeve represents a single frac stage and the packers seal against the borehole for separation between frac stages.

While there are many different types of open hole sleeve systems, they function similarly. Frac balls or darts are successively dropped from the surface to shift each frac sleeve open and then provide the isolation and diversion necessary to pump the fracture treatment in that stage. The open hole sleeve system allows numerous fractures to be performed along the lateral in a short period of time, e.g. 60 stages in a 2-3 days.

Plug and perf (P-n-P) completions typically consist of the lateral wellbore being cased and cemented, then perforated in stages with limited entry stimulation techniques. Each frac stage in a P-n-P completion has a number of perforations, referred to as a perforation cluster. Composite bridge plugs set on wireline or coiled tubing are used to separate each frac stage and provide the mechanical diversion to stimulate each selected zone efficiently, . Once the stages are completed, coiled tubing is used to drill out the composite bridge plugs and provide access along the wellbore.

P-n-P completions are the most widely applied of the two methods, perhaps because this approach to horizontal well multi-fracturing has been around longest (Casero et al., 2009), or because perforations provide more specific fluid entry points compared to the sleeve and open hole between packers. However, since multiple perforation clusters are typically used in each stage of a P-n-P completion, fractures may initiate from one or more of the perforation clusters depending on reservoir geomechanics.

Since the introduction of openhole multi-stage horizontal well fracturing systems in 2001 (Snyder et al., 2011), there has been great interest in comparing the two completion methods to determine which system provides a more productive completion, and if productivity differs as a function of reservoir type or fluids produced. Some comparisons based on field studies are summarized and shown in Table 1.1.

Table 1.1. Field studies comparing OHMS with P-n-P completions (Modified from Theppornprapakorn et al., 2014)

Source	Reservoir	Time interval	Indicator	Results
Samuelson et al., 2008	Cleveland sand (tight gas)	3 months	Cumulative gas production	OHMS > P-n-P
Thomson et al., 2009	Tight gas (British Columbia)	N/A	Gas rate per interval	OHMS = P-n-P
Lohoefer et al., 2010	Barnett shale (shale gas)	3 years	Cumulative gas production	OHMS > P-n-P
Edwards et al., 2010	Granite wash (tight gas)	12 months	Cumulative gas production	OHMS > P-n-P
Kennedy et al., 2012	Tight gas and Shale gas (Overview)	N/A	N/A	OHMS = P-n-P
Snyder and Seale, 2012	Marcellus (shale gas)	12 months	Cumulative gas production	OHMS > P-n-P
Casero et al., 2013	Red oak (tight gas)	N/A	N/A	OHMS > P-n-P
Burton, 2013	N/A	N/A	Economics, cumulative production and operational efficiency	OHMS = P-n-P

Field comparisons continue to be reported in the literature. In 2015, Remier et al., compared the performance of openhole packer systems to cemented liner completion systems across 30 horizontal wells in northern Montney gas play. The OHMS completions consistently outperformed P-n-P completions, and the author presented a new method of stimulation analysis which explains the high performance of OHMS systems.

Srinivasan et al., (2016) discussed the progression of stimulation strategies and completion methods in the Williston basin since 2009 where the operators tested with sliding sleeves and plug-n-perf oil well completions. After conducting various tests in multiple areas in the basin, in regions where net pressure was high, plug-n-perf completions performed better than OHMS completions. In areas of low net pressure, both the completions had almost same production.

It is important to note that all of the field studies reported in the literature compare production from OHMS and P-n-P completions the low permeability shales. There are no studies focusing on these completions in high permeability, primarily because the horizontal well multi-stage fracturing approach is most beneficial in lower permeability reservoirs.

1.1. COMPUTATIONAL FLUID DYNAMICS COMPARISONS OF OHMS AND P-n-P COMPLETIONS

Augustine (2011) provided the first flow performance model comparison of OHMS and P-n-P completions. He built a two-dimensional reservoir model using a steady-state edge drive mechanism to analyze the performance of transverse fractured horizontal wells with both openhole and cemented completions. Figure 1.3 shows the $1/4^{th}$ reservoir model considered in the study.

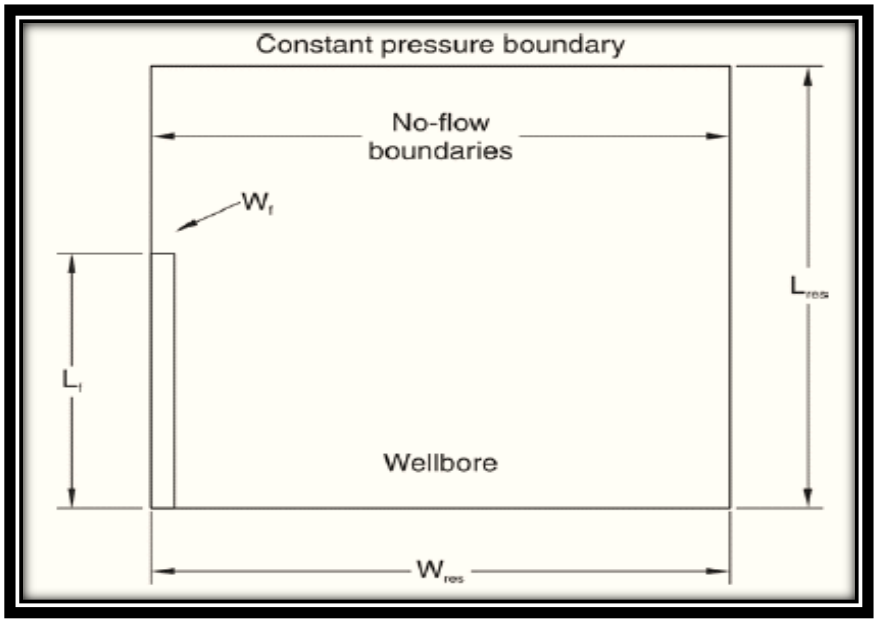

Figure 1.3. Augustine reservoir model (Augustine, 2011)

In Figure 1.3, L_f refers to the fracture-length, L_{res} is the reservoir length, w_f is the fracture width, and w_{res} is the reservoir width.

Steady-state flow with a constant pressure edge-drive was assumed, and Non-Darcy flow effects were not included. Fracture height was considered to be the same as reservoir height. A concept called “equivalent length” was developed by the author to depict the resistance of the radial flow component and to link this length with the reservoir length (L). Figure 1.4 shows the half of the edge-drive reservoir model of Augustine.

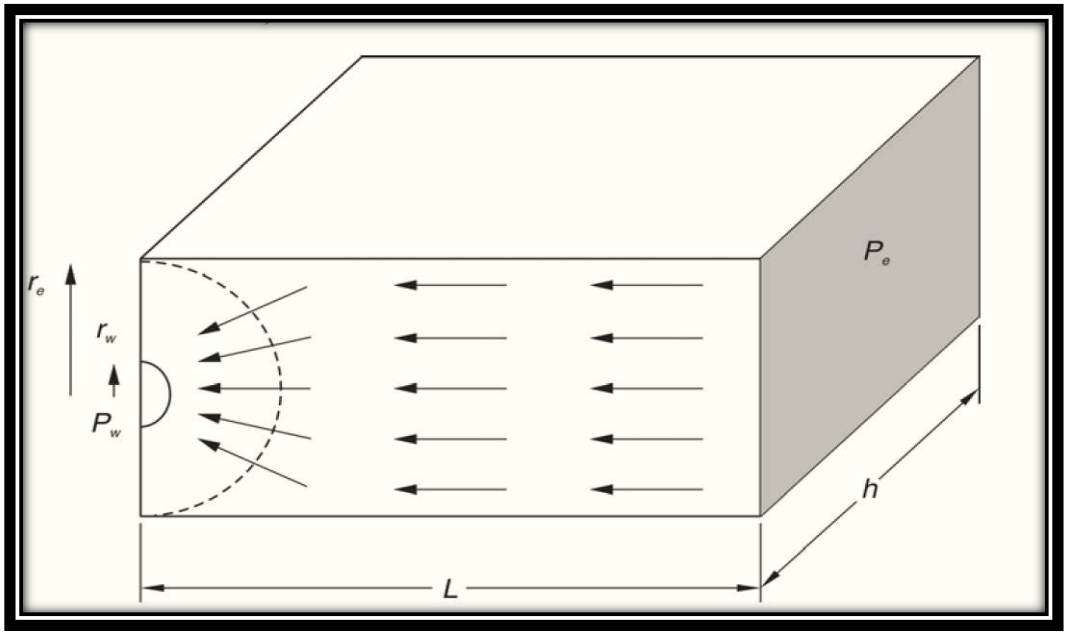

Figure 1.4. Edge-drive reservoir model (Augustine, 2011)

In Figure 1.4, r_e is the reservoir radius, r_w is the wellbore radius, P_w is the well pressure, P_e is the reservoir pressure and h is the reservoir height.

A 2-D CFD analysis was performed using SINDA/FLUINT software for a range of permeabilities using both open hole and cemented completions. The effects of vertical to horizontal permeability ratio, penetration ratio, reservoir aspect ratio and reservoir height were also included in this two-dimensional simulation work.

A productivity index ratio of the stimulated horizontal well compared to an unstimulated horizontal well was determined for all cases. Augustine presented the

results in terms of productivity index ratio versus relative conductivity. Reservoir permeability ranging from 1 milliDarcy to 1 nanoDarcy and fracture permeabilities of 10, 100, and 1000 Darcy were considered in this study. Figure 1.5 shows the results of this work for the full range of every variable considered.

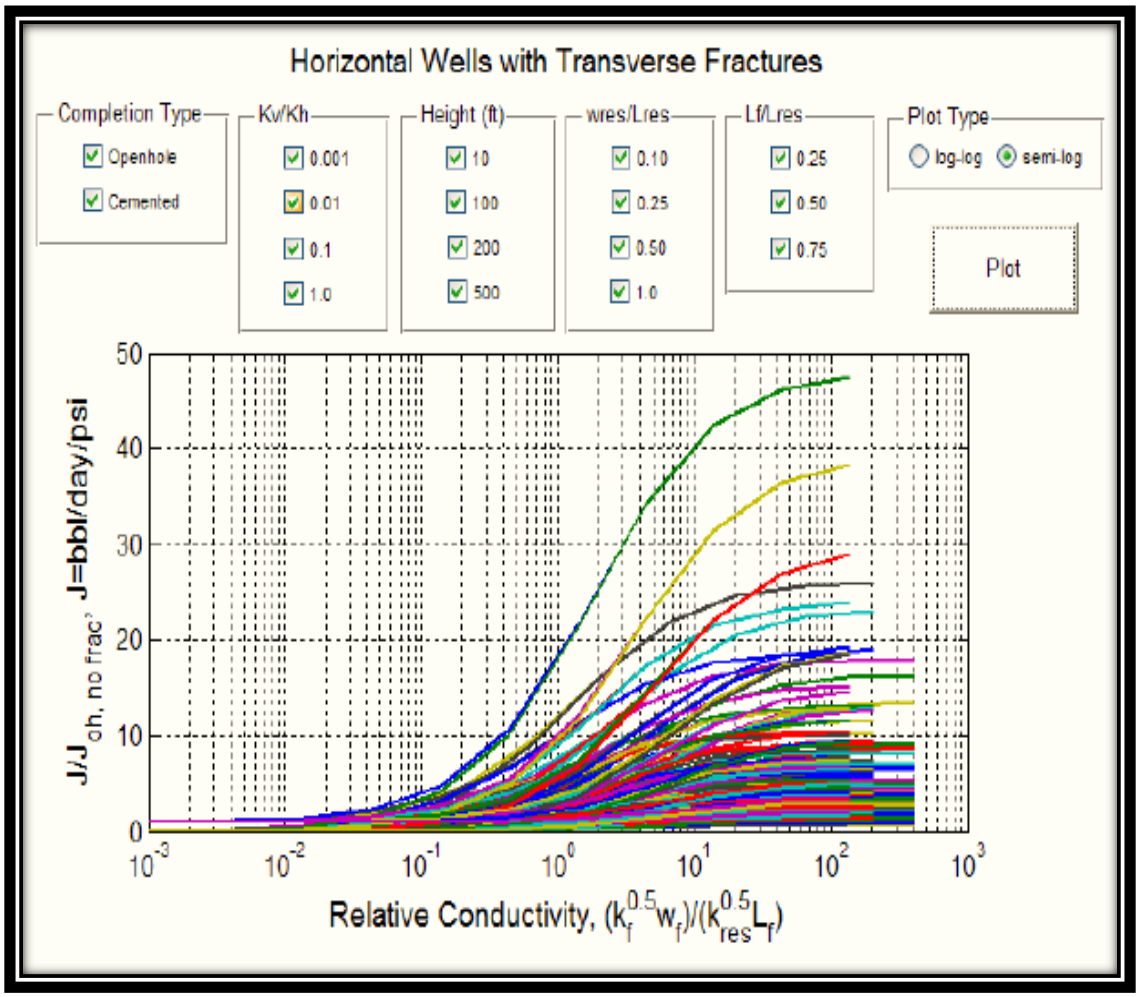

Figure 1.5. Results from Augustine's work (Augustine, 2011)

The term relative conductivity was redefined by the author to eliminate the influence of the fracture width (w_f) even though the mathematical justification for the same was not provided in the study.

For all the variable ranges considered, open hole completion outperformed cemented completion as reservoir permeability increases and the production was almost same for both the completions as reservoir permeability decreases. The results from the simulation are also displayed similar to McGuire-Sikora curves as shown in the Figure 1.6. This figure illustrates Augustine's predicted production difference between two completion types.

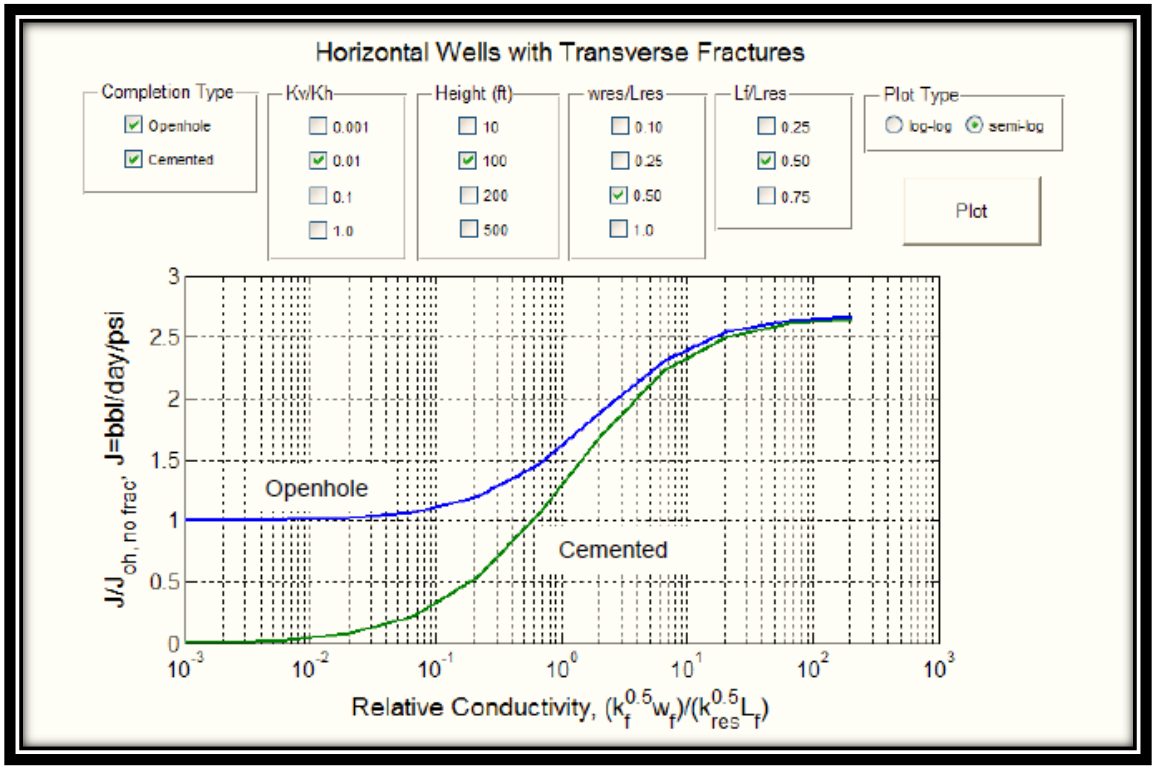

Figure 1.6. Production difference between two completions (Augustine, 2011)

The difference between the two curves in the high permeability range is defined as "production penalty" by Augustine. In the figure, relative conductivity decreases as reservoir permeability increases and vice-versa.

The production difference between open hole and cemented completion in high reservoir permeability is due to the reason that open hole completions allow for flow

across the wellbore face whereas, in cemented completions, all the flow is directed to wellbore through the fracture. This is illustrated in Figure 1.7.

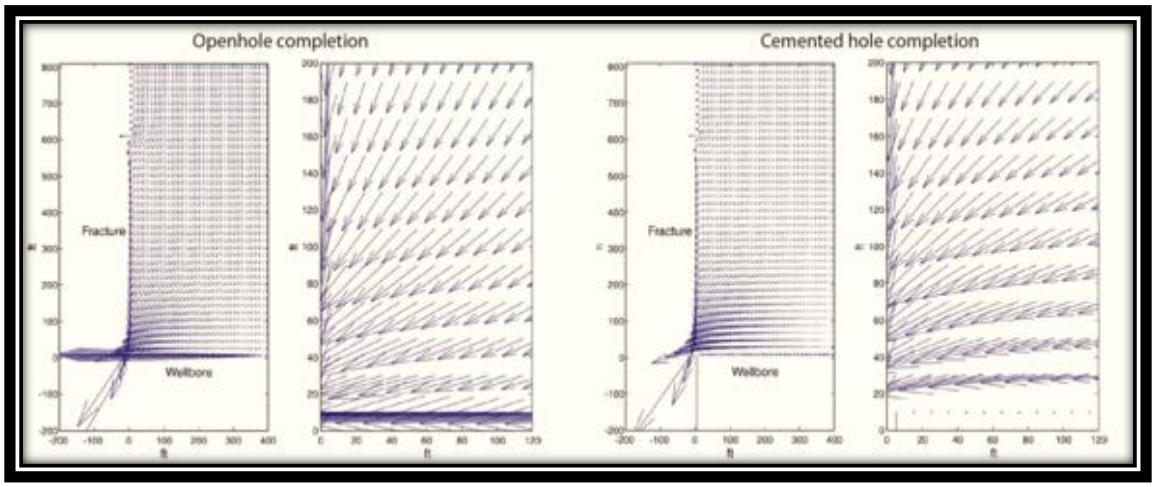

Figure 1.7. Flow profile in the 2-D reservoir model (Augustine, 2011)

It was concluded from the study that for horizontal wells with transverse fractures, assuming same fracture geometry, open hole completions outperformed cemented completions and open hole completion allows natural fractures to produce if there are any. Also, the author suggests to checking the fracture geometry in cases where cemented completions are outperforming open hole completions.

Theppornprapakorn et al., (2014) built a three-dimensional model for comparing OHMS and P-n-P completions in tight gas reservoirs, extending Augustine's two dimensional flow. A three-dimensional computational fluid dynamics (CFD) horizontal well model was constructed based on the concept of steady state edge drive reservoir model used by Augustine (2011). CFD model was developed using ANSYS FLUENT 14.0 to compare the production difference between OHMS and P-n-P completions in multi-stage fractured wells. A 6-inch wellbore in a tight gas reservoir (0.01 mD), under steady state flow with no formation damage, was considered. The OHMS completion assumed a sandface flow and the P-n-P completion was perforated with 0.22 in. perforations with 180° phasing. The simulation results were analyzed to compare the

productivity index ratio (J/Jo) with dimensionless fracture conductivity (C_{fd}) for both the completion over a range of fracture conductivity values (k_fw) obtained from carbo ceramic proppant data. Simulations were also done by varying fracture width, fracture half-length and vertical to horizontal permeability ratio to understand their influence on completion.

A horizontal well model without fracture was developed first, and validated with steady-state natural gas production equation by Economides et al., (1994), including Non-Darcy flow effects. A single-phase natural gas with laminar flow under isothermal condition was assumed. The unstimulated well model developed for this study is shown in Figure 1.8.

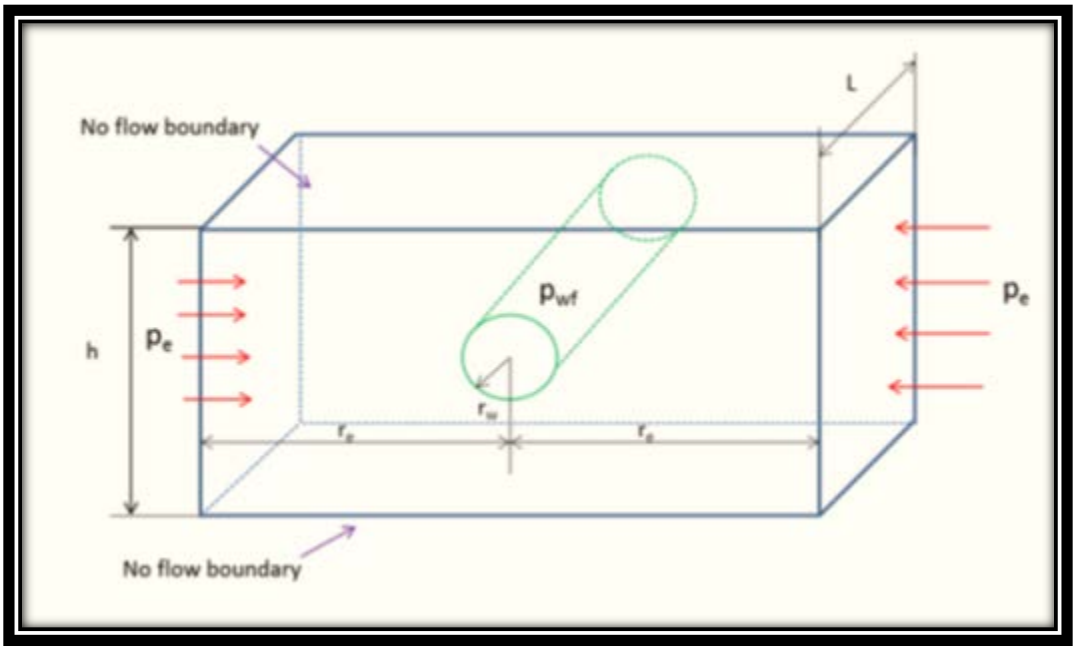

Figure 1.8. Unstimulated conceptual model (Theppornprapakorn et al., 2014)

In the stimulated model developed in CFD, the transverse fracture is created at the center of the domain, and the fracture half-length (x_f) is assumed to be equal on both sides. The reservoir pressure (p_e) is supposed to act at the boundaries of the model and

the well pressure (p_{wf}) is considered to act perpendicular to the sandface. Figure 1.9 shows the conceptual stimulated model.

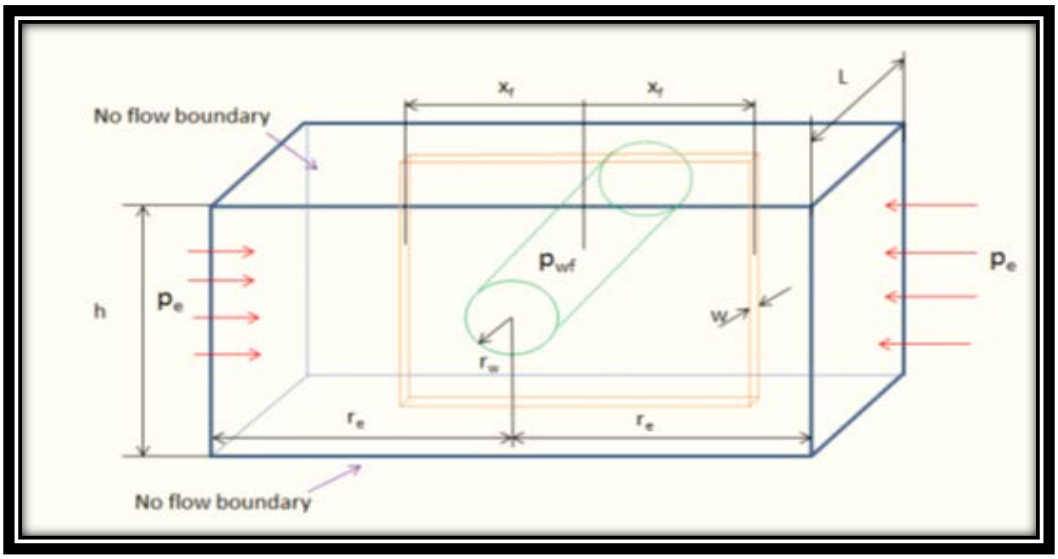

Figure 1.9. Stimulated conceptual model (Theppornprapakorn et al., 2014)

The reservoir data was obtained from the work of Magalhaes et al., (2007) with an assumption for vertical to horizontal permeability ratio (0.1). The length of the well and the distance to the outer boundary was taken as 300 ft. to validate with the horizontal well equation. Figure 1.10 shows the 3-dimensional model developed for this study.

The results were plotted in terms of productivity ratios as a function of dimensionless fracture conductivity considering the effects of fracture conductivity, penetration ratio and vertical to horizontal permeability ratio. It was concluded that OHMS completions have slightly higher production than P-n-P completions, and these results were in agreement with Augustine's (2011) two-dimensional work.

Another work in the same direction was performed by Chumkratoke et al., (2016) in which a three-dimensional CFD model was developed to analyze gas flow in extremely tight gas reservoirs (0.00001 mD). Flow from natural fractures was included in the model, which was developed using ANSYS FLUENT. Both open hole and cased hole completions were included in this study. The results from the simulation experiments

were validated with the results of the flow tests performed by the author and was compared with the historical works of Augustine and Theppornprapakorn.

The results from this study showed that open hole completions outperform cased hole completions. The trend of the curves was consistent with previous works done by Augustine and Theppornprapakorn although the magnitude of the productivities found were different.

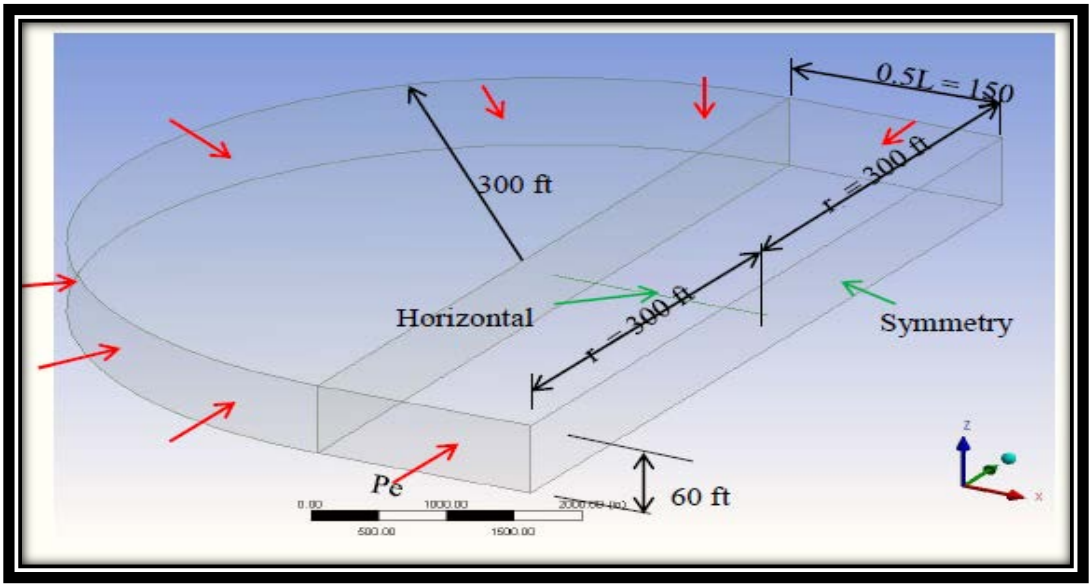

Figure 1.10. Three-dimensional CFD model (Theppornprapakorn et al. 2014)

1.2. OBJECTIVES OF THIS STUDY

The primary objective of this thesis work is to analyze and compare the performance of OHMS and P-n-P completions in high-permeability gas reservoirs by using the 3-D Computational Fluid Dynamics (CFD) model developed by Theppornprapakorn (2013). Theppornprapakorn performed simulation studies gas wells over the tight permeability range (0.01 mD) while Chumkratoke (2016) extended this work to nanoDarcy permeability.

Three high permeability reservoir cases were evaluated, including 1mD, 10 mD and 100 mD. Results of the 3-D simulations compared to the 2-D results of Augustine

(2011). High permeability is of interest because turbulent flow has greatest impact in high permeability gas reservoirs. Turbulence effects are believed to have greater impact in transverse fractures in high-permeability applications (Valko, 1996). The limited contact between the transverse fracture and the wellbore generates an additional pressure drop and a choking effect. The pressure drop can also be attributed to skin effect when fluid converges from linear to radial flow within the fracture (Mukherjee and Economides, 1991). This fluid flow inside fracture leads to convergent and Non-Darcy flow effects which drastically reduces the production (Soliman, 2006).

Theppornprapakorn included only one transverse fracture in the original horizontal well CFD model, since most horizontal well completions in tight reservoirs utilize transverse fractures. This study extends that evaluation to include two transverse fractures. Figure 1.11 depicts a horizontal well drilled in the direction of minimum stress, with multiple transverse fractures.

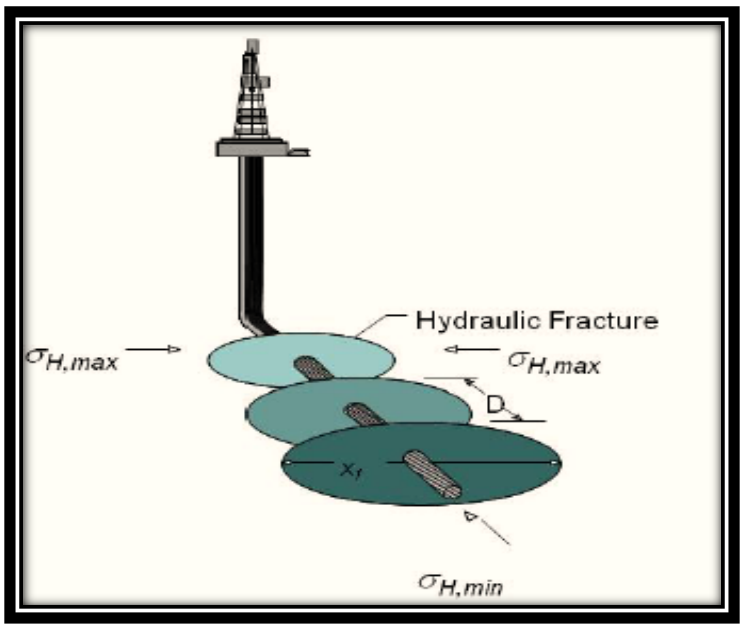

Figure 1.11. Transverse fractures in horizontal well (Economides et al. 2010)

The second objective of the study was to extend the 3-D horizontal well model to include one longitudinal fracture and compare production performance of transverse and

longitudinal fractures using 3-D CFD simulation. Figure 1.12 depicts a horizontal well drilled in the direction of maximum stress, with a single longitudinal fracture.

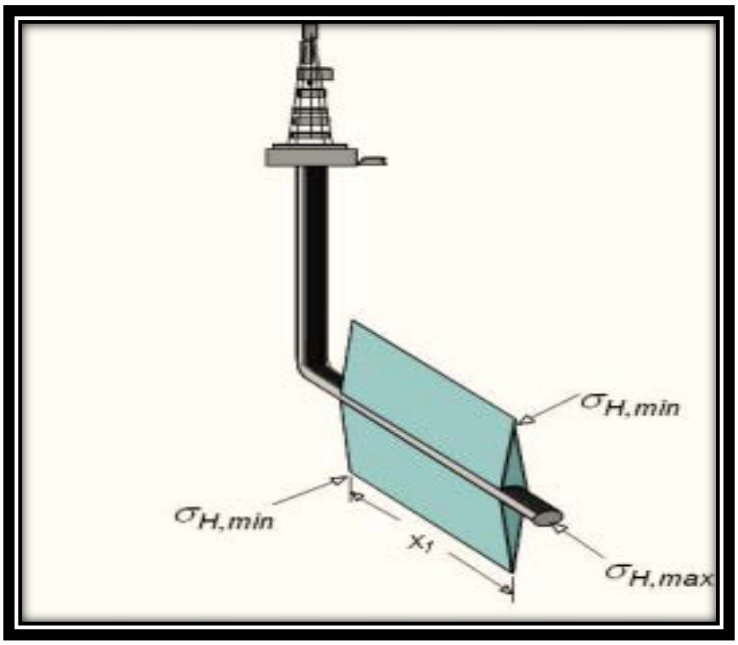

Figure 1.12. Longitudinal fracture in horizontal well (Economides et al. 2010)

Longitudinal fractures are suggested for use in moderate to high-permeability reservoirs due to the comparatively large contact area between wellbore and fracture resulting in the removal of choke effect at the contact area (Liu, 2012).

Yang (2015) provides a comparison of transverse and longitudinal horizontal fractured well performance using SITMPLAN simulation software. Her work compares up to 40 transverse fractures to 4 longitudinal fractures, and includes both oil and gas. The gas and oil reservoir simulation results based on production rate, recovery, and economics suggests that there is a critical reservoir permeability value beyond which longitudinal fractures outperform transverse fractures in horizontal wells. The results are presented in Table 1.2.

Table 1.2. Critical permeability values (Yang et al., 2015)

	IP	Ann 1st Yr Q	EUR	DR	PV	NPV
Gas	0.003 mD	0.008 mD	0.10 mD	0.04 mD	0.04 mD	0.03 mD
Oil	0.08 mD	0.20 mD	0.10 mD	0.40 mD	0.40mD	0.40mD

Yang (2015) concluded there is no significant difference in performance for transverse fractures below reservoir permeability of 0.10 mD even if the well is cased or open hole. Above reservoir permeability of 0.05 mD, the open ole longitudinal completion, and the open hole and cased multiple fractured transverse wells outperform cased hole longitudinal wells. Also, for reservoir permeability of over 0.4 mD, an open hole longitudinal well outperforms an open hole transverse well. For reservoirs in the permeability range of 0.00005 – 5 mD, a cased hole longitudinal well underperforms a cased hole transverse well. The field production data of Hugoton Gas Field in Chase Formation with a permeability in the range of 0.1 to 50 mD confirmed that longitudinally fractured horizontal wells have the highest cumulative gas production compared to two transverse fractured horizontal wells.

Results of this study are compared against the results of Yang for consistency, but are not intended to identify crucial permeability. The choice of completion method in gas reservoirs of 1 mD, 10 mD and 100 mD gas reservoirs is the primary consideration.

Results of this study are presented as folds of increase (FOI) which shows production difference between longitudinal and transverse fractures in both completions. The production difference between single and two transverse fractures are also plotted in terms of folds of increase. Parametric studies are performed by varying the propped fracture width (w), penetration ratio (x_f/r_e) and vertical to horizontal permeability ratio (k_v/k_h). Parametric studies were performed to understand the impact of these changes in fracture design.

2. BACKGROUND AND LITERATURE REVIEW

2.1. POST-FRACTURE WELL BEHAVIOR

2.1.1. Productivity Index. Productivity index of a well, both before and after the fracture treatment should be analyzed. Productivity index is a measure of the well potential. Productivity index is the ratio of the total liquid flow rate to the pressure drawdown. The expression for productivity index in natural gas wells is shown in equation 2-1.

$$J = \frac{q}{P^2e - P^2wf} \tag{2-1}$$

Where, J is the productivity index in gas wells (MSCF/D-psi^2), q is gas flow rate (MSCF/D), p_e is the outer boundary pressure (psi) and p_{wf} is the bottom hole flowing pressure (psi) (Wang et al. 2009).

2.1.2. Folds of Increase. Improvement of productivity index under steady state are expressed in terms of folds of increase (FOI). FOI is defined as (Economides et al. 2004):

$$FOI = \frac{J}{Jo} \tag{2-2}$$

Where, J is the productivity index after the stimulation and J_O is the productivity index before the stimulation.

2.1.3. Characterization of Fracture. The primary objective of hydraulic fracturing is to create and maintain a stable fracture with sufficient conductivity to maximize well productivity and ultimate recovery. Every hydraulic fracture can be characterized regarding length, width, height and conductivity.

The fracture length is assumed to consist of two equal half-lengths (x_f) in both sides of the well. This means that fracture grows equally in both directions. Half-length is presented as the conductive length through which liquids flow and not the created length by hydraulic activity.

The width of the fracture is shown as propped fracture width (w) and is an average of fracture width created. Constant fracture width has been assumed in this study.

The fracture height (h_f) is measured vertically in both transverse and longitudinal fractures. In this study, the fracture is considered to penetrate the entire pay zone thickness. Figure 2.1 shows the fracture half-length, propped fracture width, and height of the fracture in the case of a transverse fracture.

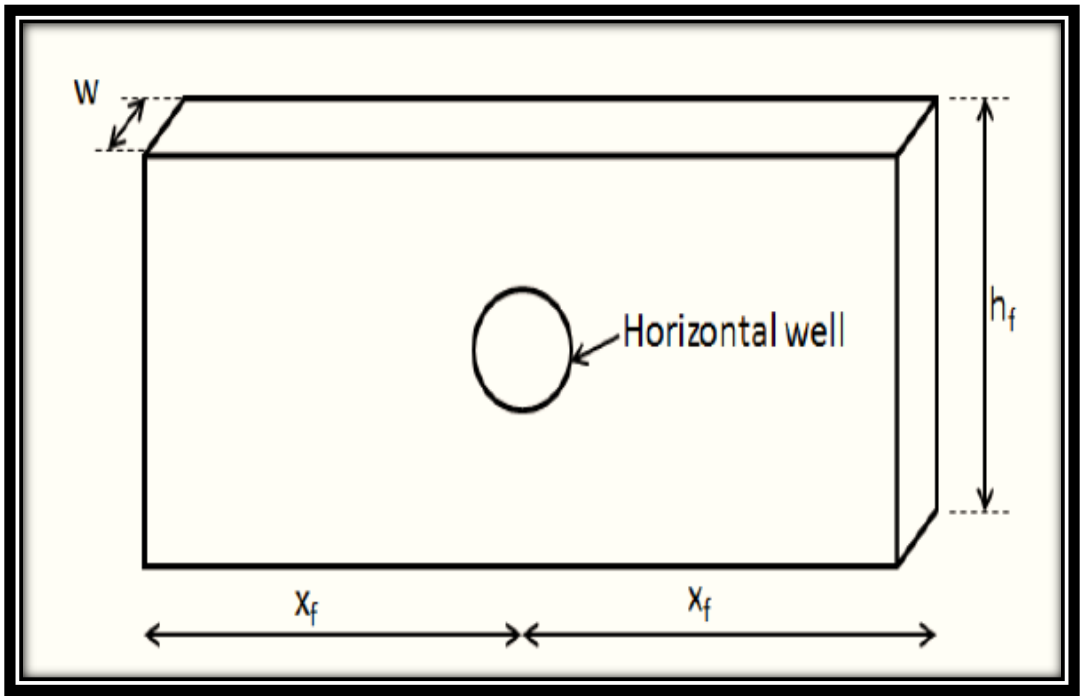

Figure 2.1. Notations of hydraulic fracture (Theppornprapakorn et al. 2014)

The interdependence of these variables is best described by the dimensionless fracture conductivity, F_{CD}:

$$F_{CD} = \frac{k_f w}{k x_f} \quad (2\text{-}3)$$

Where, k_f is the permeability of fracture (mD), and k is the permeability of reservoir (mD).

A high-dimensionless fracture conductivity indicates that flow through the fracture is much easier than flow into the fracture whereas a low dimensionless fracture conductivity shows that flow along the fracture is restricted.

The measure of how conductive or how easily fluid moves through a fracture is given by fracture conductivity, C_f (mD-ft):

$$C_f = k_f w \quad (2\text{-}4)$$

2.2. FLUID FLOW IN FRACTURED HORIZONTAL WELLS

Economides et al. (2007) pointed out that the folds of increase between fractured and non-fractured vertical gas and oil wells are quite similar at low permeabilities. He states, “folds decline as permeability increases. But as permeability increases, the trends diverge: a fractured gas well performs far better than a non-fractured high permeability gas well because of the considerable reduction in turbulence effects that adversely affect well performance.” Gas wells in high-permeability reservoirs are swayed by turbulence, and it is so severe that the gains from fracturing horizontal wells may be entirely lost.

Horizontal gas wells which are longitudinally fractured are preferred in high-permeability reservoirs due to the reduction in turbulence effects. The studies mentioned in the literature review corroborates this opinion. Transverse fractures enhance the turbulence effects due to a very small contact area between the well and the fracture.

2.2.1. Flow Into Transversely Fractured Horizontal Well. The flow direction of fluids in a transverse fracture intersecting horizontal wellbore is shown in Figures 2.2 and 2.3.

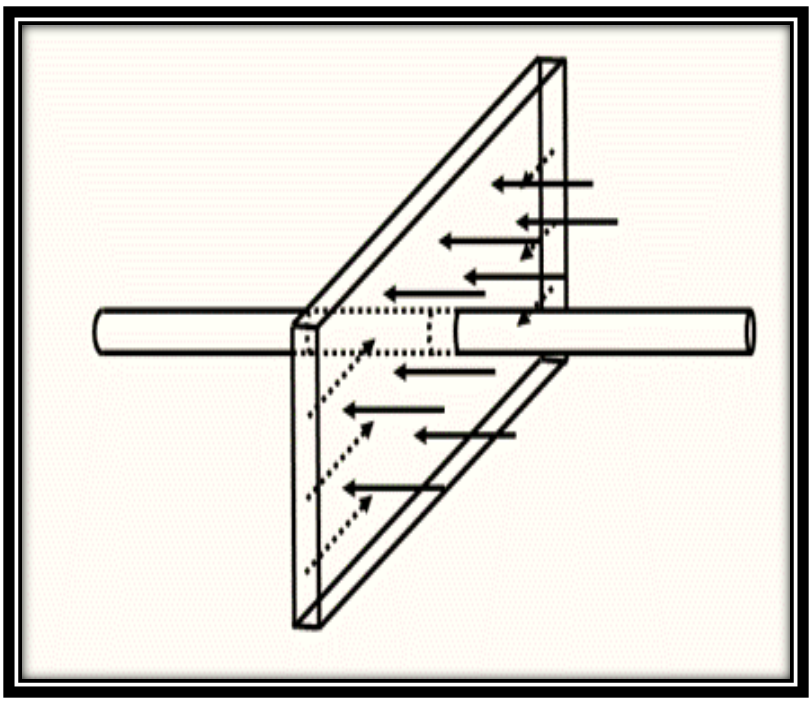

Figure 2.2. Bilinear flow (www.fekete.com/flow_regimes)

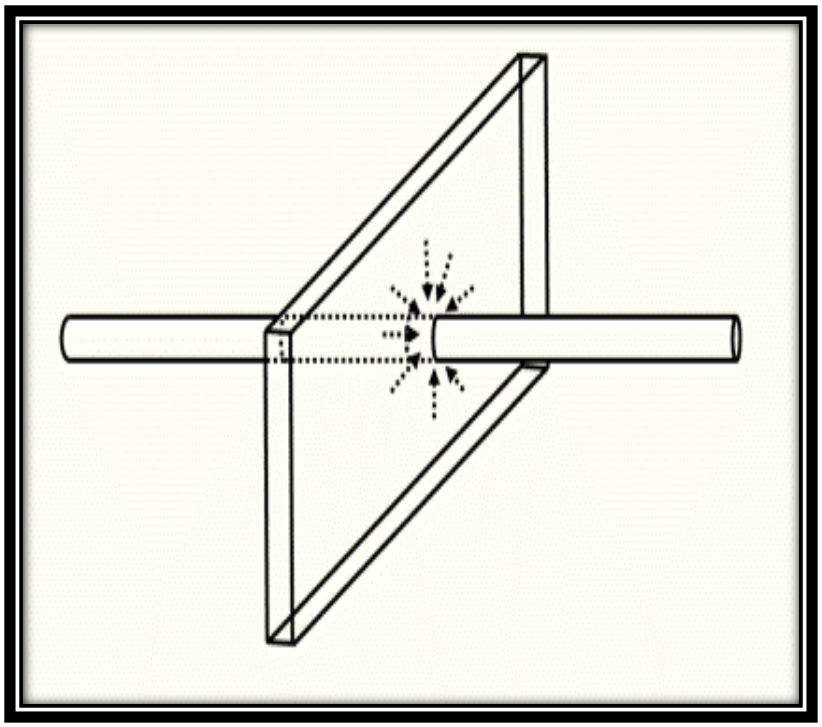

Figure 2.3. Radial flow within the fracture (www.fekete.com/flow_regimes)

Bilinear fracture flow occurs early in transversely fractured horizontal wells. In this flow regime, two linear flows exist: one towards the well within the fracture and another towards the fracture within the formation. At a later time, radial flow can be observed inside the fracture creating additional pressure drop which concerns production. This is the reason why transverse fractures are not recommended for higher-permeability formation.

2.2.2. Flow Into Longitudinally Fractured Horizontal Well. The performance of longitudinally fractured wells is usually compared with transverse fractures and fractured vertical wells. Fluid from the reservoir to the longitudinal fracture will flow in the horizontal plane when the fracture conductivity is infinite or almost infinite. Vertical permeability has minimal effect on the flow regimes and performance of both longitudinal and vertical fractured wells.

The high performance of longitudinal fracture is due to the short distance; fluid has to travel inside the fracture which leads to lower pressure drop.

Fluid flow through a porous medium or a fracture is usually assumed to be laminar with the exception in high rate gas wells. Convergent and Non-Darcy flow can drastically affect horizontal well performance early in the life of the well and can, therefore, have a critical and adverse impact on recovery. The Non-Darcy flow may exist in either the formation or the fracture, and it reduces the productivity index by introducing an additional pressure drop (skin) which reduces flow. In transversely fractured horizontal wells convergent Non-Darcy flow can be a huge problem. The negative effects of Non-Darcy on the performance of stimulated wells are well-known and documented by several authors (Lolon et al., 2004; Vincent et al., 1999).

McGuire and Sikora in 1960 (McGuire and Sikora, 1960) studied the effect of vertical fractures on the productivity of wells in a square drainage area. Their results were illustrated in the form of a chart which showed the dependency of well productivity on fracture length and conductivity. They came up with a conclusion that at large relative conductivity (low reservoir permeability), productivity can be increased by increasing the half-length (x_f) and not the conductivity. Figure 2.4.shows the McGuire-Sikora chart.

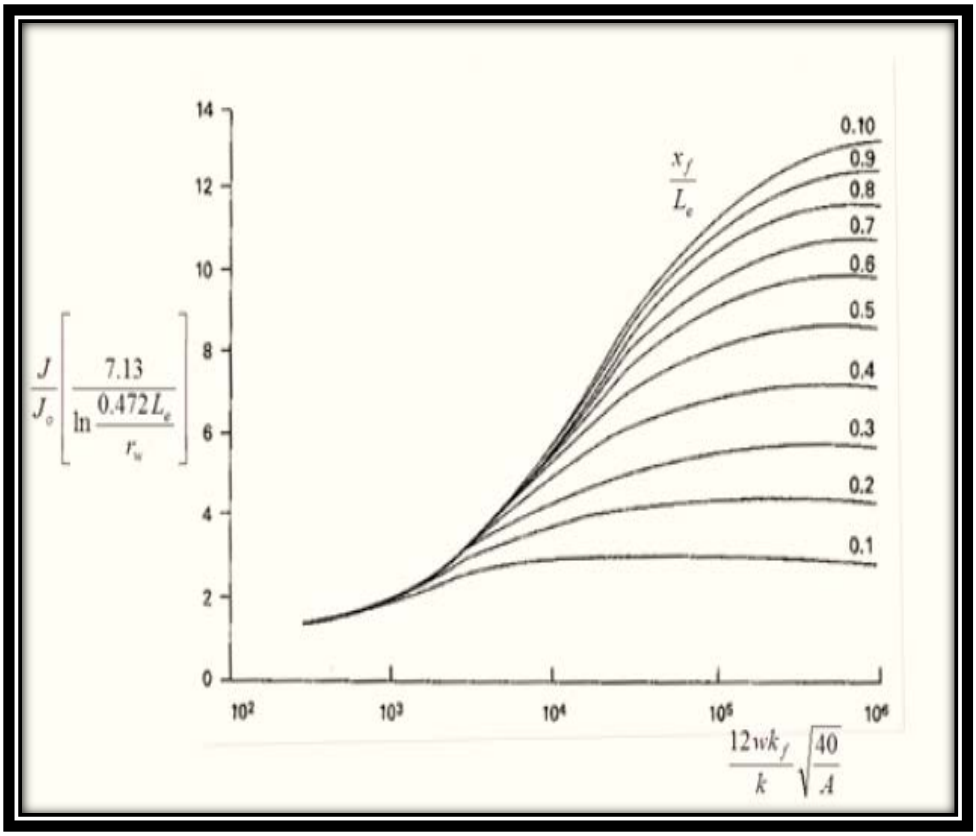

Figure 2.4. McGuire-Sikora chart (Cholet, 2000)

From the chart:

$$\text{Relative conductivity} = \frac{12wk_f}{k}\sqrt{\frac{40}{A}} \tag{2-1}$$

Where A is the square drainage area in acres and the penetration ratio (I_x):

$$I_x = \frac{x_f}{L_e} \tag{2-2}$$

Where L_e is the distance from well drainage area boundary (ft), x_f is the fracture half- length (ft).

The resultant folds of increase is obtained from the below expression

$$\frac{J}{J_o}\left[\frac{7.13}{\ln\frac{0.472L_e}{r_w}}\right] \tag{2-3}$$

Another conclusion form McGuire-Sikora work was that for a given fracture length, there exists an optimum conductivity ratio.

2.3. EVALUATION OF FRACTURED WELL PRODUCTIVITY MEASURES

This work focuses on CFD simulations which are then compared to the McGuire-Sikora fractured well productivity curves given by Augustine (2011). The question then is how do McGuire-Sikora curves compare to Pratt's (1961) fractured well productivity curve? No studies were found comparing these two measures in gas reservoirs. Britt (1994) in collaboration with Amoco Corporation, compared the two fractured well productivity measures for oil reservoirs. He suggested the use of Prats Curve (Economides et al., 1994) instead of McGuire-Sikora curves for analyzing the productivity improvement after fracturing as the results from McGuire-Sikora curve are "pessimistic for low values of relative conductivity and optimistic for high values of relative conductivity." Thus, McGuire-Sikora curves should be used with caution for high permeability oil reservoirs.

Despite the questions regarding how appropriate McGuire-Sikora curves may be over the permeability range of this study and the lack of historical comparisons in gas reservoirs, the simulations generated in this work are compared to the McGuire-Sikora curves and the results of Augustine (2011).

2.4. TRANSVERSE VS LONGITUDINAL FRACTURE ORIENTATION

Hydraulically fractured horizontal wells have become increasingly popular in unconventional gas reservoirs to improve well productivity. Depending on stress orientation relative to the wellbore, the fractures may be transverse or longitudinal. In this section, we briefly review the publications relevant to the performance analysis of transverse and longitudinal fractures in high-permeability gas reservoirs. They will set the background material for the developments in this thesis.

Valko et al., (1996) compared production rates and cumulative production from both longitudinally fractured horizontal wells and vertical wells, both fractured and un-fractured. He demonstrated the "Frac-Pack" process used for fracturing high permeability formations, where wider but shorter fractures are made by developing screen-outs. The concept of "discounted revenue," i.e., "time-value for money" was employed for economic analysis and calculations were done to estimate the net present value (NPV), discounted return on investment (DROI), and discounted profit-to-investment ratio (DPIR). The results showed that longitudinally fractured horizontal wells outperformed transversely fractured horizontal wells for reservoir permeability of 1 mD and 10 mD. Valko also indicates the need for further research to demonstrate the performance of longitudinally fractured horizontal wells.

The broad acceptance of fracturing of horizontal wells led to a comparative study of the performance of longitudinal fracture with fractured vertical well and a transverse fractured horizontal well by Soliman et al., (1996). The author recommends the use of longitudinal fractures instead of transverse fractures in high permeability formations as the width of transverse fracture near the wellbore is small leading to convergent flow which causes problems such as 'choke skin' effect, high friction pressure, and early screen out. Similar work done by Villegas et al., (1996) points in the same direction.

Turbulence effects are the dominant features in the production of higher (~10 mD) permeability gas wells and are so severe that it may lead to a reduction in the expected production rate. Transverse fractures enhance turbulence effects due to a very small contact area between the well and the fracture. Economides developed an iterative procedure to account for turbulence effects which have been explained in detail by Wei et al., (2005). Example calculations were done by the author using the iterative procedure

for a range of permeabilities, and it was concluded that transverse fractures are not attractive if formation permeability is larger than 1 mD.

The turbulence effect in transverse fractures are well explained by Soliman et al., (2006) with the help of flow regimes. The convergence of linear flow to radial flow in a transverse fracture results in additional pressure drop inside the fracture which considerably reduces the overall production, and in high permeability applications, the convergence of fluid is increased with the presence of Non-Darcy effects. The effects of Non-Darcy flow on the performance of hydraulically fractured gas wells has been well documented by Smith et al., (2004) with field case examples. Soliman performed a numerical simulation analysis to compare the performance of transverse and longitudinal fractures over a range of reservoir permeabilities. The results from the analysis favored the use of longitudinal fractures in the permeability range of 1- 5 mD and transverse fractures were preferred for reservoirs with permeability less than 1 mD.

In 2010, Economides et al. conducted a large number of fracture simulations for gas wells to evaluate the results from transverse, longitudinal and vertical fractured wells. Permeability range varied from 0.001 mD to 500 mD. Unified fracture design approach using proppant number as a correlating parameter was used in this study. Innumerable results were acquired from this study based on the permeability of the gas reservoir.

The results from this study for gas reservoirs were tabulated and are shown in Table 2.1. These results have been widely cited in studies since.

Table 2.1. Options for fracturing gas wells (Economides et al. 2007)

Permeability range, mD	Best Technical solution	Comments
>5	Horizontal wellbore, Longitudinal Fractures	In all cases
0.5-5	Horizontal wellbore, Longitudinal Fractures OR Vertical Well with Fracture	Dependent upon project economics and the relative costs of vertical and horizontal wellbores and zonal isolation techniques

Table 2.1. Options for fracturing gas wells (cont.)

0.1-0.5	Horizontal wellbore, Transverse Fractures	Above 0.5mD, the "choked" connection between the fracture and the wellbore makes transverse fractures relatively inefficient
<0.1mD	Horizontal wellbore, Transverse Fractures OR Vertical Well with Fracture	Dependent upon project economics and the relative costs of vertical and horizontal wellbores and zonal isolation techniques

The first study using unified fracture design approach for comparing transversely and longitudinally fractured horizontal wells in moderate permeability gas reservoirs (0.01 to 5 mD) was carried out by Liu et al., (2012). The unified fracture design was deployed in the study to account for Non-Darcy flow effects in the gas production. This study was based on a field example from Asia. Comparison of the net present value of nine transverse fracture configurations to three longitudinal fracture configurations with different well and fracture spacing was made. Multi-laterals were also examined in this study. Liu asserted that the completion strategies with the highest productivity were not the key to obtaining the best value and that well performance was highest when drainage optimization and flow mechanisms were properly accounted for.

A multi-phase study comparing the performance of transverse and longitudinal fractures in the permeability range of 0.000001 mD to 10 mD was done by Kassim et al., (2016). Kassim extended the results from the single phase flow comparison performed by Yang et al., (2015) by adding multiphase flow dimensions and incorporating Non-Darcy flow effects, the effect of relative permeability on fluid flow in the fracture, and impact of stress-dependent permeability on fracture conductivity. Many parameters such as lateral length, the importance of lateral direction as a function of reservoir permeability, fracture half-length, fracture conductivity and well completion type were reviewed in this work. The results from this study based on fracture orientation are shown in Table 2.2.

Table 2.2. Suitable options for fracturing wells (Kassim et al., 2016)

Best Option	Critical Permeability condensate reservoirs (API 48)	Black oil type reservoirs (API 38)	Dry gas reservoirs
Longitudinal Fractures	K> 1.8 mD	K> 2 mD	K> 0.9 mD
Transverse Fractures	K< 0.07 mD	K< 0.3 mD	K< 0.05 mD

The fracturing of horizontal wells, as a primary completion technique, is becoming more and more desirable, and all the previous studies which compared the performance of longitudinal and transverse fractures were limited by the range of reservoir permeability considered. This research provides CFD simulations that corroborate the critical permeability suggested by Yang et al., (2015) and Kassim et al., (2016) for deciding the fracture orientation based on the reservoir permeability and also on the completion technique employed. A 3-D CFD model for understanding the gas flow in high permeability reservoirs was developed for this research work.

3. SIMULATION SOFTWARE

The simulation software used is a Computational Fluid Dynamics (CFD) software. CFD can be described as the use of computer-based simulation to analyze systems involving fluid flow and heat transfer. It is a powerful technique and has a broad range of applications in industrial and non-industrial areas. Some of the fields where CFD is applied are aerospace, power plants, chemical processes and automobile industry, etc. Versteeg et al. (2009). Figure 3.1 shows CFD stress analysis image of a subsea gate-valve.

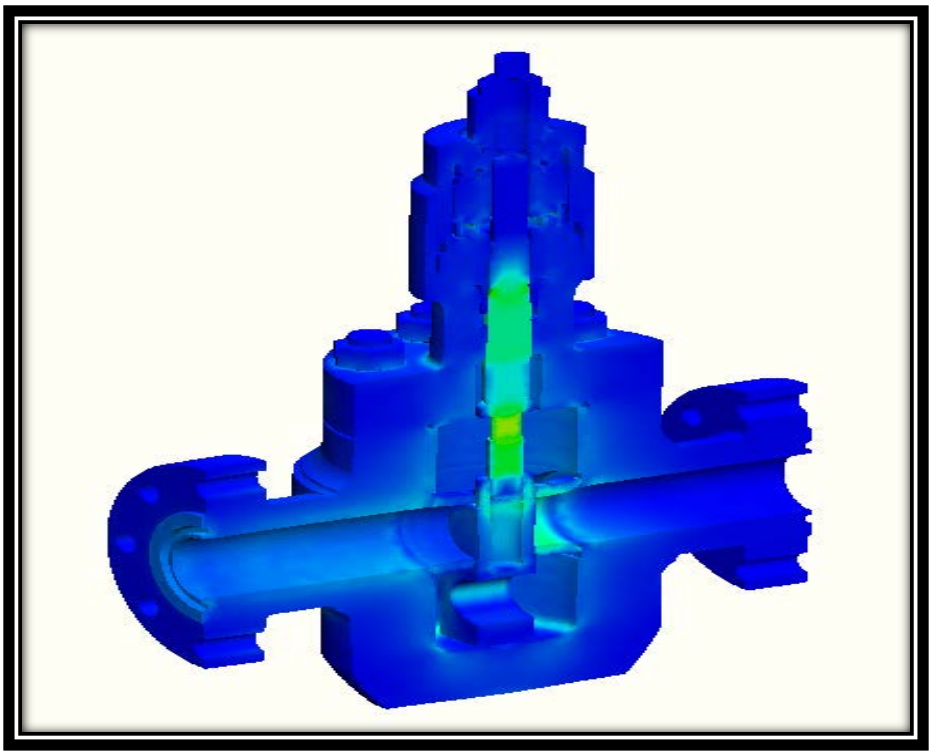

Figure 3.1. A CFD model image. (http://www.pretechnologies.com/sectors/oil-and-gas/subsea-processing)

CFD has been successfully used in the oil and gas industry in many applications. Predicting fracture propagation behavior, analyzing inflow performance in hydraulically fractured wells taking into account completion complexities, understanding of flow along

horizontal wells and building models to compare the performance of perforations are some of its applications. Jimenez et al. (2009), Zeboudj et al. (2010), Sun et al. (2011) and Byrne et al. (2011) are some of the authors who used CFD to analyze well performance and near well bore damage in oil and gas industry.

This research uses CFD to describe inflow to the wellbore, flow into and through the fracture, and then flow through the different types of well completions. CFD has been used for the work because traditional reservoir simulators describe reservoir flow at large scale, and the detailed aspects of the completion are difficult to model in simulators such as CMG and ECLIPSE. Jimenez et al. 2009 demonstrates the use of CFD to model inflow in vertical and deviated wells, with a hydraulic fracture producing from in a layered reservoir. The work included different perforating schemes and shows the utility of CFD in modeling well completions.

3.1. SIMULATION PROCESS

CFD analysis takes place in three stages: Pre-processing, Solving, and Post-processing.

Pre-processing is the first step in CFD simulation process, which helps to describe the geometry in best possible way. ANSYS Geometry is used in this research. All the boundaries such as inlets, outlets and walls are defined in this step. The fluid domain of interest is also identified in this step. Next step is the mesh generation step where the domain of interest is divided into smaller segments. ANSYS Meshing is used in this case. The mesh is then imported to ANSYS FLUENT 15.0 for generating the flow field solutions at mesh points. Inside FLUENT, the problem physics are identified and are solved using a computer.

It is important that proper boundary conditions such as wall temperature, inlet velocity, and gauge pressure are applied in the computational domain. The CFD Solver FLUENT generates the flow field data at each mesh point after solving the appropriate governing equations.

Once the results are obtained, they are analyzed using different plots like contour plots, line plots, etc. ANSYS CFD-Post is employed in this work to analyze the results. Figure 3.2 shows the basic processes involved in CFD modeling.

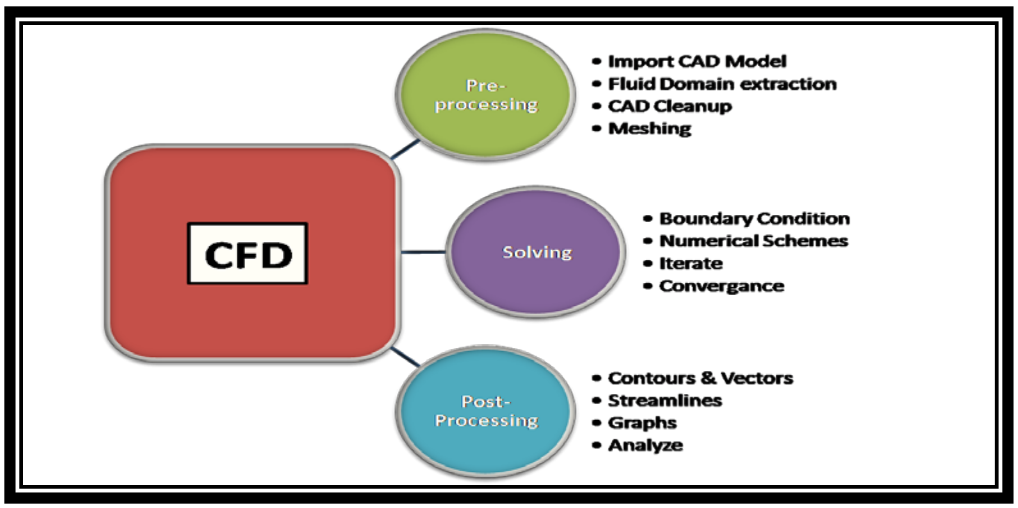

Figure 3.2. Basic CFD processes

3.2. GOVERNING EQUATIONS IN CFD

CFD modeling is based on fundamental laws of fluid dynamics: the conservation of mass, momentum and energy. These equations are used to find out the three primary unknowns in fluid dynamics (Esionwu, 2014):

- Velocity vector, ∇
- Pressure, p
- Temperature, T

Four quantities are obtained by resolving the governing equations (Esionwu, 2014):

- Density, ρ
- Enthalpy, h or internal energy, e
- Viscosity, μ
- Thermal conductivity, k

Since this work is based on gas, the governing equations for compressible flow is given below:

3.2.1. The Continuity Equation. (Esionwu, 2014)

$$\text{Continuity equation} = \frac{\partial p}{\partial t} + \overline{V}.(\rho\vec{V}) = 0 \qquad (3\text{-}1)$$

Where "$\vec{V}.\vec{V}$= time rate change of volume moving fluid element per unit volume."(Esionwu, 2014)

3.2.2. The Momentum Equation (Navier-Stokes Equations). Momentum equations can be expressed in x, y and z direction.

In x-direction (Esionwu, 2014),

$$\frac{\partial(\rho u)}{\partial t} + \nabla.\left(\rho u\vec{V}\right) = -\frac{\partial p}{\partial x} + \frac{\partial \tau xx}{\partial x} + \frac{\partial \tau yx}{\partial y} + \frac{\partial \tau zx}{\partial z} + \rho fx \quad (3\text{-}2)$$

In y-direction (Esionwu, 2014),

$$\frac{\partial(\rho v)}{\partial t} + \nabla.\left(\rho v\vec{V}\right) = -\frac{\partial p}{\partial y} + \frac{\partial \tau xy}{\partial x} + \frac{\partial \tau yy}{\partial y} + \frac{\partial \tau zy}{\partial z} + \rho fy \quad (3\text{-}3)$$

In z-direction (Esionwu, 2014),

$$\frac{\partial(\rho w)}{\partial t} + \nabla.\left(\rho w\vec{V}\right) = -\frac{\partial p}{\partial z} + \frac{\partial \tau xz}{\partial x} + \frac{\partial \tau yz}{\partial y} + \frac{\partial \tau zz}{\partial z} + \rho fz \quad (3\text{-}4)$$

Where u, v and w are the velocities in x, y and z direction, respectively.

3.2.3. The Energy Equation. The principle of energy conservation governs temperature variations in the reservoir. In this work, reservoir temperature is assumed to be constant (isothermal reservoir). Hence, energy conservation equation is redundant. Energy equation can be found in many CFD publications such as Versteeg et al. (2009).

3.3. OVERVIEW OF ANSYS WORKBENCH AND FLUENT

3.3.1. ANSYS Workbench. The ANSYS Workbench platform is based on an innovative project schematic view which connects the entire simulation process. The ANSYS Workbench Geometry Interfaces provide a two-way connection with all the main CAD systems, which helps in making design decisions based on efficient simulation results. ANSYS meshing compresses the review process, ensuring accurate solutions. The robust workflow schematic changes the way people work with simulation. Workflow is represented as connected systems in flowchart form which makes it easy to comprehend. Figure 3.3 shows the ANSYS Workbench schematics.

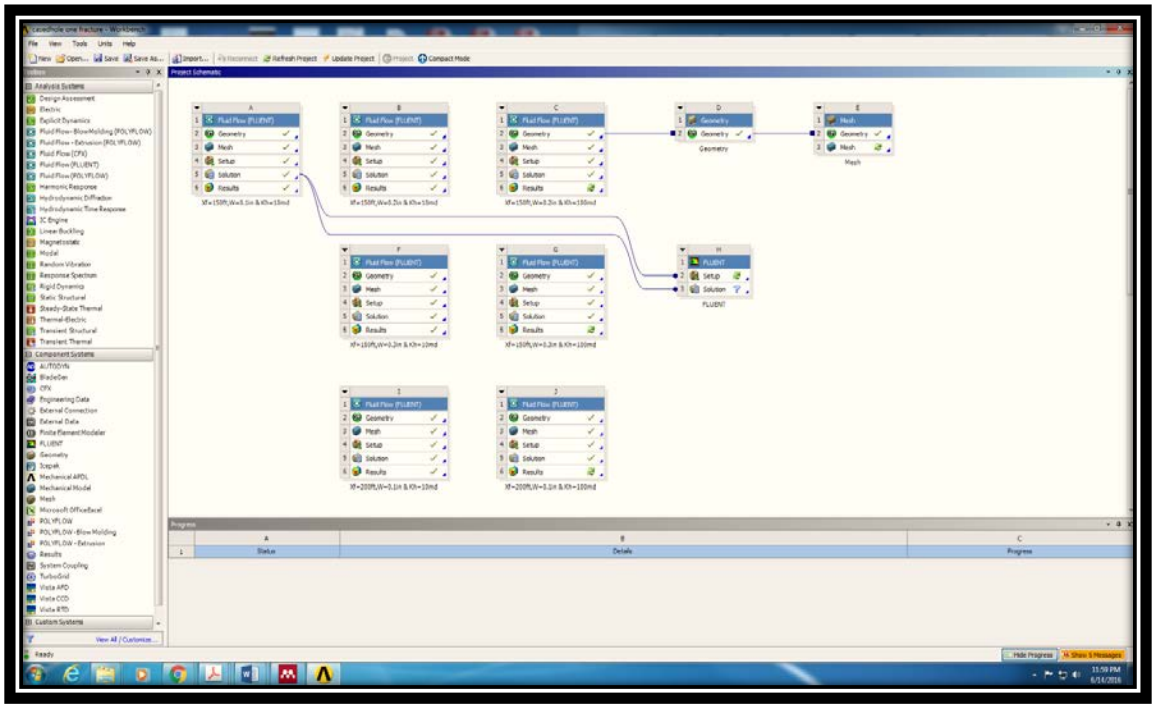

Figure 3.3. ANSYS Workbench

3.3.2. ANSYS FLUENT. FLUENT is an analysis system available in ANSYS Workbench. The system consists of four modules: DesignModeler, Mesh, Setup and Solution, and Results.

The desired geometry is built in the DesignModeler, and all the pressure/velocity outlets and inlets are named here. The geometry is then transferred to the mesh module where the complex geometry is broken down into nodes. The software calculates the relevant governing equations at each node to render the flow field. The larger the density of meshing, the greater is the accuracy of evaluation, and greater is the difficulty in solving the problems. Figure 3.4 shows the meshing process in ANSYS Meshing.

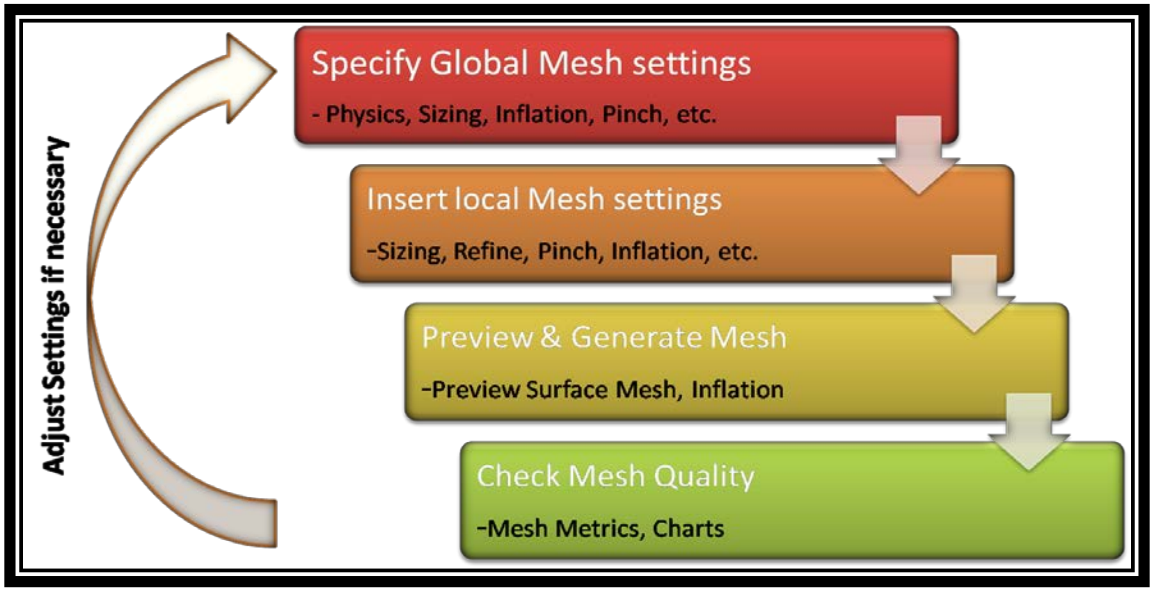

Figure 3.4. ANSYS Meshing process (ANSYS, 2014)

Global mesh settings are used in this study. The quality of mesh should be checked and improved if it doesn't meet the required criteria. Important geometric details are well captured in a high-quality mesh, and a bad mesh will have convergence difficulties. Figure 3.5 shows the mesh quality recommendations based on skewness and orthogonal quality.

The meshed model is then imported into the setup module which is the last pre-processor in ANSYS FLUENT. All the boundary conditions, cell zone conditions and material properties of the model are defined here. A cell zone is a group of cells for which all active equations are solved. The accuracy of the simulation result depends on

these conditions. Since this study is related to the production of natural gas, species transport is turned on. “Porous Zone” option is enabled in the “Fluid” panel since flow through porous media is considered. The input in this section is viscous resistance which is the inverse of permeability. The conversion of permeability (k) in mD unit to viscous resistance ($1/m^2$) explained by Wang et al. (2009) is:

$$\text{Viscous resistance } (1/m^2) = \frac{1}{k(md)\times 9.9\times 10^{-16}} \tag{3-5}$$

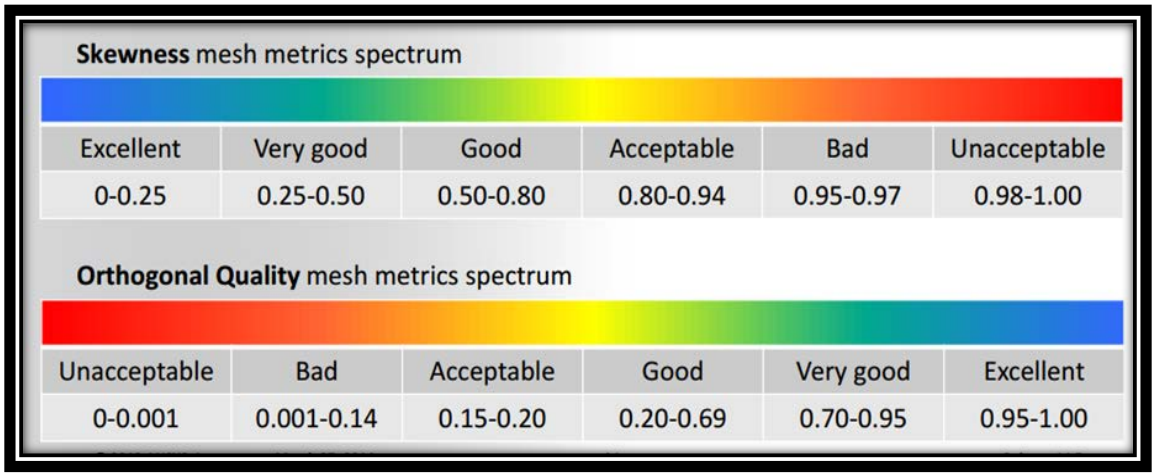

Figure 3.5. Mesh quality recommendations (ANSYS, 2014)

Material properties are obtained from the FLUENT database, or a custom user-defined database can be created if required material properties are not available in FLUENT.

The solver is set up to calculate the solution is the next process. Figure 3.6 shows a solution procedure overview. Pressure based and Density based solvers are the two types of solvers available in FLUENT. Pressure based solver is used in this study since it is applicable for high-speed compressible flow.

The simulation process is started once the setup is completed. All the solution variables are initialized before starting the iterations. A good initialization reduces the

iteration time. In this study either Hybrid or Standard initialization is used. Iterations will stop once the convergence is achieved, and the convergence criteria depend on the values set by the user. “Generally, a decrease in residuals by three orders of magnitude can be a sign of convergence (but not necessarily)” (Sofialidis, 2013). Bad mesh quality and mistakes in assumptions made can lead to difficulties in getting a convergence.

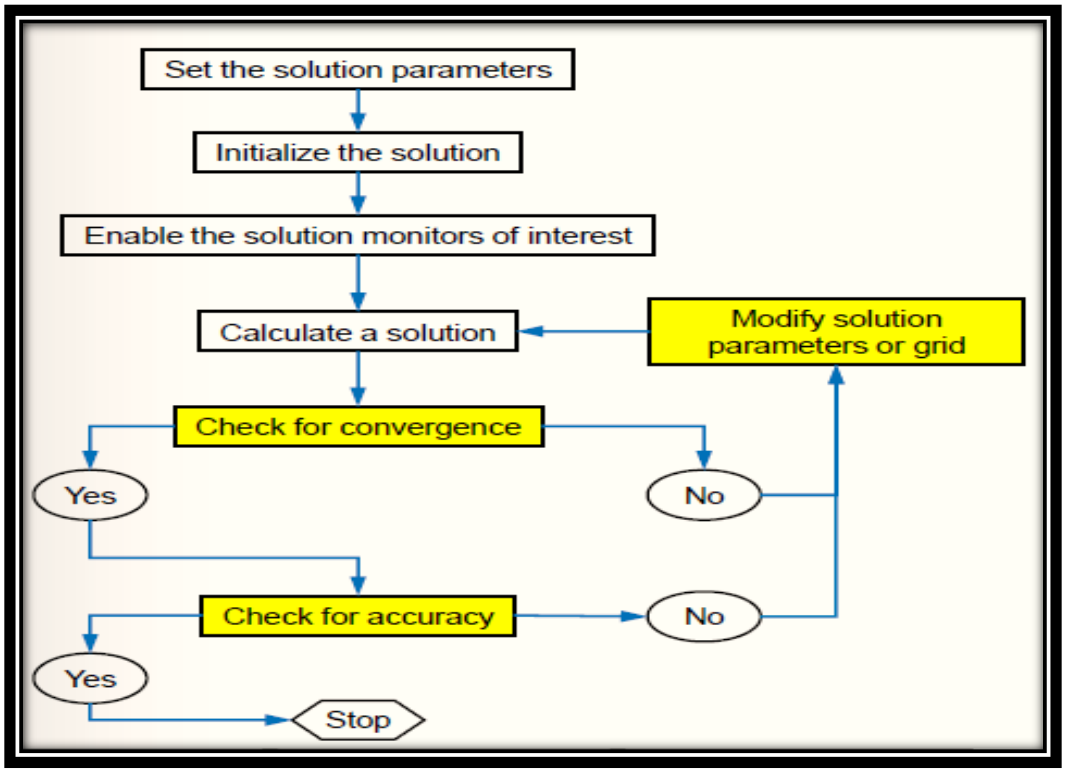

Figure 3.6. Simulation Workflow (Sofialidis, 2013)

After completing the iterations, results can be analyzed in FLUENT post-processor by plotting pressure/velocity vectors, contours, and streamlines, etc. at desired locations in the model. Though FLUENT post-processor is easy to use, it lacks in many applications when compared with CFD-Post.

CFD-Post is the last module of FLUENT in ANSYS Workbench. CFD-Post is used for analysis of results with advanced post-processing tools and simultaneous comparison of different cases. CFD-Post provides a range of functions with its integrated

calculators giving insightful solution visualizations. Each CFD-Post session includes a standard template for report generation. This module also allows multiple resolution data sets to be loaded simultaneously, making the comparison of different parameters hassle free.

A FLUENT workflow chart is shown in Figure 3.7 which shows all the processes carried out in ANSYS FLUENT and have been mentioned above in this section.

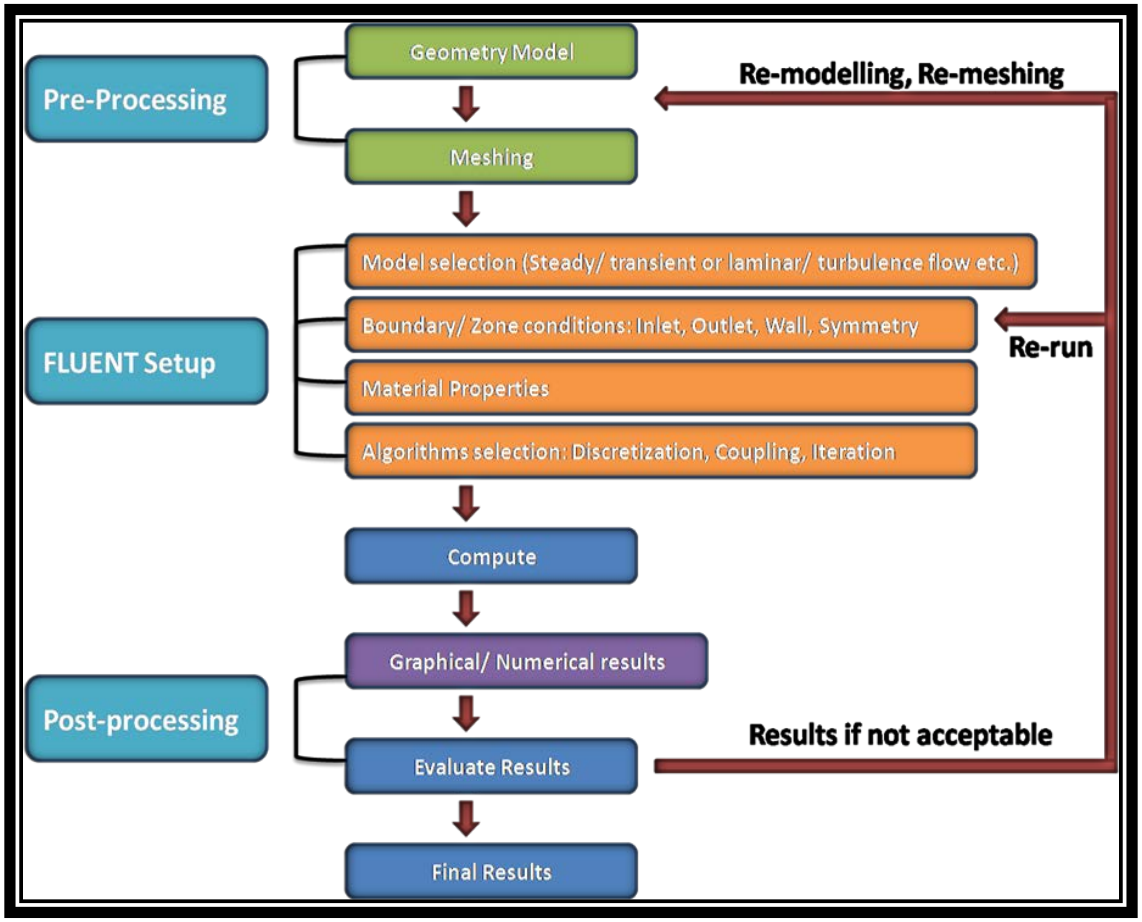

Figure 3.7. FLUENT workflow chart (Theppornprapakorn et al., 2014)

4. RESERVOIR SIMULATION

This section explains about the horizontal gas well model developed for this study. All the fundamental properties and equations necessary to build and validate the CFD model are also described in this section. The horizontal well deliverability equation of Joshi (1988), expanded by Economides et al. (1990) has been used to validate the model. The validation is made using a horizontal well model without any fracture. Validation results are presented in the form of IPR plots and tables. Parametric studies were performed and completion methods were evaluated in this study, as discussed in this section.

4.1. RESERVOIR DATA

The reservoir data used in this study is same as Theppornprapakorn et al. (2014) with a change in the horizontal permeability values. Simulations were performed with horizontal permeabilities of 1 mD, 10 mD, and 100 mD. A vertical to horizontal permeability ratio of 0.1 is assumed. Gas compositions are required for calculating the gas properties, and ethane and methane have been used in this study. FLUENT requires gas composition to solve the equation of state, as the gas properties cannot be directly given as input to FLUENT. The reservoir properties are shown in Table 4.1.

Table 4.1. Reservoir data

Reservoir and fluid properties	Value	Unit
Reservoir rock	Sandstone	-
Net pay; h	60	ft
Horizontal absolute permeability; k_h	1, 10 and 100	mD
Vertical to horizontal permeability ratio ($k_v/k_{h)}$	0.1	-
Reservoir temperature; T	254	°F
Reservoir/Boundary pressure; p_e	2800	psi
Gas compositions	93% Methane, 7% Ethane	-

4.2. NATURAL GAS PROPERTIES

Natural gas is naturally occurring mixture of light hydrocarbon gases. It consists mainly of methane. Natural gas properties are used throughout from reservoir inflow to well flow performance. This section explains the gas properties which are used in this work.

4.2.1. Mole Fraction. The composition of a natural gas mixture is expressed as the mole fraction. The mole fraction is defined as (Ikoku, 1992):

$$y_i = \frac{n_i}{\sum n_i} \tag{4-1}$$

Where y_i is the mole fraction of component i, n_i is the number of moles of component i, and $\sum n_i$ is the total number of moles of all components in the mixture.

4.2.2. Apparent Molecular Weight. Apparent molecular weight is used to characterize a gas mixture. It is a pseudo property of the mixture and is given as (Ikoku, 1992):

$$M_g = \sum y_i M_i \tag{4-2}$$

Where M_g is apparent molecular weight of mixture and M_i is molecular weight of component i. Gas component properties are shown in Table 4.2.

4.2.3. Real Gas Law. All gases deviate from ideal gas laws under most conditions. Natural gas behavior can be approximated by real gas law and is given by (Ikoku, 1992):

$$pV = ZnRT \tag{4-3}$$

Where p is the pressure (psi), V is the gas volume (ft^3), Z is the gas deviation factor which is dimensionless. It is also called Z-factor. R is the universal gas constant and it is equal to 10.73 psi ft/lb-mol-°R and T is the absolute temperature (R), which is simply °F+460°.

Table 4.2. Gas component properties

Gas components	Formula	Molecular Weight	Critical properties		Acentric factor (ω)
			T_c (°R)	P_c (psi)	
Methane	CH_4	16.043	343.338	667.029	0.011
Ethane	C_2H_6	30.070	549.906	706.624	0.100

4.2.4. Natural Gas Density. Density is defined as (Wang et al., 2009):

$$\rho_g = \frac{pMW_g}{ZRT} \tag{4-4}$$

Where ρ_g is the natural gas density (lb/ft^3).

4.2.5. Pseudo Critical Properties. Pseudo critical temperature and pressure are the average critical temperature and pressure of the mixture components. When the gas composition is known, pseudo critical temperature and pressure can be found out from (Wang et al., 2009):

$$p_{pc} = \sum y_i p_{ci} \tag{4-5}$$

$$T_{pc} = \sum y_i T_{ci} \tag{4-6}$$

Where p_{pc} is the pseudo critical pressure of natural gas (psi), p_{ci} is the pseudo critical temperature of component i (psi), T_{pc} is the pseudo critical temperature of natural gas (R) and T_{ci} is the pseudo critical temperature of component i (R).

4.2.6. Pseudo Reduced Properties. Pseudo reduced properties are defined as the actual properties divided by their critical properties. Pseudo reduced properties are also used to define the Peng-Robinson equation of state (PR EOS). The pseudo reduced pressure and temperature are given by (Wang et al., 2009):

$$p_{pr} = \frac{p}{p_{pc}} \tag{4-7}$$

$$T_{pr} = \frac{T}{T_{pc}} \tag{4-8}$$

Where p_{pr} is the pseudo reduced pressure and T_{pr} is the pseudo reduced temperature.

4.2.7. Z-factor. Standing and Katz (1942) published a chart from which Z-factor can be determined using the pseudo reduced properties. The chart is shown in Figure 4.1.

Z-factor can also be calculated directly using an equation of state. Hall and Yarborough (1974) developed a correlation to calculate Z-factor value and this correlation is used in this study in the calculation of real gas law. The correlation is (Economides and Martin, 2007):

$$z = \left[\frac{0.06125 p_{pr} t}{Y}\right] exp[-1.2(1-t)^2] \tag{4-9}$$

Where t is the reciprocal of the pseudo-reduced temperature (T_{pc}/T) and Y is the reduced density that can be obtained from:

$$F(Y) = X1 + \frac{Y+Y^2+Y^3+Y^4}{(1-Y)^3} \qquad (4\text{-}10)$$
$$-(X2)Y^2 + (X3)Y^{X4} = 0$$

Where,

$$X1 = -0.06125 p_{pr} t \, exp[-1.2(1-t)^2]$$
$$X2 = (14.76t - 9.76t^2 + 4.58t^3)$$
$$X3 = (90.7t - 242.26t^2 + 42.4t^3)$$
$$X4 = (2.18 + 2.82t)$$

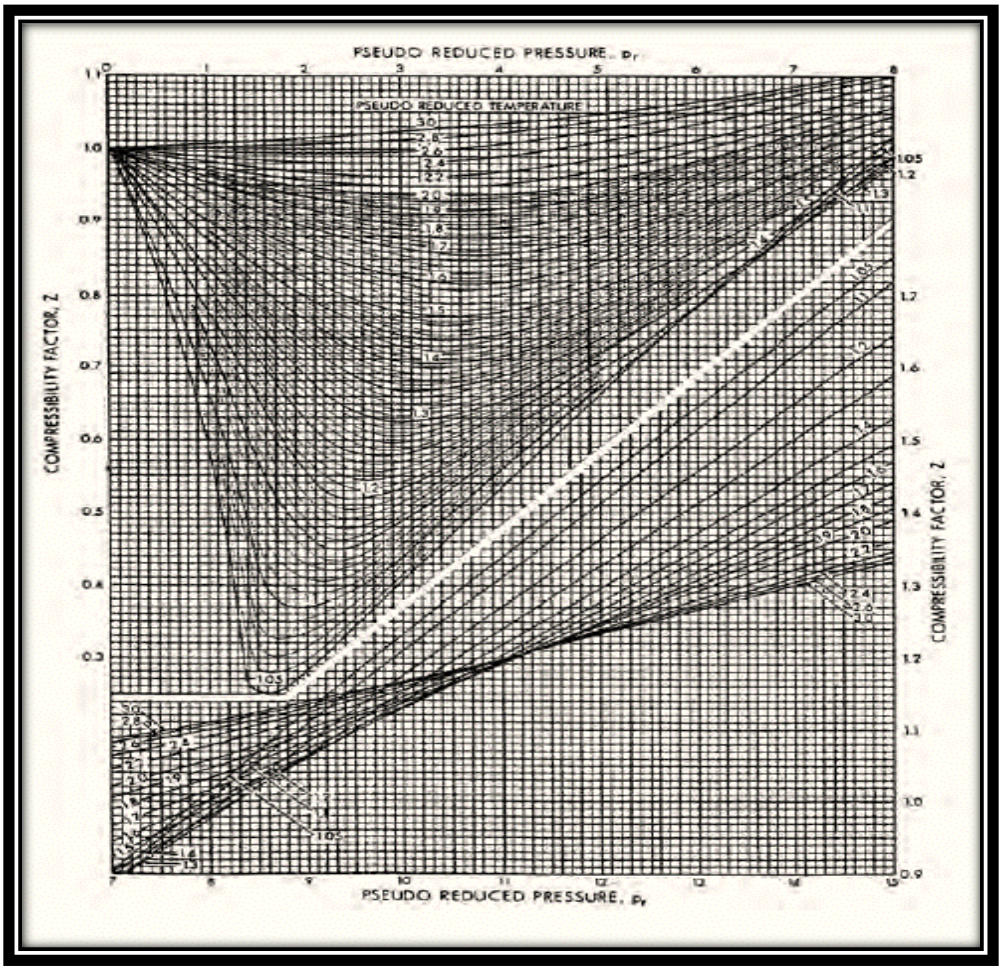

Figure 4.1. Standing and Katz (1942) Z-factor chart (Wang et al., 2009)

4.2.8. Equation of State. An equation of state uses mathematical relationships to determine properties of fluids or fluid mixtures, such as temperature, pressure, volume or internal energy. Density of fluids or fluid mixtures cannot be entered into FLUENT directly and there is no option to include Z-factor in FLUENT. Density values of known fluids are stored in the FLUENT library and the density of a mixture is calculated inside FLUENT using an equation of state. In this study Peng-Robinson equation has been used to find out the mixture density (ANSYS FLUENT User's Guide, 2011).

The Peng-Robinson equation was developed to express the fluid parameters in terms of critical properties (Peng and Robinson, 1976). It was used to determine compressibility factor and density of fluid mixture. The properties of gases employed in this study are available in the FLUENT database. Peng-Robinson equation is a three-parameter equation and requires critical mixture constants such as critical pressure (P_{cm}), critical temperature (T_{cm}) and acentric factor (ω_m).

In this study, FLUENT calculates critical mixture constants using Van der Waals mixing rules (ANSYS FLUENT User's Guide, 2011). The equations for critical mixture constants are given below (ANSYS FLUENT User's Guide, 2011):

$$T_{cm} = \frac{\left[\sum_i (x_i \frac{T_{ci}}{p_{ci}^{0.5}})\right]^2}{\sum_i (x_i \frac{T_{ci}}{p_{ci}})} \tag{4-11}$$

$$p_{cm} = \frac{T_{cm}}{\sum_i (x_i \frac{T_{ci}}{p_{ci}})} \tag{4-12}$$

$$\omega_m = \sum_i y_i \omega_i \tag{4-13}$$

Where ω_i is the acentric factor of gas component and is shown in Table 4.2 in section 4.3.2 along with other critical properties.

4.2.9. Gas Viscosity. Viscosity is a measure of fluid's internal resistance to flow. The correlation developed by Lee et al. (1966) is used in this study. Gas viscosity is given as (Wang et al., 2009):

$$\mu_g = Kexp(X\rho_g^Y) \tag{4-14}$$

$$K = \frac{(9.4+0.02MW_g)T^{1.5}}{209+19MW_g+T} \tag{4-15}$$

$$Y = 2.4 - 0.2X \tag{4-16}$$

$$X = 3.5 + \frac{986}{T} + 0.01MW_g \tag{4-17}$$

Where the gas viscosity (μ_g) is in centipoises (cp) and T is temperature in R.

4.3. HORIZONTAL WELL EQUATIONS

4.3.1. Equation for Incompressible Fluids. The horizontal well equation for incompressible fluids was developed by Joshi (1988). This relationship was based on the assumption that in the horizontal plane, flow is in steady state, and the vertical plane flow is in a pseudo-steady state. Joshi's equation, assuming Darcy flow and no skin effects, was redefined by Economides et al. (1994) and presented as:

$$q = \frac{k_H h(p_e - p_{wf})}{141.2B\mu\left(\ln\left\{\frac{\left[a+\sqrt{a^2-\left(\frac{L}{2}\right)^2}\right]}{\frac{L}{2}}\right\}+\left(\frac{I_{ani}h}{L}\right)\ln\frac{I_{ani}h}{[r_w(I_{ani}+1]}\right)} \tag{4-18}$$

Where q is the surface volume flow rate (STB/D), h is the reservoir thickness (ft), k_h is the horizontal permeability (mD), p_e is the pressure at outer-boundary (psi), p_{wf} is the bottom hole flowing pressure (psi), B is the formation volume factor of liquid (res bbl/STB), μ is the viscosity (cp), L is the horizontal well length (ft). I_{ani} is the measurement of vertical to horizontal permeability anisotropy which is given by,

$$I_{ani} = \sqrt{\frac{k_h}{k_v}} \tag{4-19}$$

Where k_v is the vertical permeability (mD). The term 'a' (ft) is related to drainage ellipse and is given by,

$$a = \frac{L}{2}\left\{0.5 + \left[0.25 + \left(\frac{r_{eH}}{L/2}\right)^4\right]^{0.5}\right\}^{0.5} \quad for\ \frac{L}{2} < 0.9r_{eH} \tag{4-20}$$

Where r_{eH} is the distance of horizontal well from the outer boundary (ft).

4.3.2. Equation for Gas Reservoir. Gas production from a horizontal well in steady-state is given by (Economides et al., 1994):

$$q_g = \frac{k_h h\left(p_e^2 - p_{wf}^2\right)}{1424\mu ZT\left(\ln\left\{\frac{\left[a+\sqrt{a^2-\left(\frac{L}{2}\right)^2}\right]}{\frac{L}{2}}\right\}+\left(\frac{I_{ani}h}{L}\right)\left\{\ln\frac{I_{ani}h}{[r_w(I_{ani}+1)]}+Dq\right\}\right)} \tag{4-21}$$

Where q_g is the gas flow rate at the surface (MSCF/D), μ is the gas viscosity (cp) measured between wellbore and reservoir outer boundary, Z is the Z-factor between

wellbore and reservoir outer boundary, T is the reservoir temperature (°F), and D is a Non-Darcy coefficient, typically used to characterize turbulent flow in high rate gas wells. An empirical relationship for D is proposed by Economides et al., (1994) which is shown below.

$$D = \frac{6*10^{-5}*\gamma*k_s^{-0.1}*h}{\mu*r_w*h_{perf}^2} \quad (4\text{-}22)$$

Where γ is the gas gravity, k_s is the near- wellbore permeability (mD), h and h_{perf} the net and perforated thickness (both in ft.), and μ is the gas viscosity (cp).
Correlations to calculate gas properties to find μ and Z-factor in the equation were described in Section 4.2.

4.4. BASIC SIMULATION MODEL

The basic model is same as the one used by Theppornprapakorn et al., (2014). A 6-inch diameter horizontal open hole well of length 300 ft was considered. The concept of planar symmetry was applied to the model to reduce the computational time and to carry out more detailed simulations with more mesh cells grouped in areas of interest. The distance from the reservoir's outer boundary to the horizontal well was 300 ft. and all the outer boundaries are applied with reservoir pressure (p_e). A constant well pressure (p_{wf}) is assumed acting normally along the well boundary. Figure 4.2 shows the basic well model developed using FLUENT.

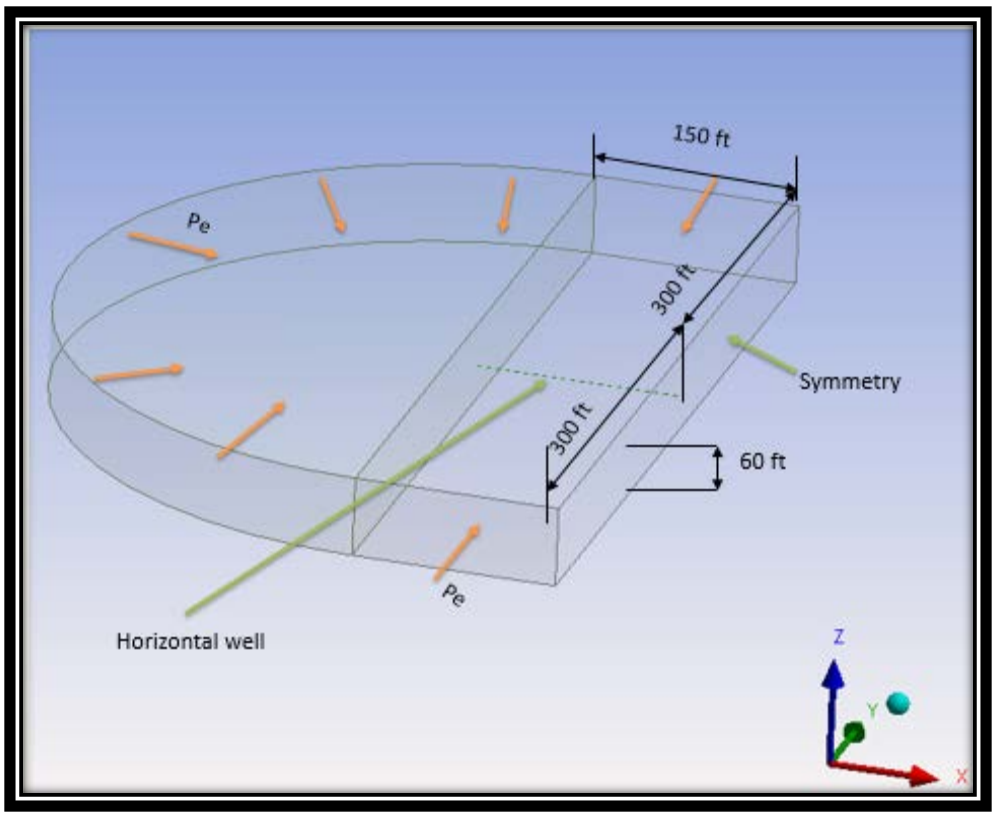

Figure 4.2. Horizontal open hole well model

4.5. MODEL VALIDATION

4.5.1. Incompressible Fluid Model. The horizontal well equation for incompressible fluids (Eq- 4-18) was used in this case. If the FLUENT simulation results matched the horizontal equation values, then the model was deemed valid. The validation process for a 10 mD reservoir using water is shown in this section. The density of water used was 998.3 kg/m^3 and the viscosity was 1.003 cp, and these values are assumed to be pressure-independent. Simulations were carried out with different well pressure cases such as 200, 500, 800, 1000, 1200, 1600, 2000, 2200 and 2500 psi. Following are the steps involved in FLUENT:

- The meshing operation is performed on the base model. The mesh qualities are checked, and if they are not in the acceptable quality range (Figure 3.5), the model has to be re-meshed.

- The acceptable mesh is opened in FLUENT. In the FLUENT launcher settings, double precision with parallel processing is selected as the processing option. As the number of processes increase, the time to calculate solution decreases. Figure 4.3 shows the FLUENT launcher settings used in this case.

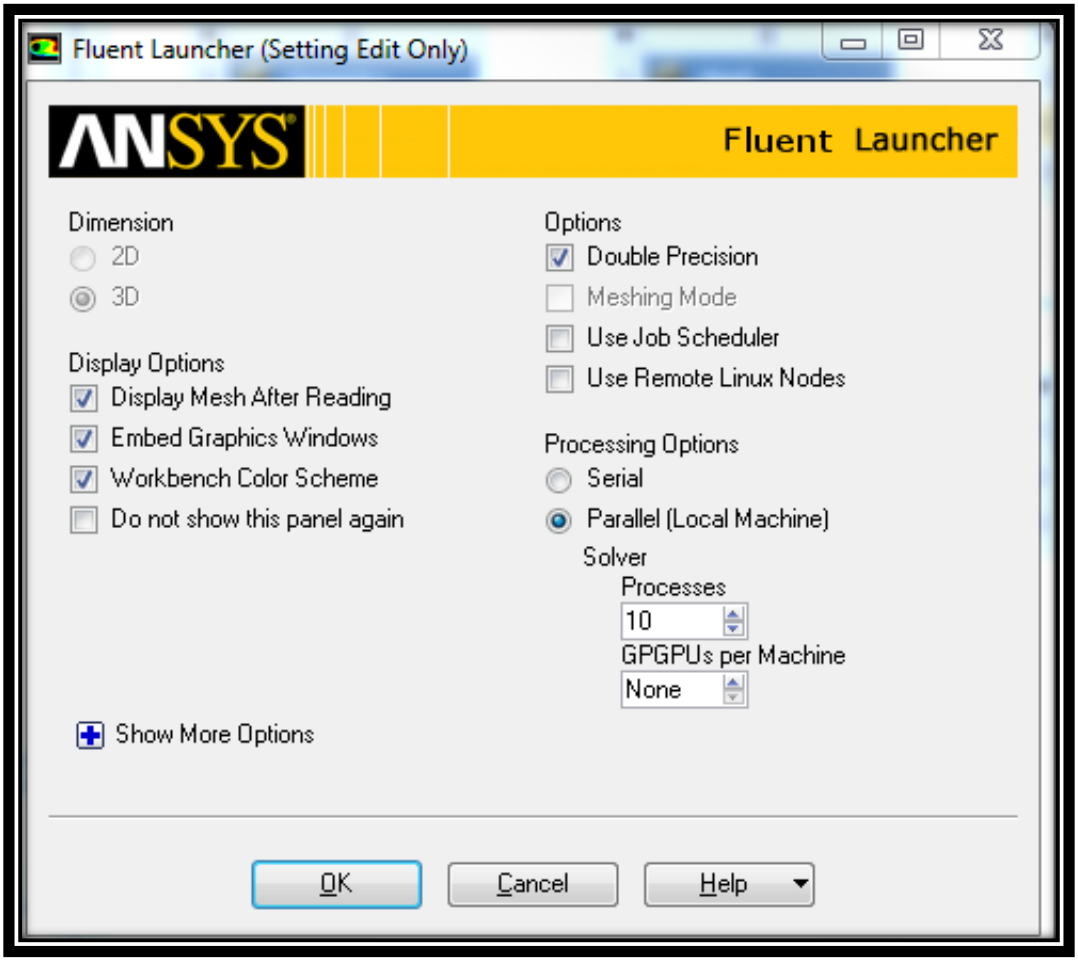

Figure 4.3. FLUENT launcher settings

- A pressure-based, absolute velocity formulation and a steady-state solver are selected for the simulation under the General tab. Gravitational force is not considered.

- Properties of the model are entered under the models tab. The energy equation is turned off since there is no heat transfer involved and the fluid flow is assumed to be laminar.
- In the cell zone conditions tab, two domains can be seen, and both the domains have porous media feature enabled. The porous zone box is checked for each domain, and the permeability of reservoir (k_h = 10 mD and k_v = 1 mD) is entered into FLUENT in the viscous resistance box. The equation for viscous resistance is shown in Equation (3.5). Figure 4.4 shows the cell zone conditions panel where viscous resistance values have to be entered.

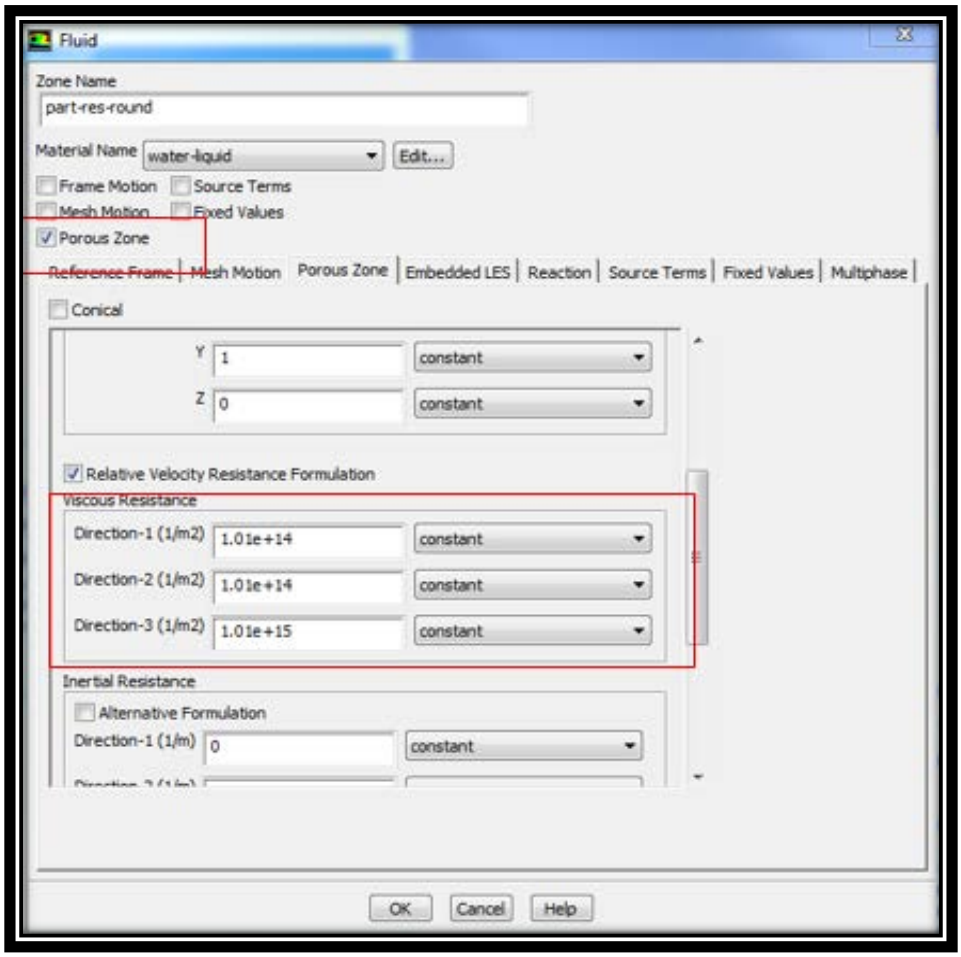

Figure 4.4. Cell zone conditions panel

In the Figure 4.4, Direction-1 and Direction-2 values are obtained from horizontal permeability value (k_h = 10 mD) and Direction-3 value is the vertical permeability value (k_v = 1 mD).

- The boundary conditions are entered next in the boundary conditions panel. Inlet pressure is same as reservoir pressure (p_e = 2800 psi). The pressure at the outlet is the well pressure (p_{wf}) and in this case, it is 1000 psi. Figure 4.5 shows the pressure-outlet zone in the boundary conditions panel. Since there is no heat transfer and a single-phase flow is assumed (completely water), no values are entered in other tabs.

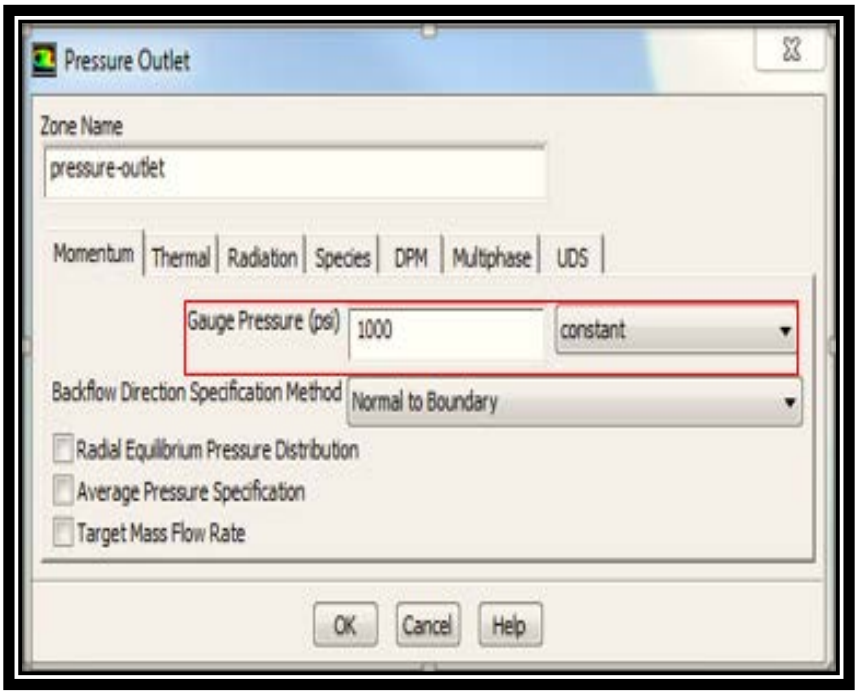

Figure 4.5. Boundary condition panel

- In solution methods, SIMPLE pressure-velocity coupling scheme is used. Least squares based, presto and second order upwind methods are employed in the Gradient, Pressure and Momentum tabs respectively and default values are used for the solution controls.

- The mass conservation between inlets and outlets and the mass flow rate at outlets are monitored by creating surface monitors, and the values are shown as plots.
- The solution is initialized using Hybrid initialization, and the simulation is started by putting the number of iterations. While using Standard initialization, the solution may converge faster.
- Once the solution is converged according to convergence criteria mentioned in Section 3.3.2, the iteration is stopped.
- The volume flow results obtained from FLUENT using different well pressures are compared with the volume flow rates obtained from Equation (4-18) in the unit of reservoir barrels per day (RVB/D). Liquid formation volume factor (B) is not considered in the equation to obtain the results in the unit of RVB/D. The results from simulation and equation are compared in the form of Inflow Performance Relationship (IPR) plot.

4.5.1.1. Inflow Performance Relationship (IPR). The IPR for a well is the relationship between the well flow rate (q) and flowing well pressure (p_{wf}). It is a mathematical tool used in production engineering. The shape of the curve is determined by reservoir fluid composition and also the behavior of the fluid phases.

4.5.1.2. Model result. The IPR comparison between simulation result and the horizontal well equation are almost identical. In Figure 4.6, shows simulation results of the model with the horizontal permeability (k_h) of 10 mD compared to results from the horizontal well equation, both in the form of IPR curve.

The results from FLUENT model and equation for different well pressures are shown in Table 4.3. The errors between FLUENT and equation results are very small and the model was deemed valid for incompressible fluid flow.

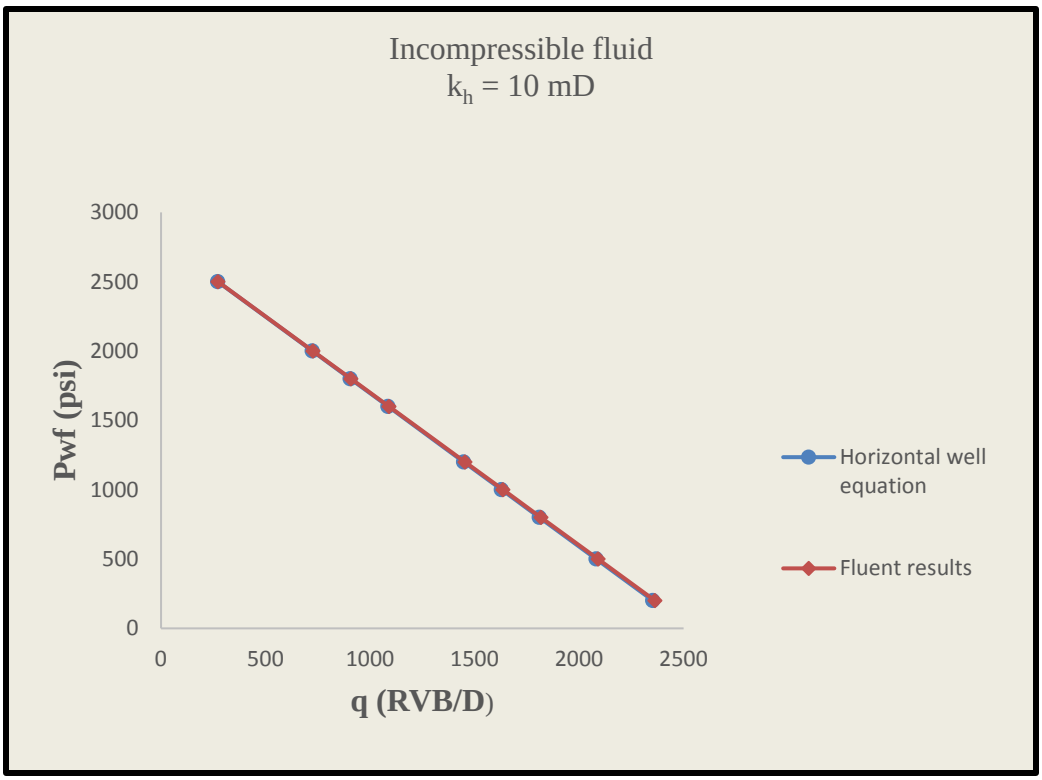

Figure 4.6. IPR comparison between results from FLUENT model and horizontal well equation

Table 4.3. Errors from the incompressible fluid model.

P_{wf} (psi)	**FLUENT result (RVB/D)**	**Equation result (RVB/D)**	**Error % from equation**
200	2363.067	2353.296	0.413
500	2091.111	2081.76	0.447
800	1817.801	1810.228	0.417
1000	1635.984	1629.205	0.414
1200	1454.197	1448.18	0.413
1600	1090.687	1086.137	0.417
1800	908.870	905.11	0.414
2000	727.114	724.09	0.416
2500	272.661	271.53	0.415

4.5.2. Non-Darcy Flow Effects. Non-Darcy flow effects are generally a concern for gas flow, especially at high flowrates through high permeability reservoirs. In order to check Non-Darcy flow effects and their importance in this work, flow simulations were performed in FLUENT using 100% air, reservoir permeability of 100 mD, gas gravity, $\gamma = 1$, perforated thickness, $h_{perf} = 60$ ft and near wellbore permeability, $k_s = 1$ mD. Results were compared with flow calculations using Eq (4-21). Eq (4-21) includes the Non-Darcy flow term given in Eq (4-22).

The results from the simulation and equation are presented in Table 4.4, and a log-log plot comparing both the results are shown in Figure 4.7. The percentage error between the results from FLUENT and the horizontal gas well equation (Eq 4-21) was about 1.38 %. Since the difference between the results was very small, Non-Darcy flow effects are believed to be considered in FLUENT. According to Economides et al (1994) the turbulence effect in unstimulated horizontal wells (Eq 4-21) usually can be neglected since they are multiplied by the scaled aspect ratio $I_{ani}h/l$. This typically gives a number as between 10^{-5} and 10^{-7} which is very small.

Table 4.4. Simulation results with percentage error.

P_{wf} (psi)	**P_e^2-P_{wf}^2 (psi^2) P_e = 2800 psi**	**FLUENT result (MSCF/D)**	**Equation result (MSCF/D)**	**Error % in result**
200	7800000	5712.60	5632.60	1.40
500	7590000	5053.36	4983.40	1.38
1.38	7200000	4394.48	4333.50	1.38
1000	6840000	3995.05	3900.35	1.38
1200	6400000	3515.62	3467.12	1.37
1600	5280000	2636.76	2600.26	1.38
1800	4600000	2197.15	2166.65	1.38
2000	3840000	1757.72	1733.42	1.38
2200	3000000	1318.29	1299.99	1.38
2500	1590000	659.16	650.01	1.38

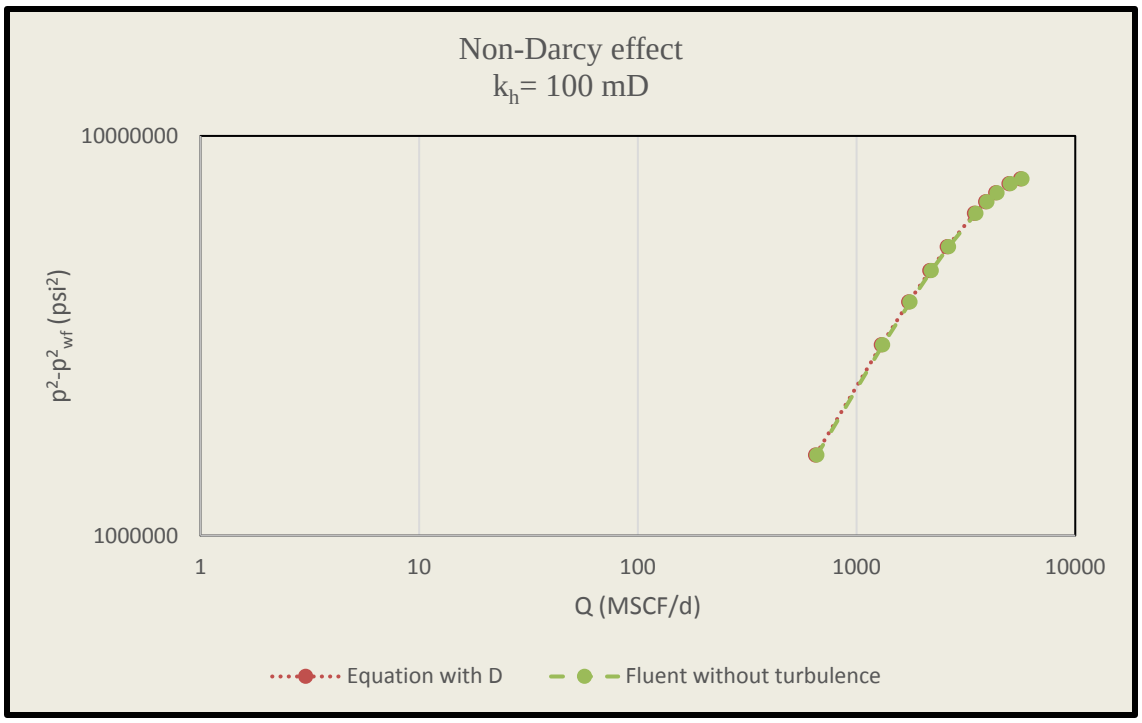

Figure 4.7. Comparison of results from FLUENT and Equation including Non-Darcy factor.

4.5.3. Compressible Fluid Model. In this section, the compressible fluid model was validated using the horizontal well Equation (4-21) without the Dq term. The FLUENT model used is the same as the one used in Section 4.5.1 and was validated using 100% air. The gas properties to be entered into FLUENT are calculated using the equations stated in Section 4.2. Reservoir permeability (k_h) of 100 mD is considered here to validate the model. If the FLUENT simulation results matched with the horizontal equation values, then the model was deemed valid. Simulations were carried out with different well pressure cases such as 200, 500, 800, 1000, 1200, 1600, 2000, 2200 and 2500 psi. Following are the steps involved in FLUENT:

- The initial meshing process and approach remains the same as in the incompressible fluid model. The solver selected is same as the incompressible model.
- The energy equation is turned ON in the Models panel and laminar flow is assumed.

- Peng-Robinson density model is defined in the materials panel to calculate the density of air in FLUENT for each well pressure cases. Figure 4.8 shows the activation of Peng-Robinson equation to calculate density.

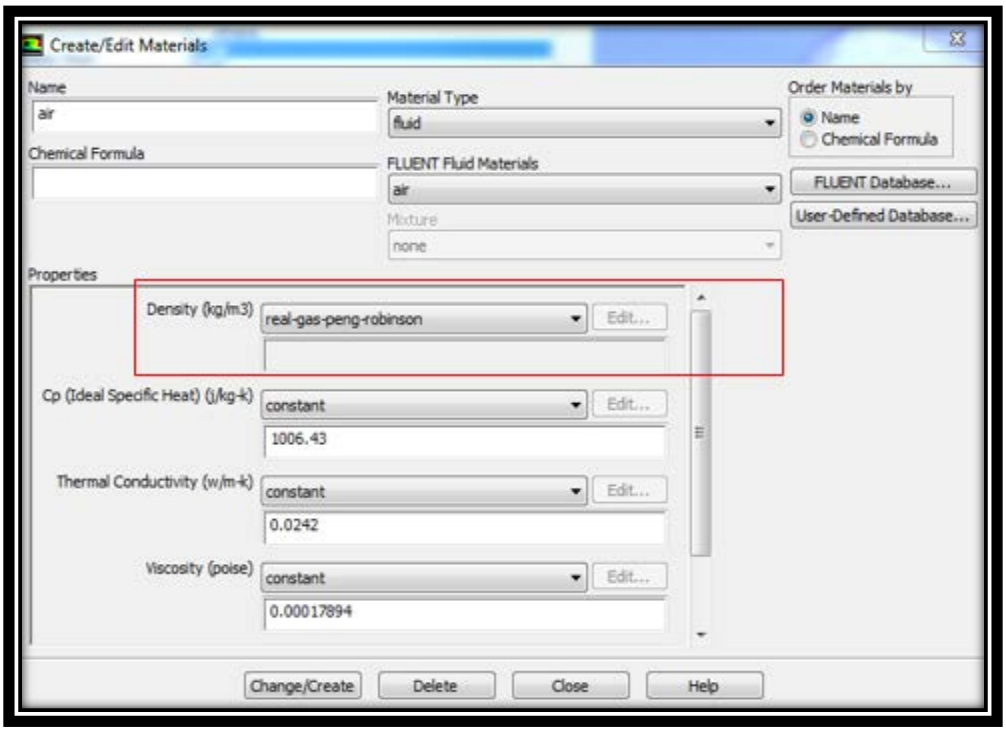

Figure 4.8. Density calculation setup

- Viscosity of air is assumed constant for each well pressure case. Viscosity is calculated using equations described in Section 4.2.9 for each well pressure case and is entered into FLUENT. The same value is used in the horizontal well equation. The viscosity calculated is the arithmetic mean of viscosity value at the well boundary and outer boundary.
- Permeability values are entered in FLUENT in the same way as incompressible fluids, in the cell zone conditions panel. In fixed values tab, the temperature value is defined to maintain the isothermal condition. Figure 4.9 shows the fixed values setup.

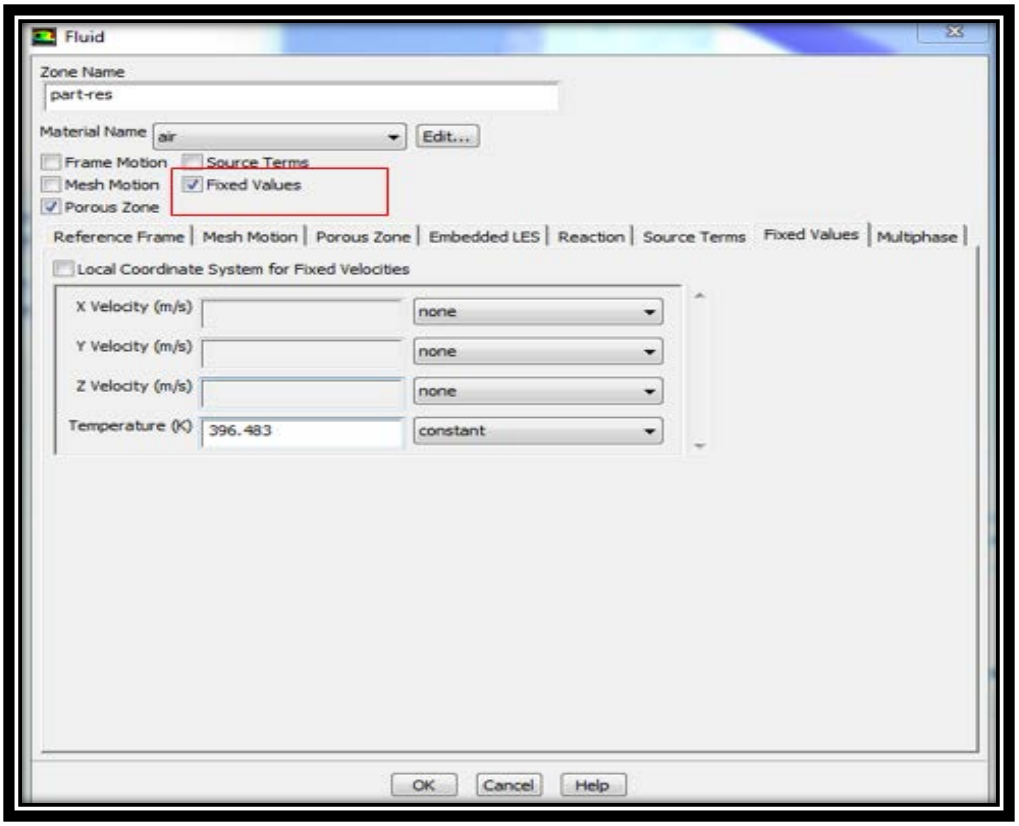

Figure 4.9. Fixed values setup

- Inlet and outlet pressures are entered in the boundary conditions panel in the same way as incompressible fluids. Simulation is carried out with default values in the solution methods and solution controls panel and the process is same as incompressible fluids. The mass flow rate values obtained from FLUENT for different well pressures are divided with the density of air (Eq.4-4) at surface condition (Pressure = 14.7 psi and temperature = 60°F) to get the volume flow rates at surface (MSCF/D).

The results from simulation and the horizontal equation are compared in the form of an IPR curve. The curve pattern and the values are almost identical with a small error at higher rates. Figure 4.10 shows the IPR comparison between simulation and equation results.

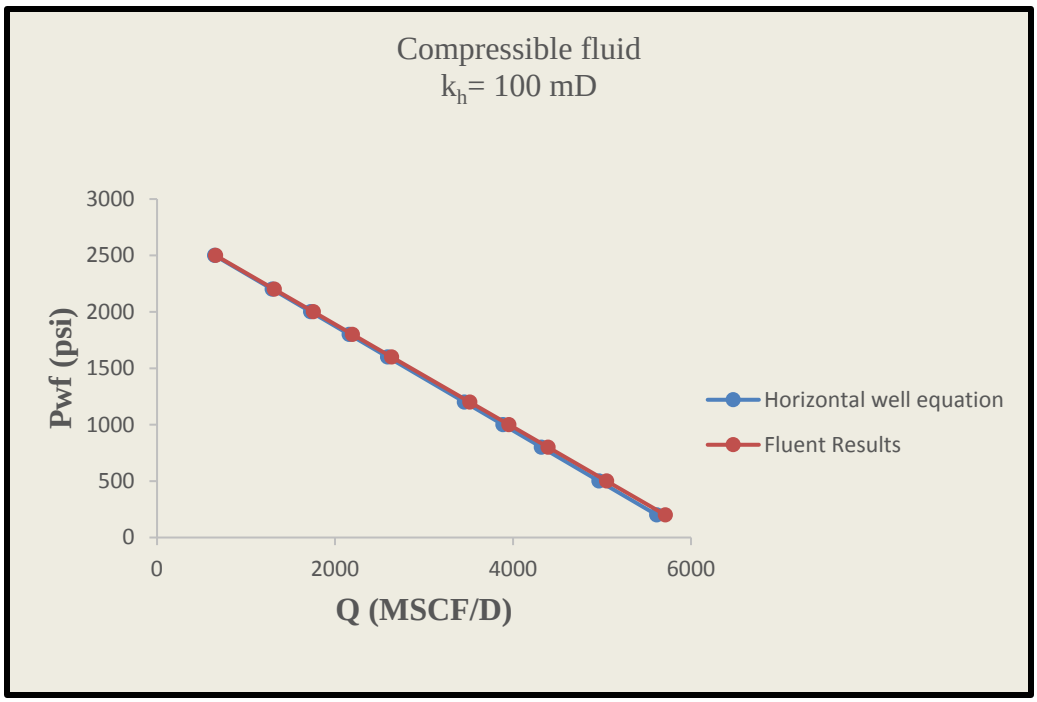

Figure 4.10. IPR comparison between results from FLUENT model and horizontal well equation

All the simulations and equation results using different well pressures are presented in Table 4.5. The compressible fluid model was deemed valid since the errors were not significant (<2%). The small variation in results were attributed to the reasons mentioned below:

- FLUENT calculates Z-factor using Peng-Robinson equation of state whereas the correlation by Hall–Yarborough in Section 4.2.7 uses Starling–Carnahan equation of state. This was considered as a factor for the difference in results.
- Also, the Z-factor value used in the horizontal well equation is the arithmetic mean of Z-factor value at the reservoir boundary and wellbore, whereas FLUENT calculates Z-factor value by assigning a value to each cell.
- Mesh quality can be another reason for the slight difference in results. Even though the mesh quality was in the acceptable range, slight improvement in mesh quality can yield better results.

Table 4.5. Errors from the compressible fluid model.

P_{wf} (psi)	FLUENT result (MSCF/D)	Equation result (MSCF/D)	Error % from equation
200	5712.60	5615.67	1.69
500	5053.36	4967.71	1.69
800	4394.48	4319.75	1.70
1000	3995.05	3887.77	1.70
1200	3515.62	3455.80	1.70
1600	2636.76	2591.85	1.70
1800	2197.15	2159.87	1.69
2000	1757.72	1727.90	1.69
2200	1318.29	1295.92	1.69
2500	659.16	647.96	1.69

4.6. FRACTURE MODELS

Transverse and longitudinal fractures are integrated into the horizontal well model developed in Section 4.4. The fractured horizontal well models were developed to analyze the completion effects and to compare the production between transverse and longitudinal fractures:

- Horizontal well with one transverse fracture.
- Horizontal well with two transverse fractures.
- Horizontal well with one longitudinal fracture.

4.6.1. Single Transverse Fracture Model. In this model, a single transverse fracture of constant width (w) is created at the center of the 300 ft. horizontal well bore. A symmetry plane is assumed at the middle of the fracture to simplify the model and reduce computation time. Thus, the fracture width (w) is modeled only in half. The height of the fracture (h_f) is assumed to be equal to the reservoir thickness (60 ft.). Figure 4.11 shows the schematic of single transverse fracture used in this study.

The created fracture is assumed to be isotropic and porous. The porous media feature is enabled in FLUENT. Fracture permeability is input into FLUENT as described in Section 3.3.2 and is considered same in all directions. The natural gas flow between

fracture and the horizontal well bore depends on the type of completion used and will be discussed in Section 4.7. Figure 4.12 shows the single transverse fracture model created in FLUENT DesignModeler.

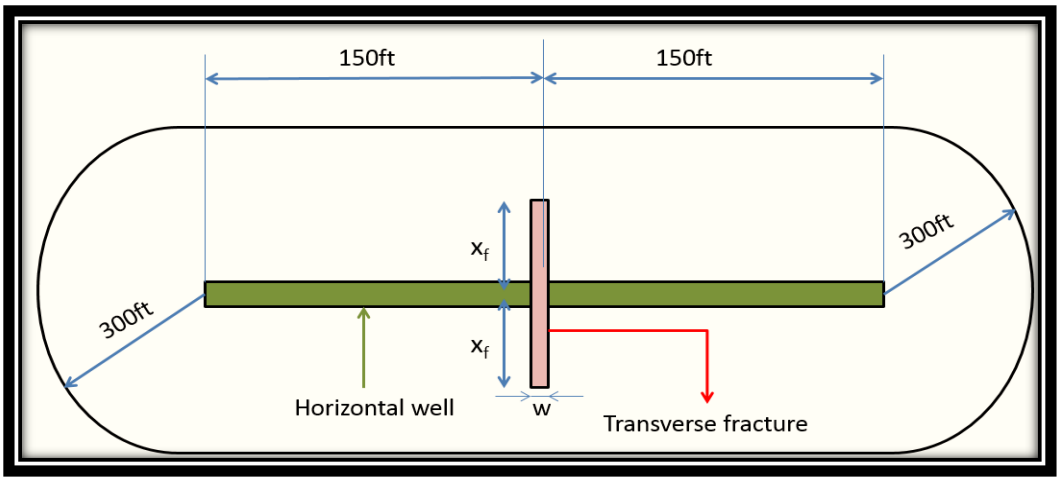

Figure 4.11. Single transverse fracture schematic

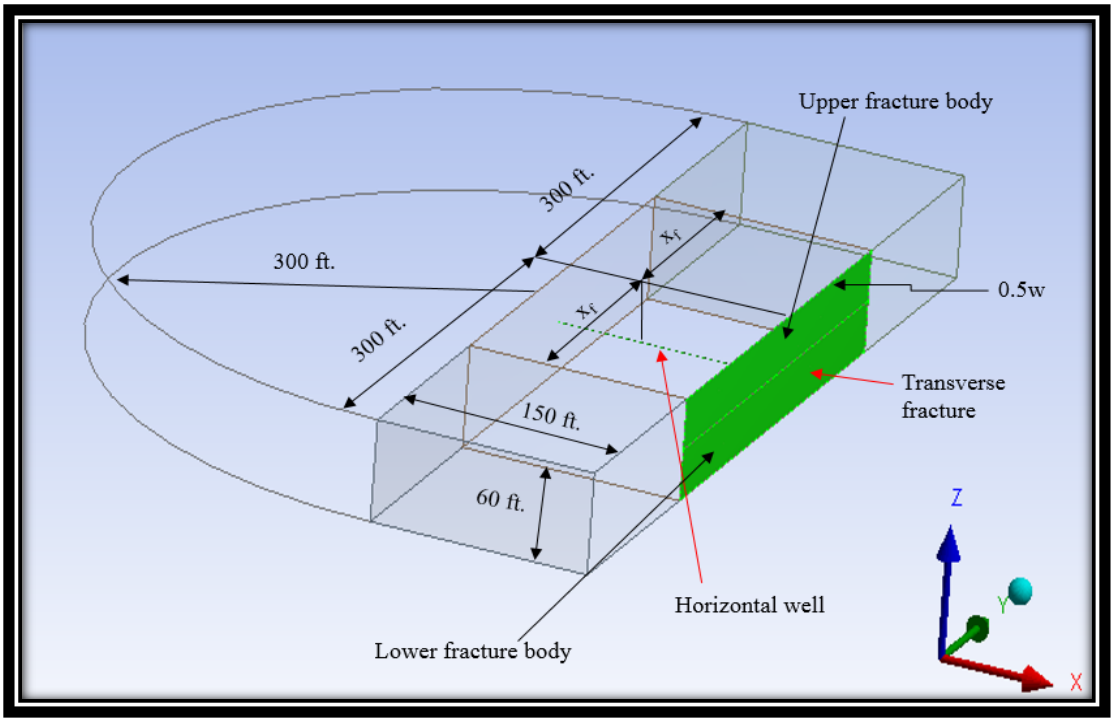

Figure 4.12. Single transverse fracture geometry in FLUENT

The rectangular part of the reservoir is divided into three sections to facilitate the meshing process and also to display the fracture.

4.6.2. Two Transverse Fracture Model. In this model, two transverse fractures are created. One fracture at the center of the well (150 ft.) and another fracture located 75 feet from the first fracture. A symmetry plane is assumed in both the fractures to reduce computation time, and fracture width is modeled in half. All the other parameters are the same as in the single transverse fracture. Figure 4.13 shows the two transverse fracture schematic used in this study.

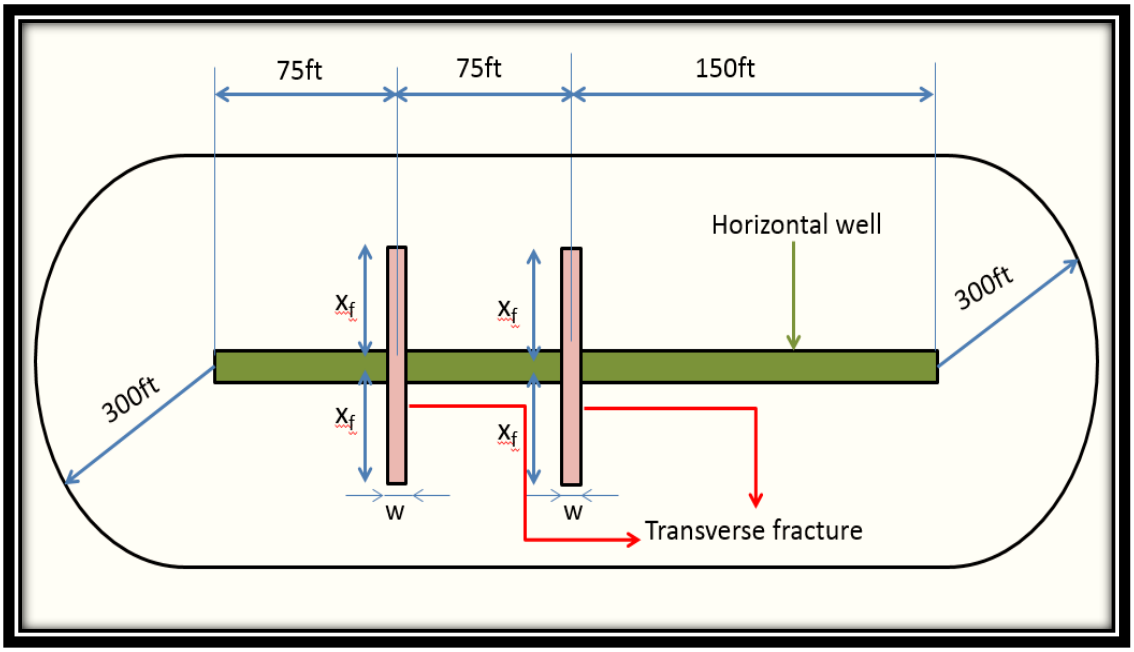

Figure 4.13. Two transverse fracture schematic

Fracture permeability used is same as in the single transverse fracture model. Figure 4.14 shows the two transverse fracture geometry created in FLUENT.

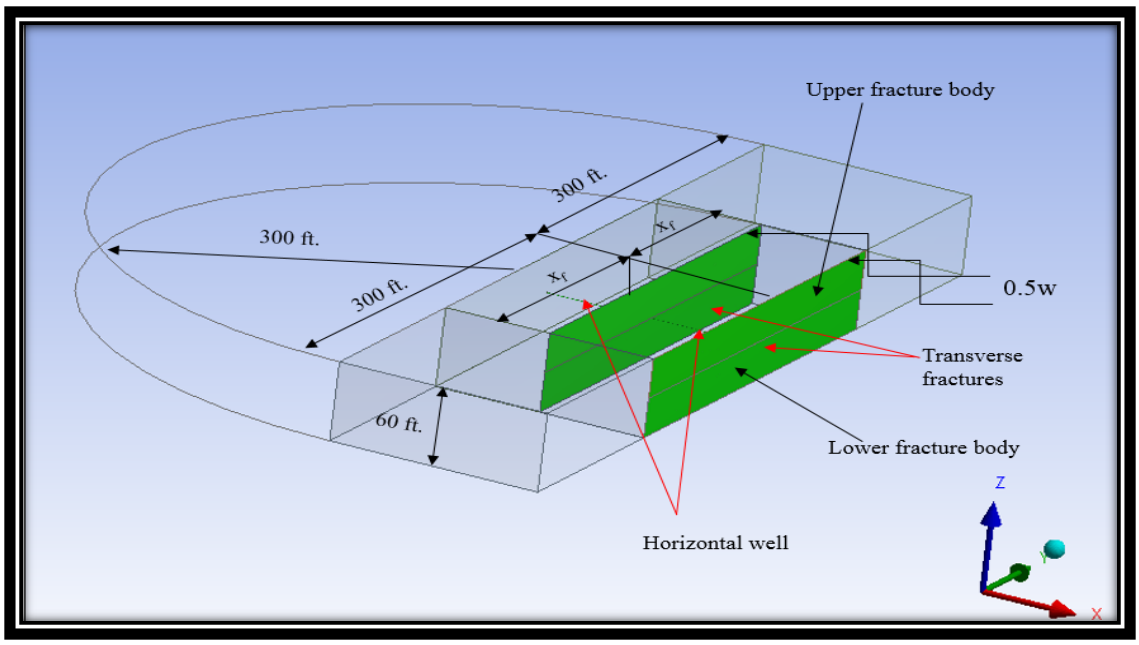

Figure 4.14. Two transverse fracture geometry in FLUENT

4.6.3. Longitudinal Fracture Model. A single longitudinal fracture model has been built in this case. The fracture was assumed to cover the entire length of the wellbore (300 ft.), and the height of the fracture (h_f) was equal to the reservoir thickness (60 ft.). A symmetry plane is assumed at the end of 300 ft. to reduce computation time. The fracture width is modeled entirely compared to transverse fractures. Fracture permeability data is same as transverse fractures, and natural gas flow from the fractures to the wellbore depend on the completion type employed.

Since the length of the horizontal well was small (300 ft.), only one longitudinal fracture could be modeled. Figure 4.15 shows the longitudinal fracture schematic used in this case and Figure 4.16 shows the longitudinal fracture model created in FLUENT. The horizontal well is perforated at the center to initiate the fracture and then the fracture, grows in both direction covering the entire length of the wellbore. The fracture initiation process is same in both OHMS and P-n-P completions.

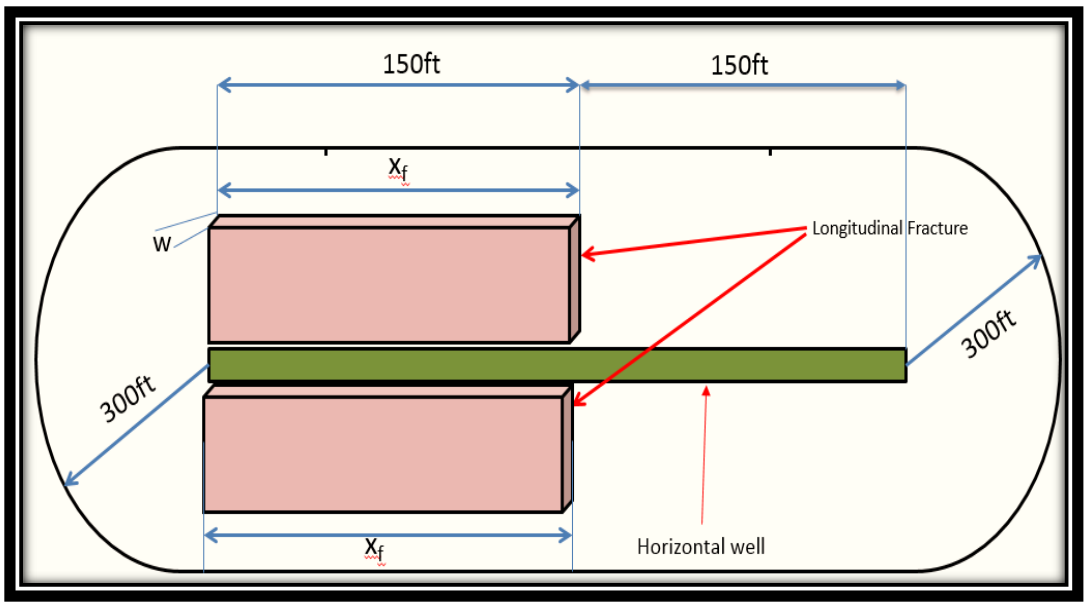

Figure 4.15. Longitudinal fracture schematic

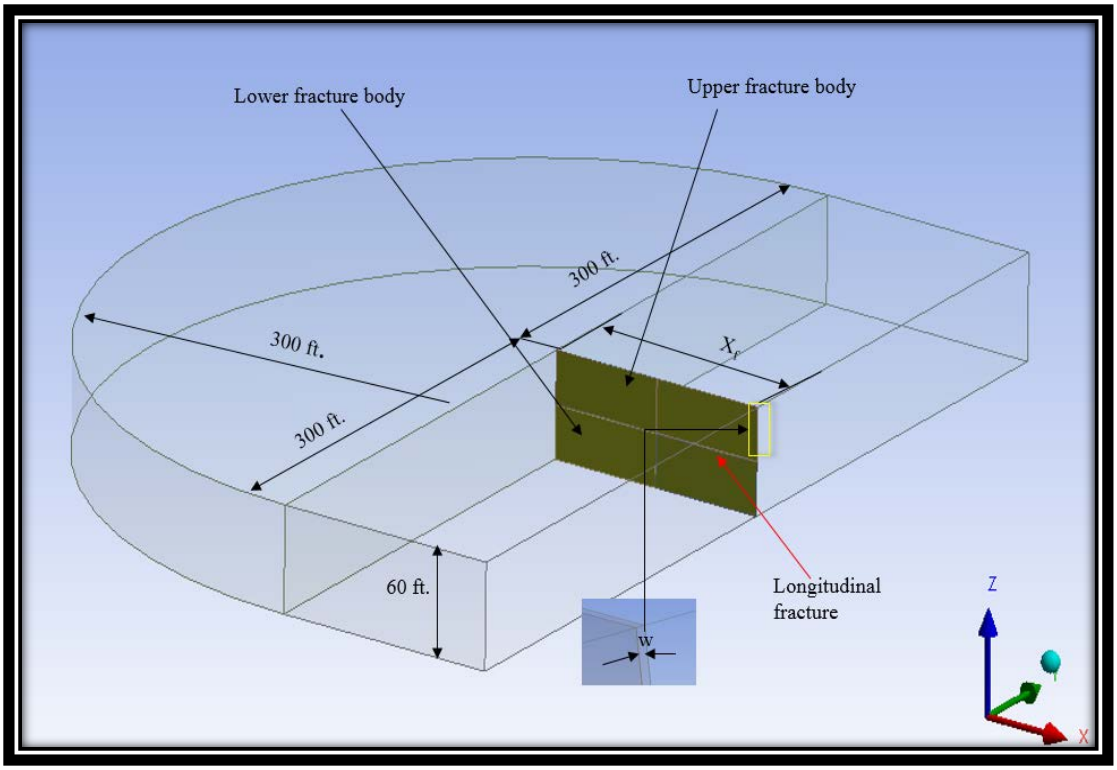

Figure 4.16. Longitudinal fracture geometry in FLUENT

4.7. COMPLETION MODELS

Open Hole Multi-stage and Plug-n-Perf are the two types of horizontal well completion systems analyzed in the study. The effect of both completion methods on natural gas production are assessed and compared.

4.7.1. Plug-and-Perf Model. In this model, natural gas flows from the fracture to the wellbore through the perforations. The perforations are assumed to be at 180° phasing and are created based on Baker Hughes FracConnect perforating system. The diameter of the perforated hole is 1 inch, and the penetration depth is assumed to be 1.5 times the diameter of the wellbore which is equal to 9 inches (Wutherich et al., 2012). Economides et al., (1994) also states that there will be an unacceptable fracture width reduction if the perforated length is more than 1.5 times the well diameter. The perforations provide the connection between upper and lower fracture body.

Since fractures are initiated through these perforations, good connectivity between fractures and perforations has to be created. The perforated zone is assumed to be a non-porous zone. In FLUENT geometry, the horizontal well is designed as a wall without any frictional losses, and the two perforation holes are considered as the reservoir outlets. Well pressure (p_{wf}) is taken as 1000 psi, and it is assumed to act in the normal direction at the end of perforation holes (outlets).

In real field cases, a cluster of perforations in different stages are made to create the fractures. Due to modeling limitations, these type of perforations is not included in this study. Figure 4.17 shows the outlets and perforations in the FLUENT geometry.

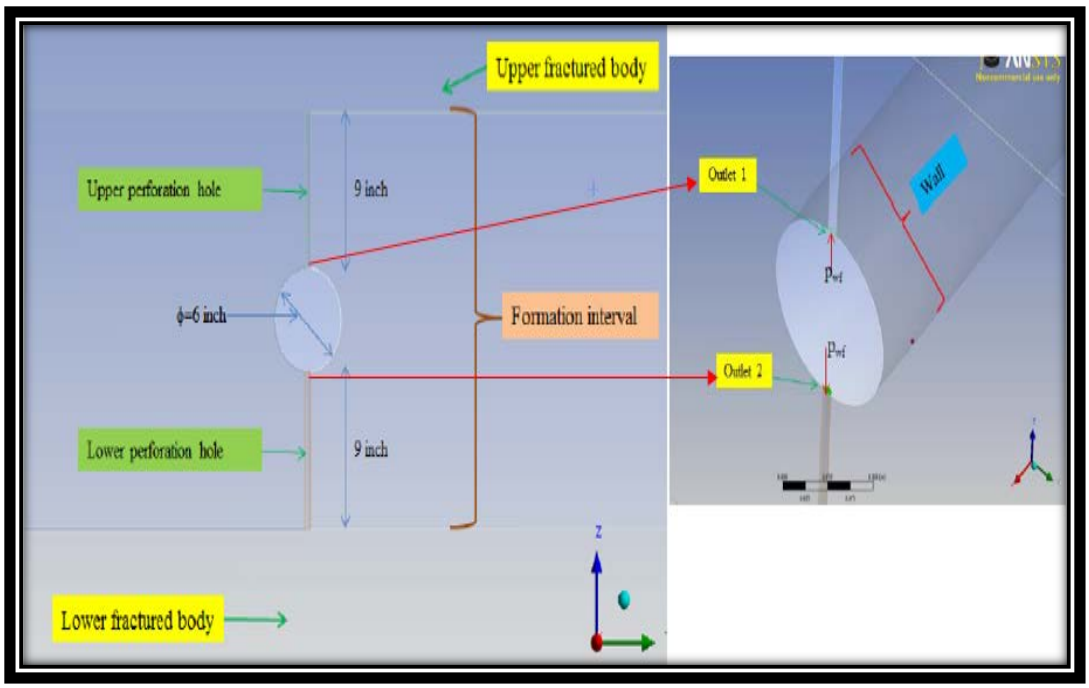

Figure 4.17. Outlets and perforations (Theppornprapakorn et al., 2014)

4.7.2. Open Hole Multi-Stage System Model. In OHMS model, the horizontal wellbore is not cased and cemented, and it acts as an open hole without any formation damage. The entire horizontal wellbore section without fracture is assumed to be open hole. The fracture is considered to intersect the open hole directly, and the full open hole section is expected to be the outlet. The natural gas from formation flows through the open hole and fracture bodies. The fracture is divided into two parts: Upper fracture body and Lower fracture body. Well pressure of 1000 psi (p_{wf}) is assumed to act in the normal direction at the outlets.

The OHMS packer profile and components are not considered in order to reduce the complexity of the model. Figure 4.18 shows the outlets in OHMS model.

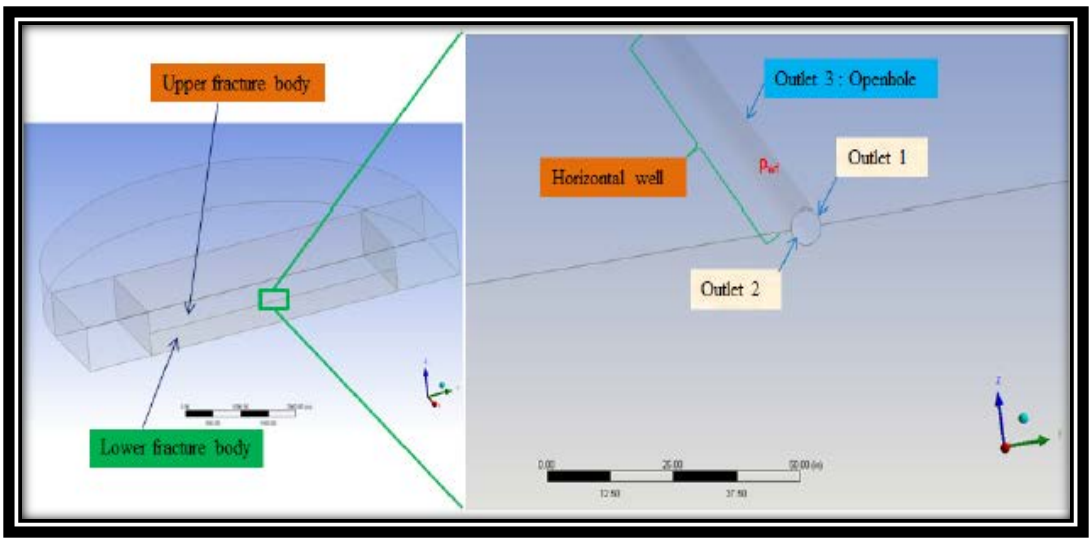

Figure 4.18. Outlets in OHMS model (Thepornprapakorn et al., 2014)

4.8. BASE CASE SIMULATION

The base case model uses the reservoir data given in Table 4.1. Simulations for all the three fracture models: Single transverse fracture, two transverse fracture, and longitudinal fracture are performed. Both P-n-P and OHMS completions are included. A 20/40 Ottawa sand is assumed to be used for fracturing. Based on this assumption, a constant fracture width (w) of 0.1 inches is utilized in the base model, as the minimum fracture width should be three times the size of proppant. The mean particle diameter of Ottawa sand was approximately equal to 0.03 inches (Kullman, 2011). The fracture half-length (x_f) is taken as 150 ft. The vertical to horizontal permeability ratio (k_v/k_h) of the reservoir is taken as 0.1. A base case simulation is performed to compare the performance of transverse and longitudinally fractured wells in gas reservoirs. Simulations are carried out for all the three reservoir permeability values. The results are presented as plots in which folds of increase (FOI) of both transverse and longitudinally fractured wells are compared with unstimulated horizontal wells for different fracture conductivity values. The bottom hole flowing pressure or the well pressure (p_{wf}) is taken as a constant 1000 psi for all the cases. The base case results are shown as plots with fracture conductivity (C_f) on the X-axis and the folds of increase (FOI) on the Y-axis. Fracture conductivity (C_f) values for 20/40 Ottawa sand at 250°F are taken from CARBO

ceramic proppant data (Kullman, 2011). The fracture conductivity values used are 2000, 3700, 6000, 8900 and 10700 mD-ft. Viscous resistance values to be entered into FLUENT are calculated using the fracture permeability (k_f) values given in the proppant data chart (Kullman, 2011).

From the base case simulation results, production comparison of P-n-P and OHMS completions are made for the reservoir permeability (k_h) range used in this study.

4.9. PARAMETRIC STUDIES

Parametric studies were performed to assess the impact that changing parameters will have on the natural gas production from the three fracture models.

4.9.1. Propped Fracture Width (w). The effect of fracture width on natural gas production from transverse and longitudinal fractures using both the completions was studied. The reservoir data was same as in the base case. Fracture half-length (x_f) was taken as 150 ft. Simulations were performed by changing fracture widths to 0.2, and 0.3 inches and results were compared with the base case. “Typical average widths of a hydraulic fracture are of the order of 0.25 in. (or less)” (Economides et al., 2004). The fracture conductivity (C_f) values were same as in the base case.

4.9.2. Penetration Ratio (x_f/r_e). This study was carried out applying reservoir data used in the base case. The effect of penetration ratio on natural gas production from transverse fracture models with both completion types was analyzed by changing half-length (x_f) to 200 and 250 ft. Longitudinal fractures are not considered in this study since the longitudinal fracture in base case covers the entire length of the wellbore (150 ft.). The simulation results were compared with the base case. Constant fracture width of 0.1 inches was used in all simulations. The fracture conductivity (C_f) range is same as in the base case.

4.9.3. Vertical to Horizontal Permeability Ratio (k_v/k_h). In this case, simulations were made by changing vertical to horizontal reservoir permeability ratio to 0.5 and 1, and the results were compared with the baseline scenario. This study was done to understand the effects of vertical to horizontal reservoir permeability ratio on natural gas production from transverse and longitudinal fractured horizontal wells. Reservoir data and fracture conductivity (C_f) values used are same as in the base case.

5. SIMULATION RESULTS

5.1. BASE CASE RESULTS

The base case simulation results are shown in this section. Figure 5.1 illustrates the relationship between folds of increase (FOI) and fracture conductivity (C_f) for all the three fracture models using P-n-P completion for reservoir permeability (k_h) of 1 mD.

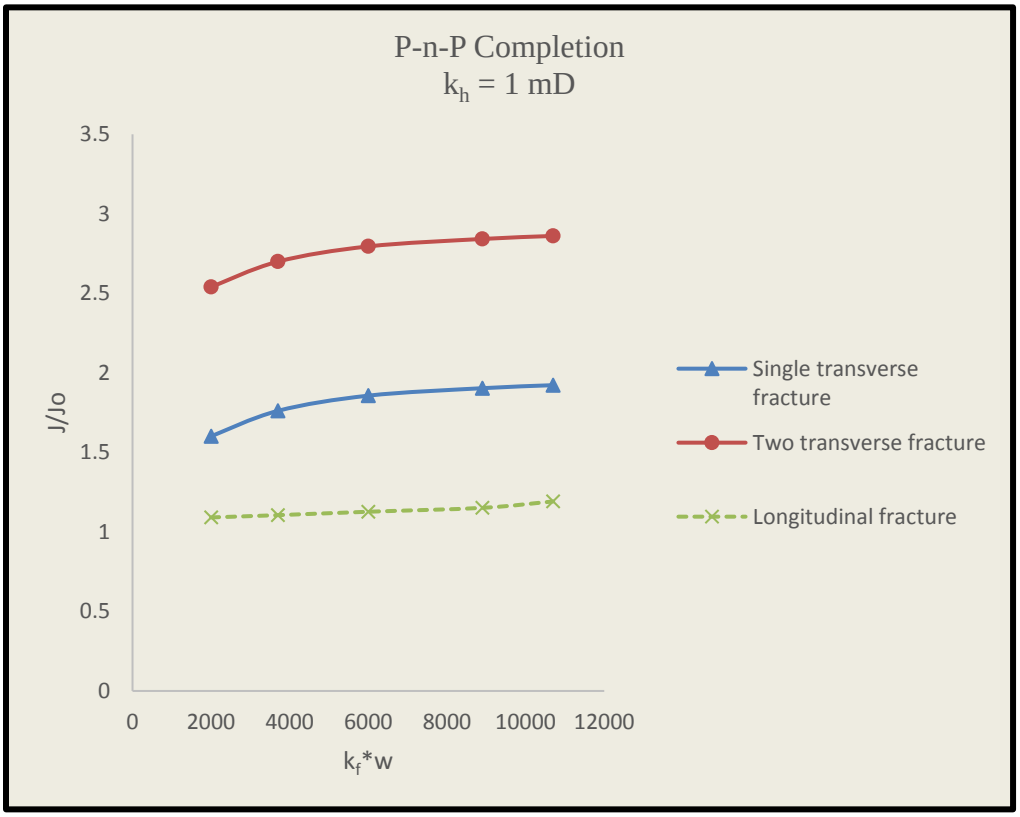

Figure 5.1. P-n-P model comparison results of 1 mD reservoir

The plot shows that two transverse fracture model outperforms both single transverse and longitudinal fracture model. All the three curves illustrate the same pattern with increasing fracture conductivity (C_f).

Figure 5.2 and 5.3 shows the results for all the three fracture models using P-n-P completion for a reservoir with permeability (k_h) of 10 mD and 100 mD respectively.

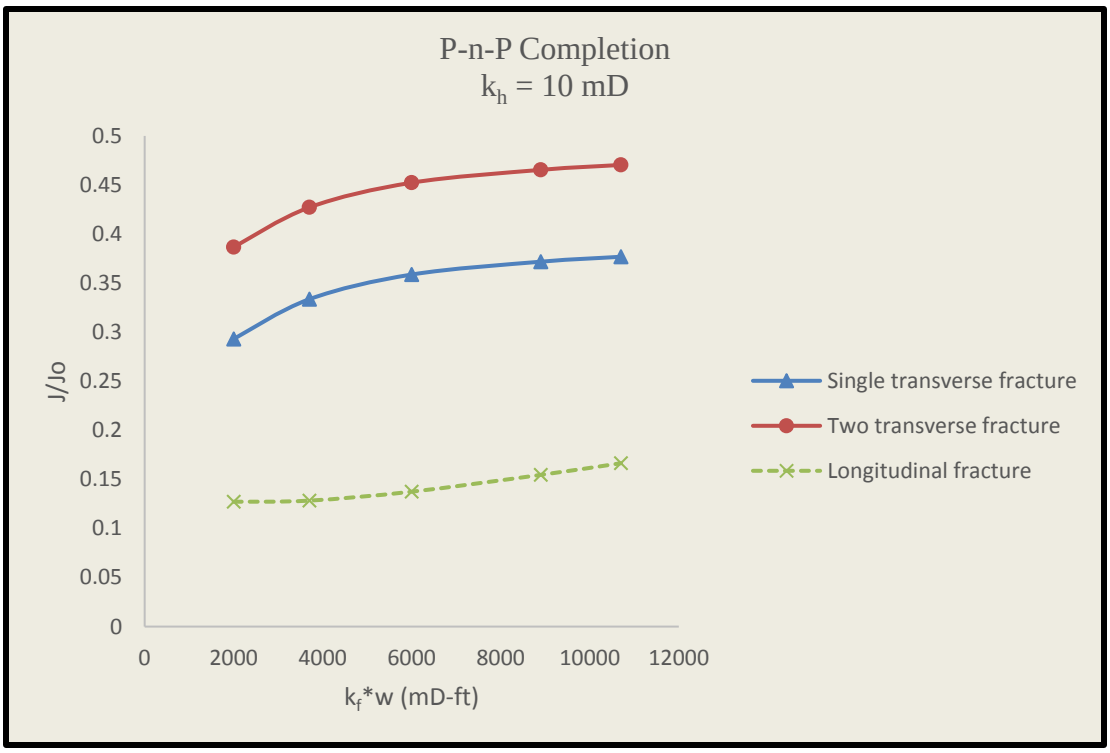

Figure 5.2. P-n-P model comparison results of 10 mD reservoir

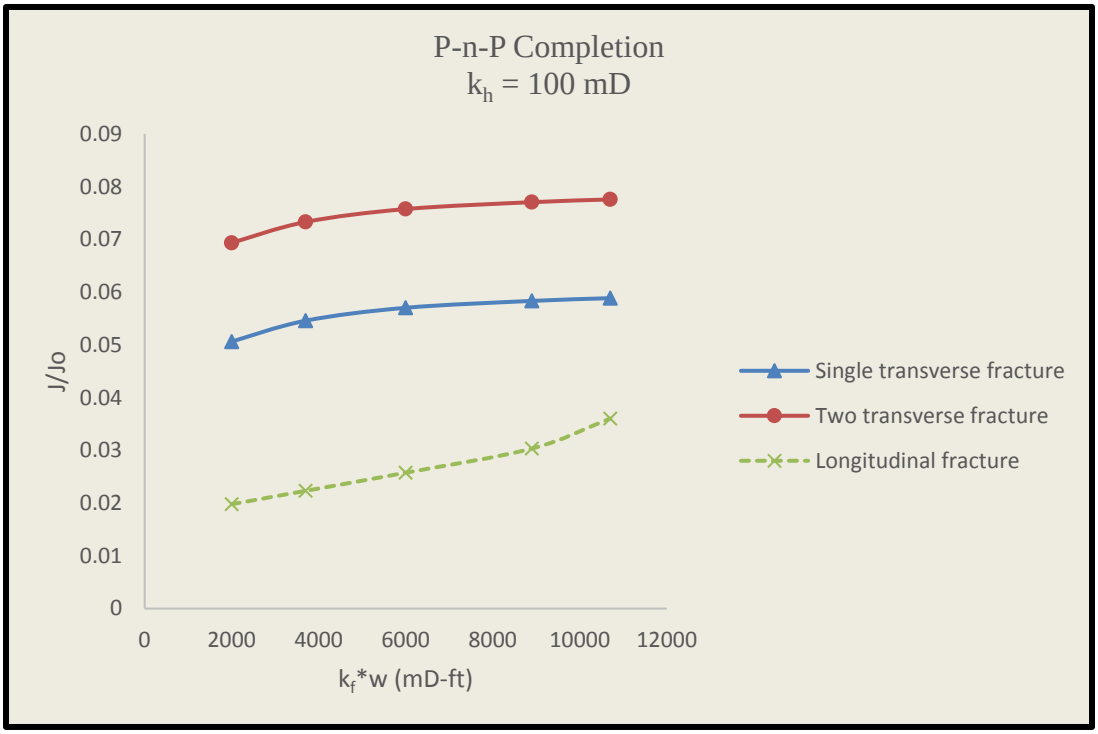

Figure 5.3. P-n-P model comparison results of 100 mD reservoir

Figures 5.2 and 5.3 follow the same trend. For increasing fracture conductivity (C_f), and two transverse fracture model has better folds of increase (FOI) compared to other two fracture models. The folds of increase (FOI) of two transverse fracture model is approximately 55% more than the longitudinal fracture type in all the three permeability (k_h) cases.

Figure 5.4, 5.5 and 5.6 shows the relationship between folds of increase (FOI) and fracture conductivity (C_f) for all the three fracture models using OHMS completion method for reservoir permeability (k_h) of 1 mD, 10 mD, and 100 mD respectively.

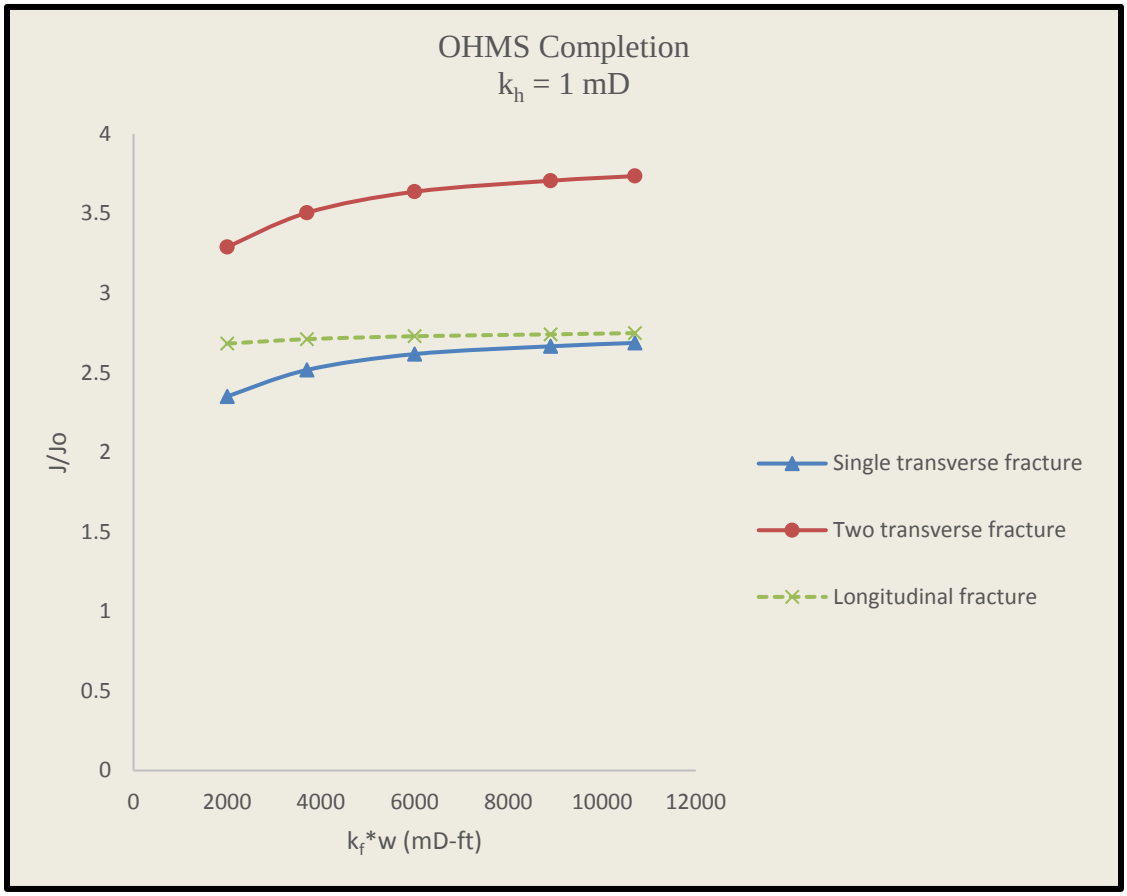

Figure 5.4. OHMS model comparison results of 1 mD reservoir

The plot shows that all the three curves follow the same pattern and longitudinal fracture performs better than a single transverse fracture.

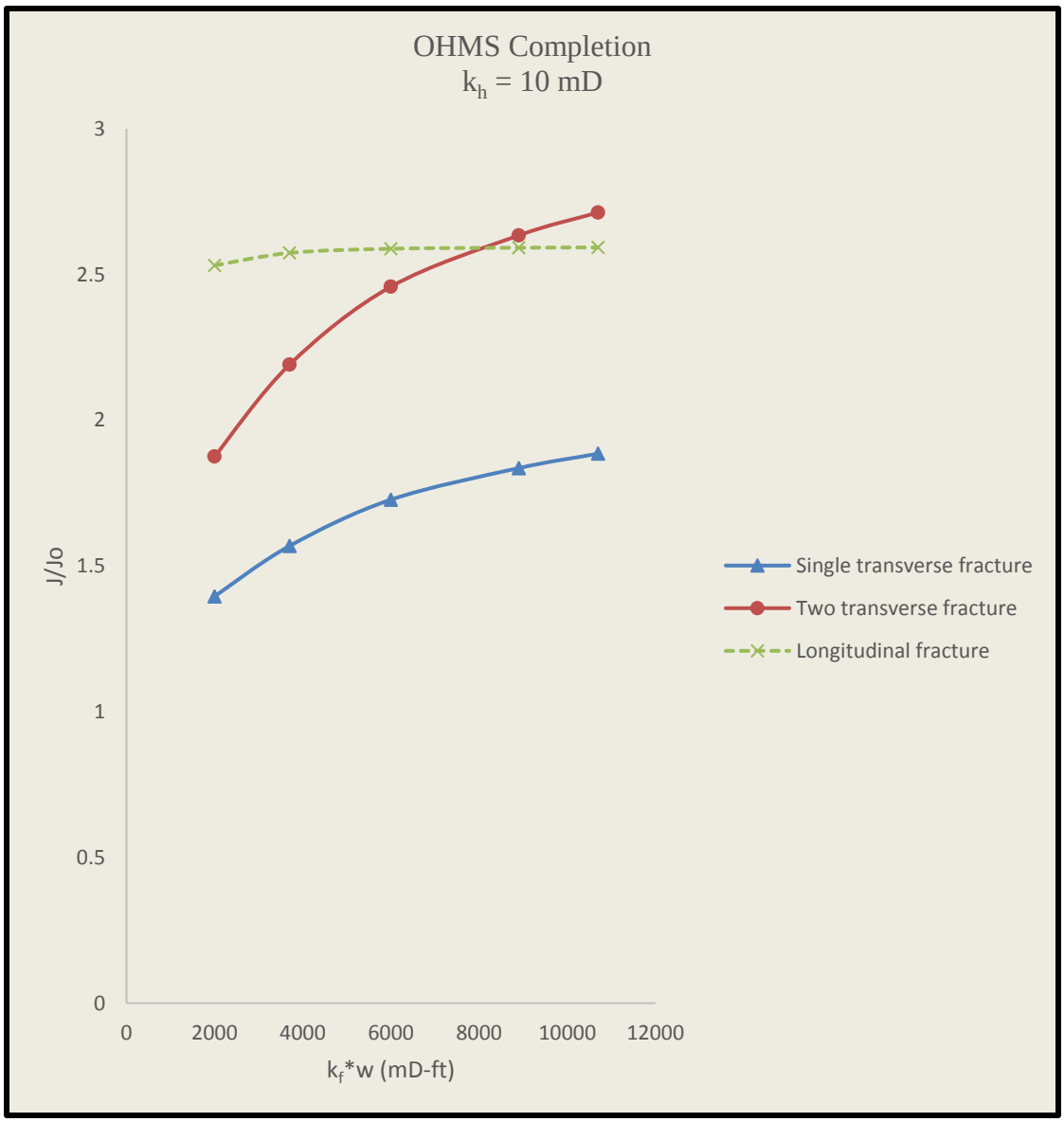

Figure 5.5. OHMS model comparison results of 10mD reservoir

In this case, longitudinal fracture outperforms transverse fracture models for low fracture conductivity (C_f) and as the fracture conductivity (C_f) increases, two transverse fracture model yield better results compared to other fracture patterns.

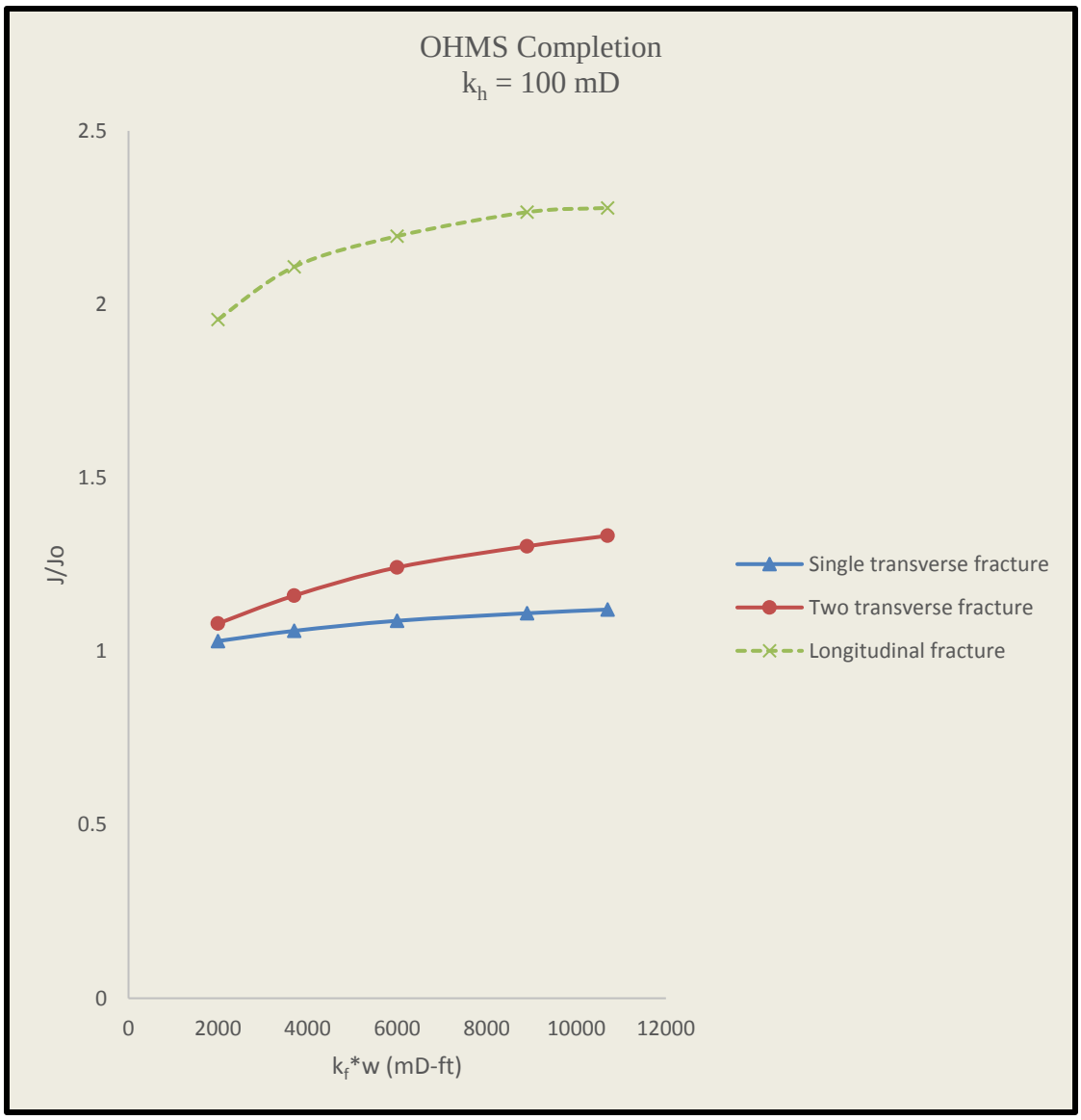

Figure 5.6. OHMS model comparison results of 100mD reservoir

From the plot, it is clear that folds of increase (FOI) of longitudinal fracture are higher than transverse fractures at 100 mD. All the three curves show a similar pattern with increasing fracture conductivity (C_f), and there is no significant increase in natural gas production for higher fracture conductivity (C_f).

Figure 5.7, 5.8 and 5.9 shows the production comparison of OHMS and P-n-P completions for the base case with reservoir permeability (k_h) of 1 mD, 10 mD, and 100 mD respectively.

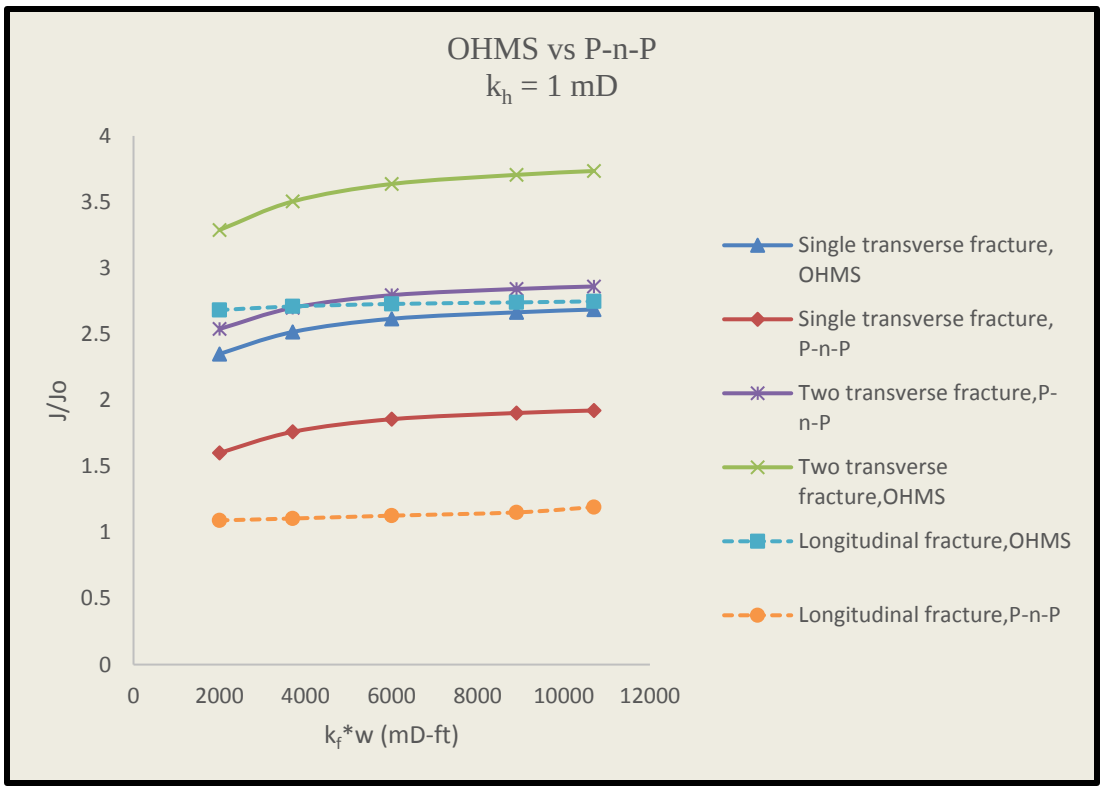

Figure 5.7. OHMS vs. P-n-P completion results of 1 mD reservoir

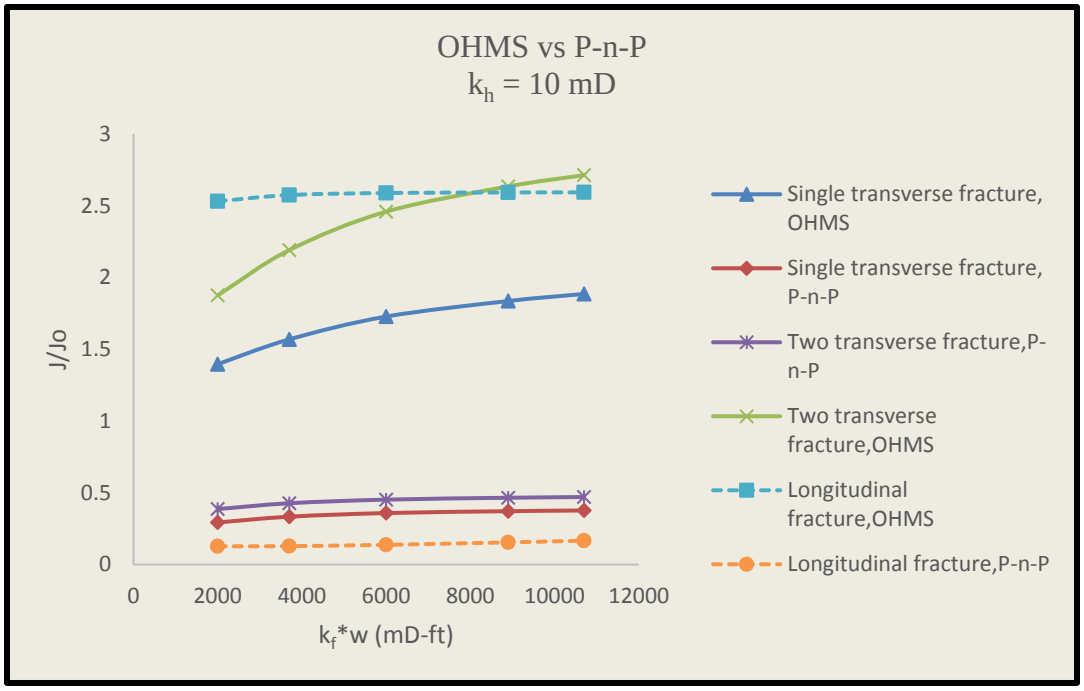

Figure 5.8. OHMS vs. P-n-P completion results of 10 mD reservoir

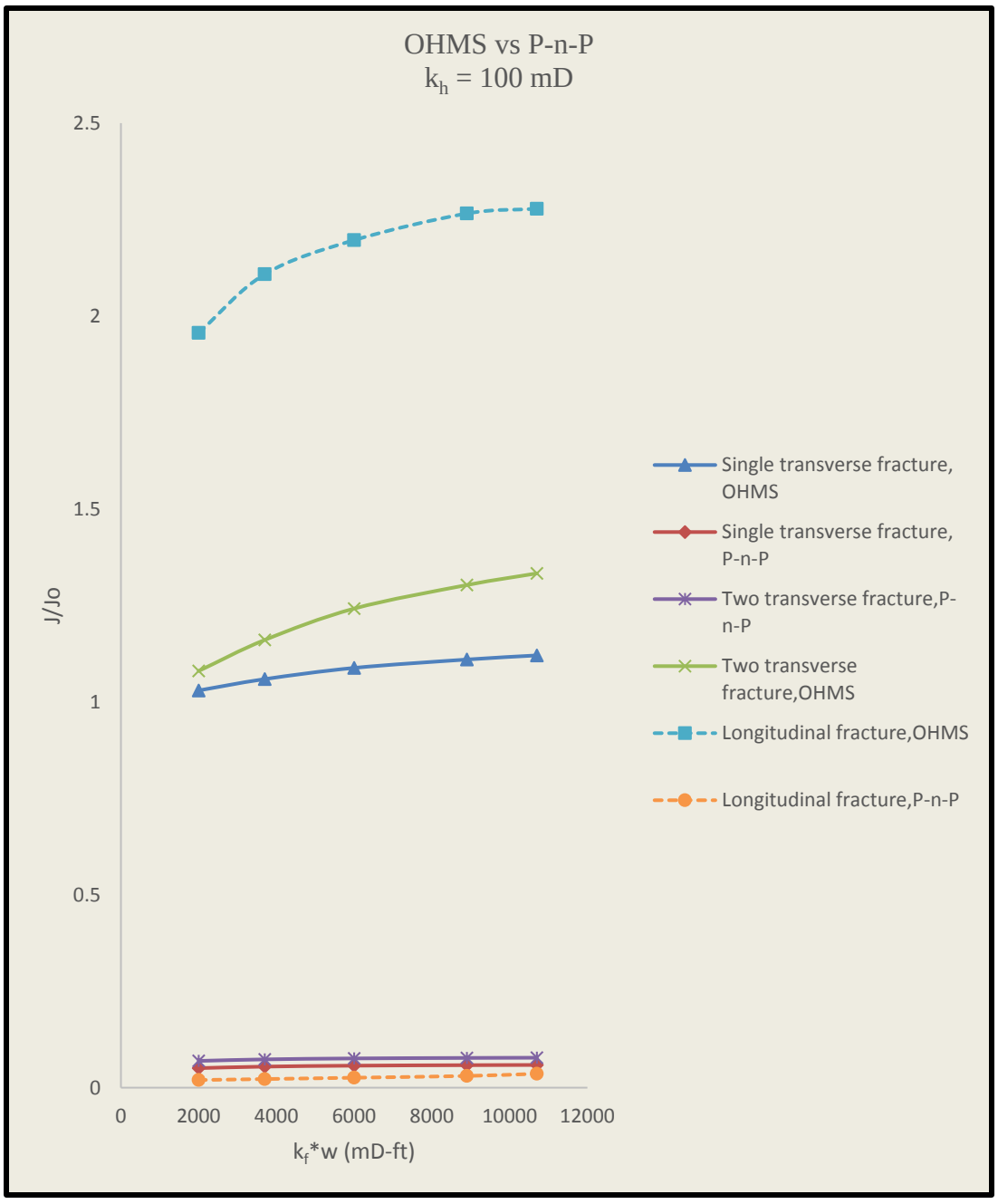

Figure 5.9. OHMS vs. P-n-P completion results of 100 mD reservoir

Figures 5.7 to 5.9 show that the performance of wells with OHMS completions is better than wells with P-n-P completions in the permeability (k_h) range used for this study. Except for the reservoir with permeability (k_h) of 1 mD, the folds of increase (FOI) of P-n-P completed wells are less than 1.

5.2. PARAMETRIC STUDY RESULTS

5.2.1. Effect of Propped Fracture Width (w). The results of simulations which analyzed the effects of changing propped fracture width (w) on natural gas production are presented in this section. The effect of increasing fracture width (w) effect is shown for both completions. The folds of increase (FOI) after changing the fracture width (w) to 0.2 and 0.3 inches are compared with base case. Figure 5.10 shows the effect of propped fracture width (w) in a single transverse fracture model with P-n-P completion for all the reservoir permeability (k_h) values.

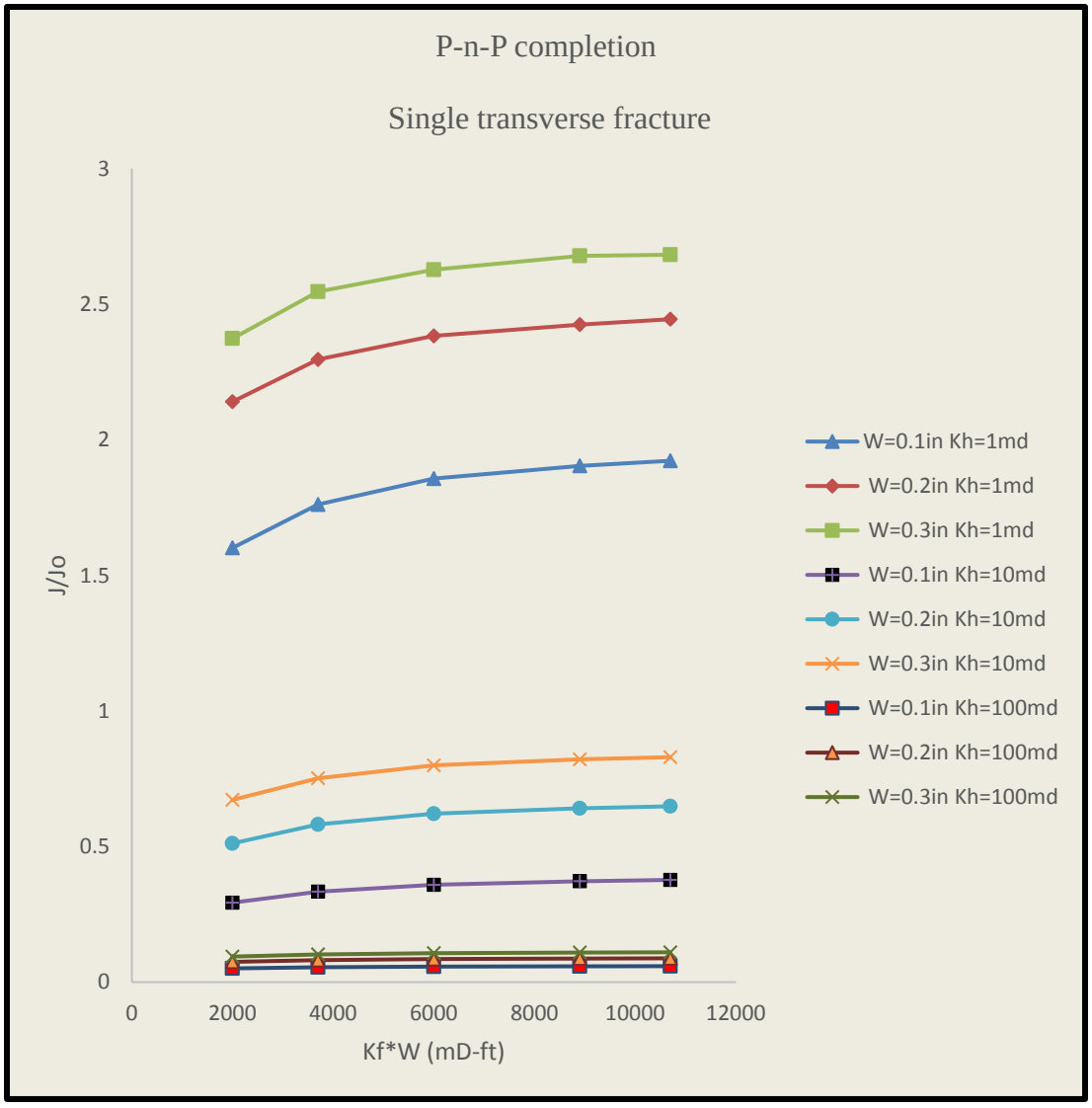

Figure 5.10. Results: fracture width study: Single transverse fracture; P-n-P

The results show that folds of increase (FOI) for fracture widths (w) 0.2 and 0.3 inches are greater than the base case. Figure 5.11 shows the two transverse fracture model with P-n-P completion.

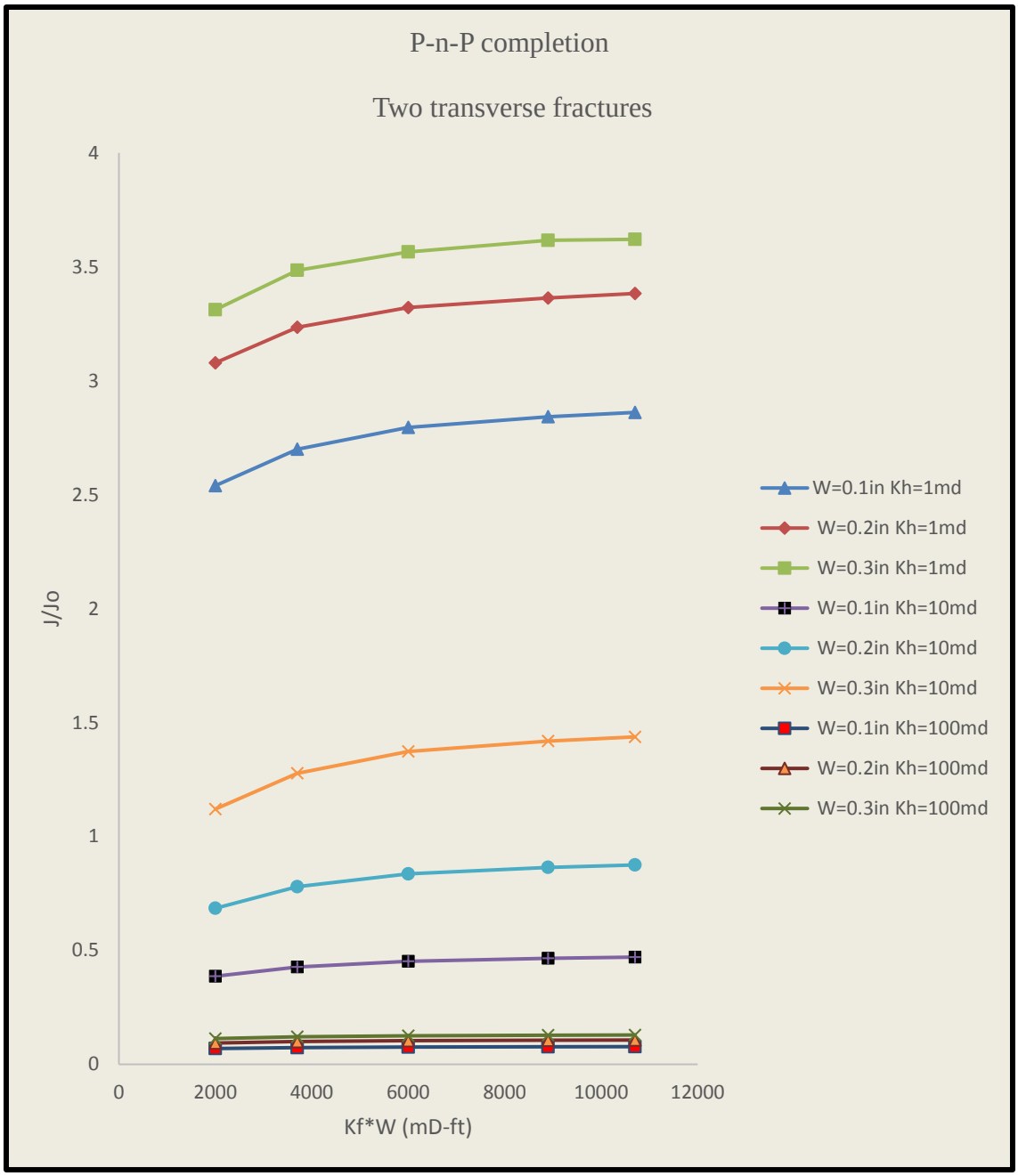

Figure 5.11. Results: fracture width study: Two transverse fracture; P-n-P

The effect of a change in fracture width (w) for two transverse fractures model is the same as for single transverse fracture type in P-n-P completions.

Figure 5.12 and 5.13 shows the effect of fracture width (w) in wells completed with OHMS method for single transverse fracture and two transverse fracture wells respectively.

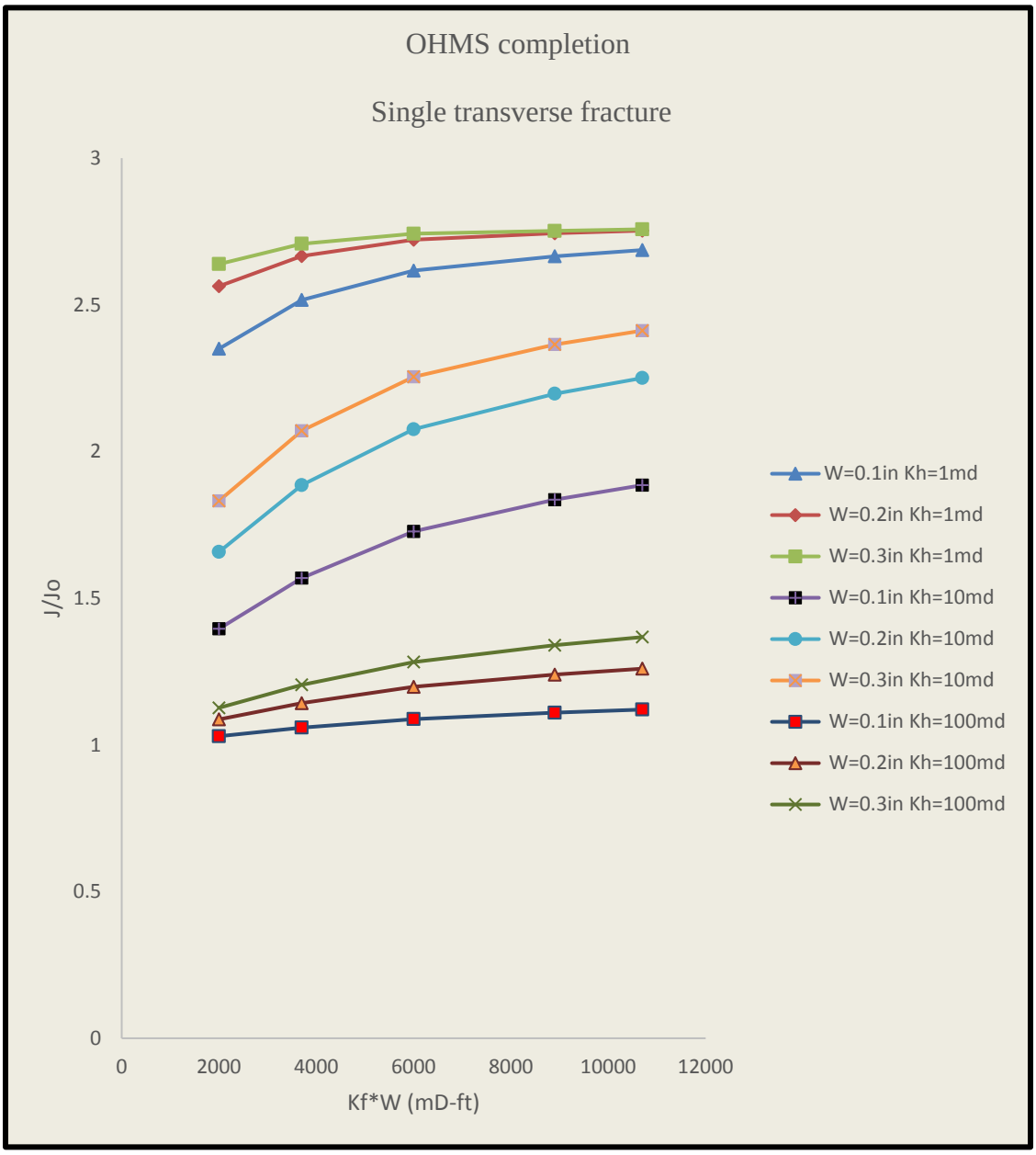

Figure 5.12. Results: fracture width study: Single transverse fracture; OHMS

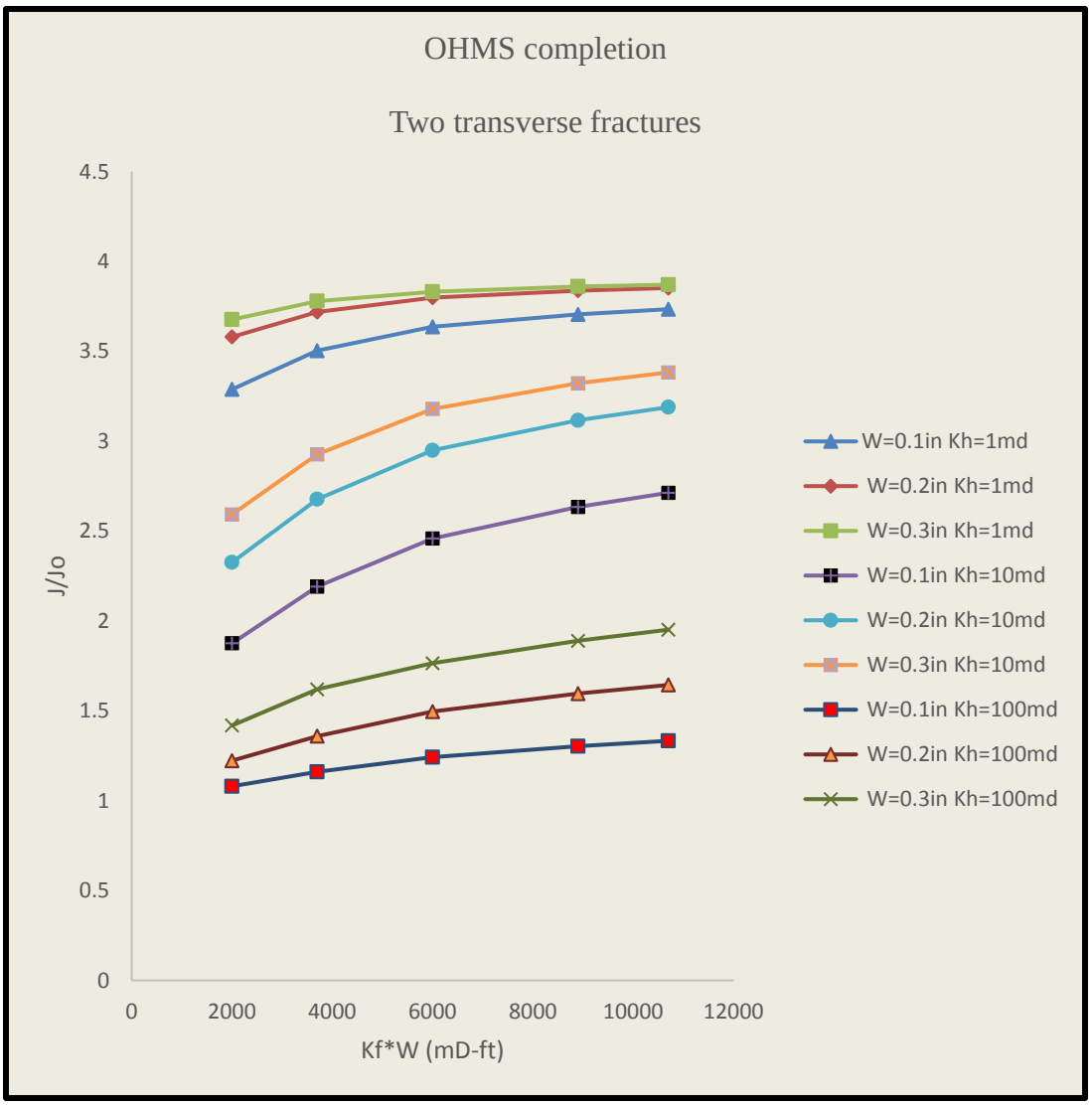

Figure 5.13. Results: fracture width study: Two transverse fracture; OHMS

Both Figure 5.12 and 5.13 show that for a reservoir with permeability (k_h) of 1 mD, folds of increase (FOI) for fracture widths (w) of 0.2 and 0.3 inches have almost the same values as fracture conductivity (C_f) increases. The general pattern in both the figures is the same.

Figure 5.14 and 5.15 shows the effect of fracture width (w) on longitudinal fractures using P-n-P and OHMS completions respectively.

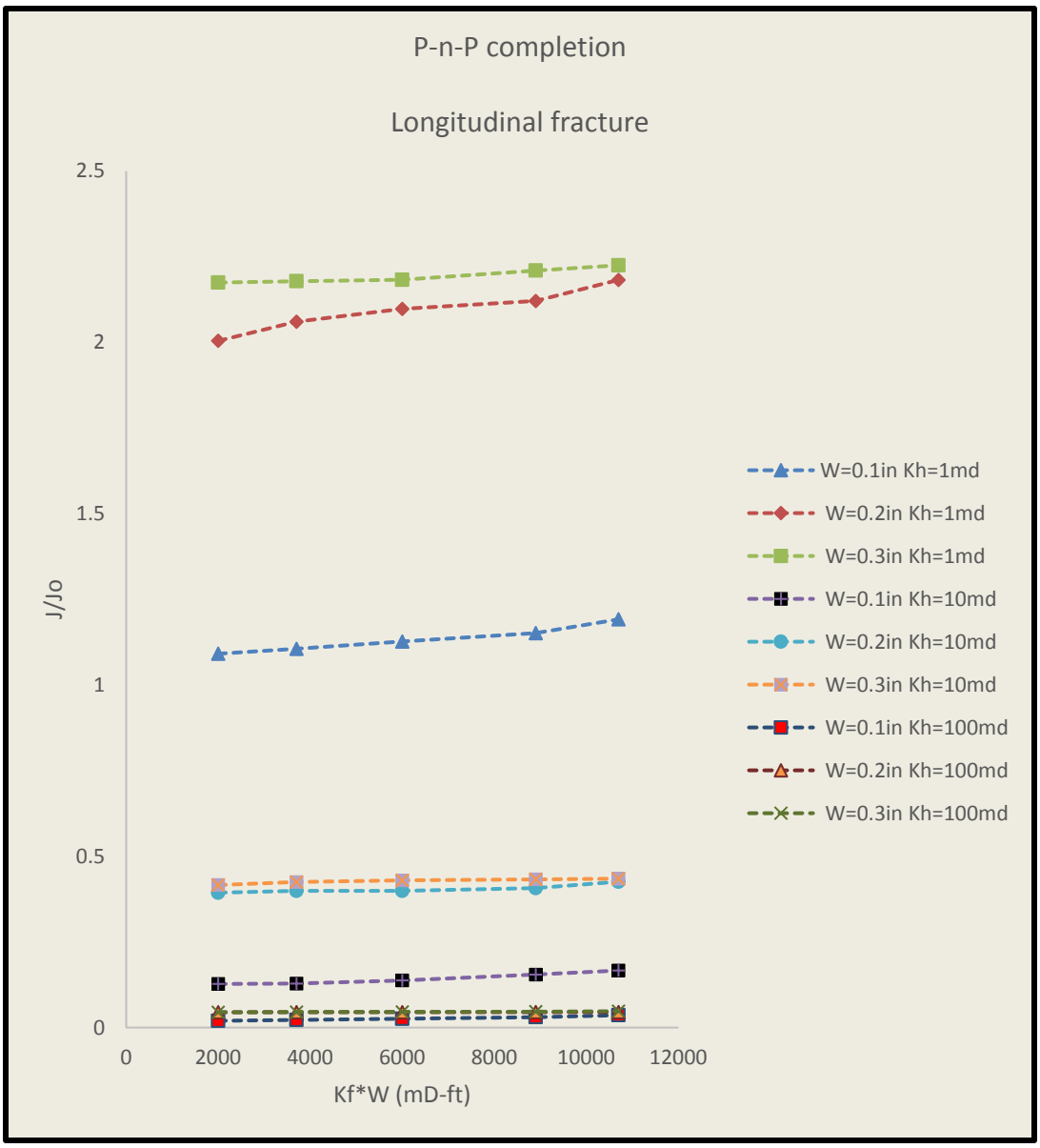

Figure 5.14. Results: fracture width study: Longitudinal fracture; P-n-P

According to Figure 5.14, natural gas production increases with fracture widths (w) of 0.2 and 0.3 inches compared to base case width of 0.1 inches. However, there is no significant change in the folds of increase (FOI) for a 100 mD reservoir with the change in fracture width (w).

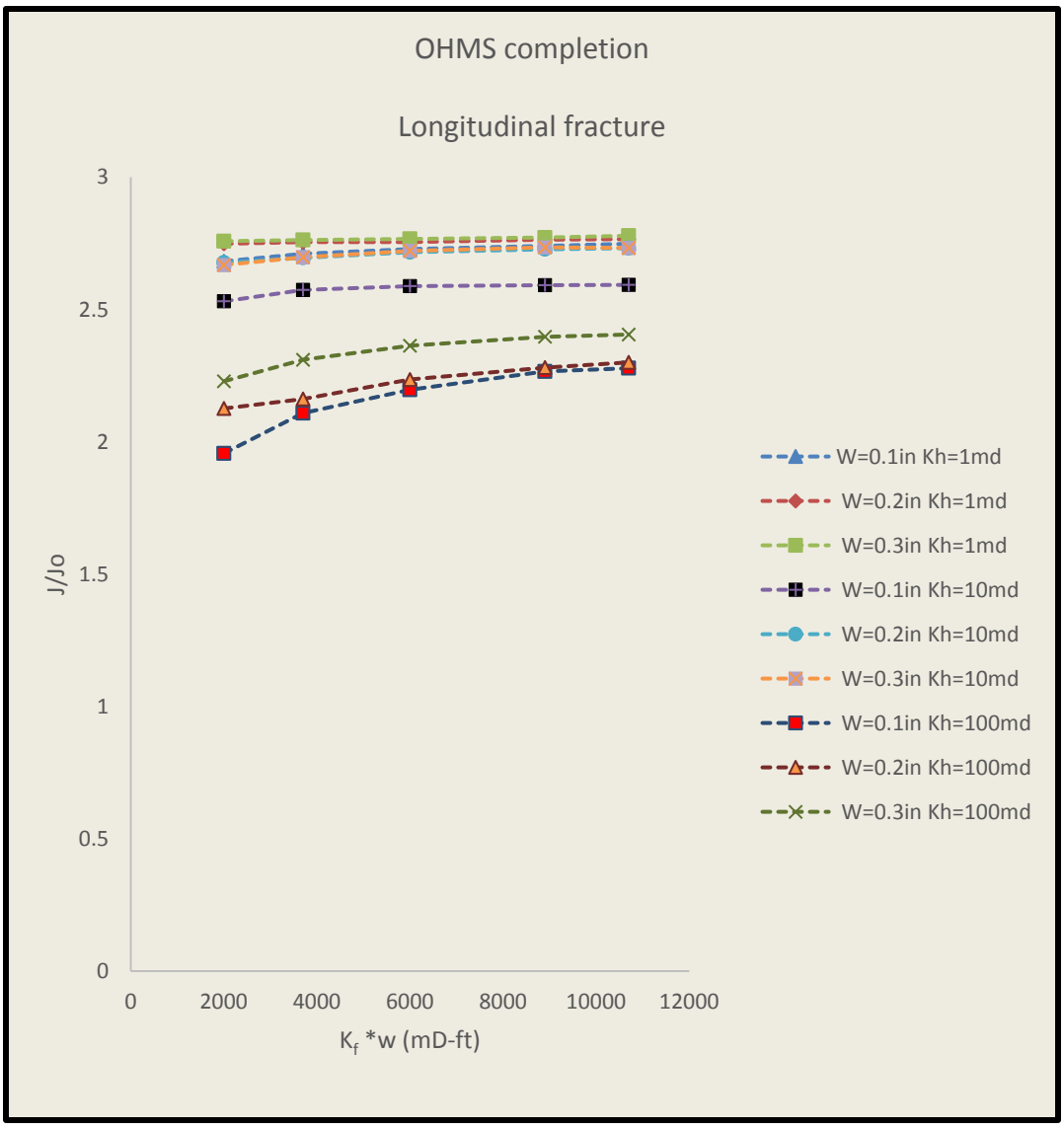

Figure 5.15. Results: fracture width study: Longitudinal fracture; OHMS

Figure 5.15 shows that for reservoirs with permeability (k_h) of 1 mD and 10 mD, the folds of increase (FOI) with the change in fracture width (w) is negligible. For 100 mD case, an increase in fracture width increases production.

5.2.2. Effect of Penetration Ratio. Results of the parametric study on the penetration ratio (x_f/r_e) are given in this section. Results for single transverse and two transverse fracture wells completed with P-n-P and OHMS methods are presented

separately. Figure 5.16 and 5.17 shows the results of single transverse and two transverse fracture well completed with P-n-P method respectively.

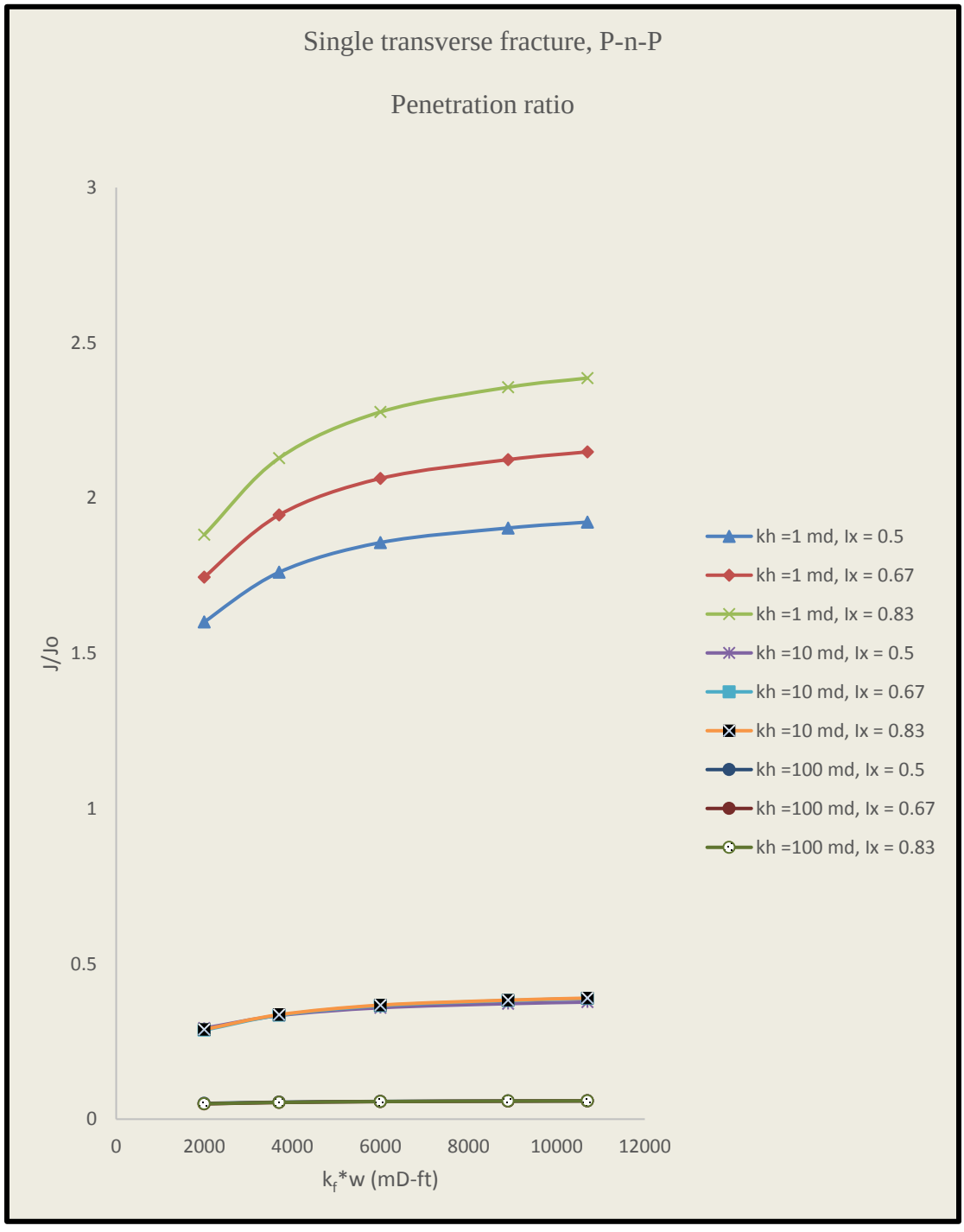

Figure 5.16. Results: Penetration ratio effect: Single transverse fracture; P-n-P

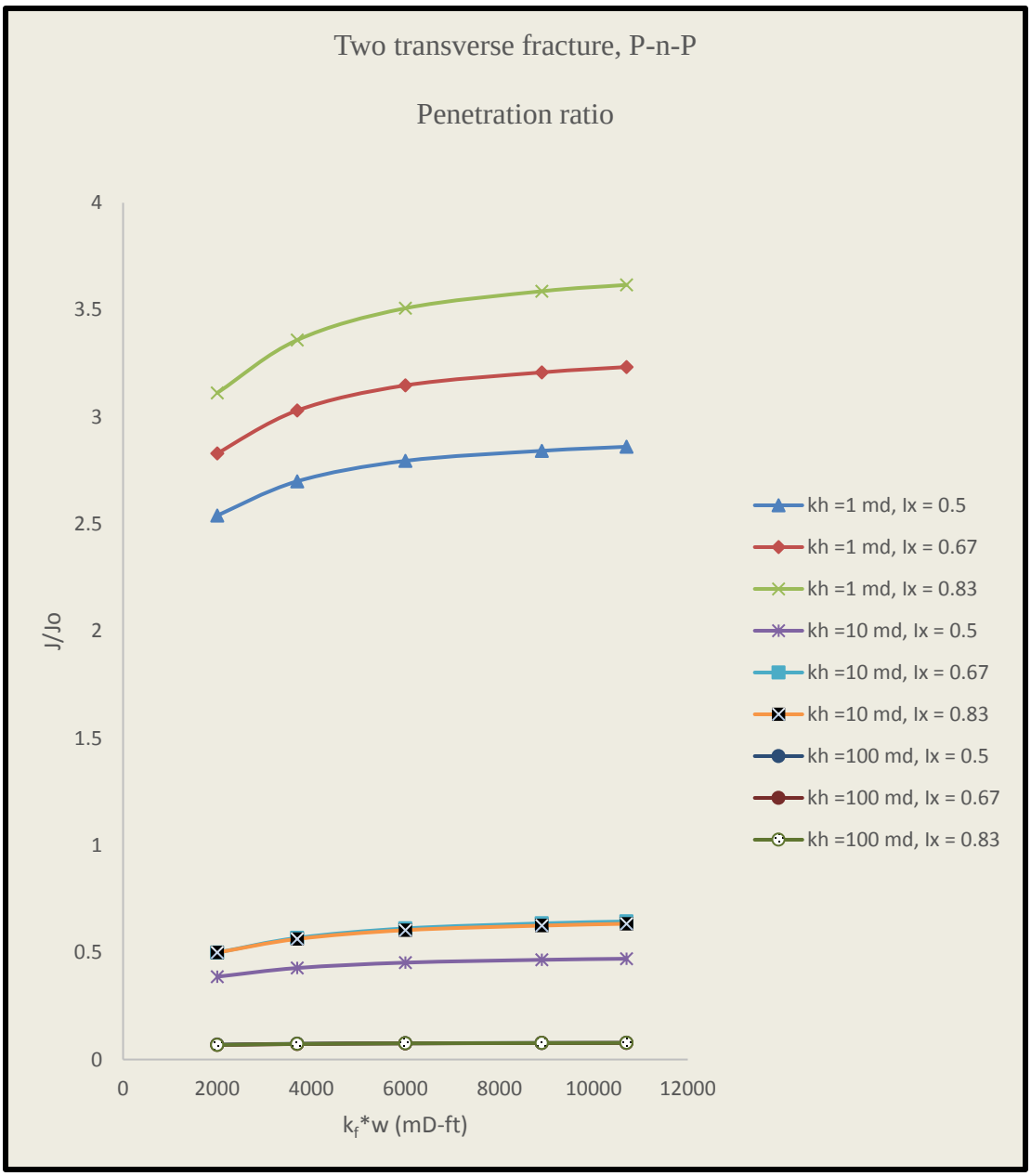

Figure 5.17. Results: Penetration ratio effect: Two transverse fracture; P-n-P

According to Figure 5.16 and 5.17, there is a considerable increase in production for a 1 mD reservoir with the increase in half-length (x_f) whereas there is only a small increase in production for 10 and 100 mD reservoirs.

Figure 5.18 and 5.19 shows the results of single transverse and two transverse fracture well completed with OHMS method respectively.

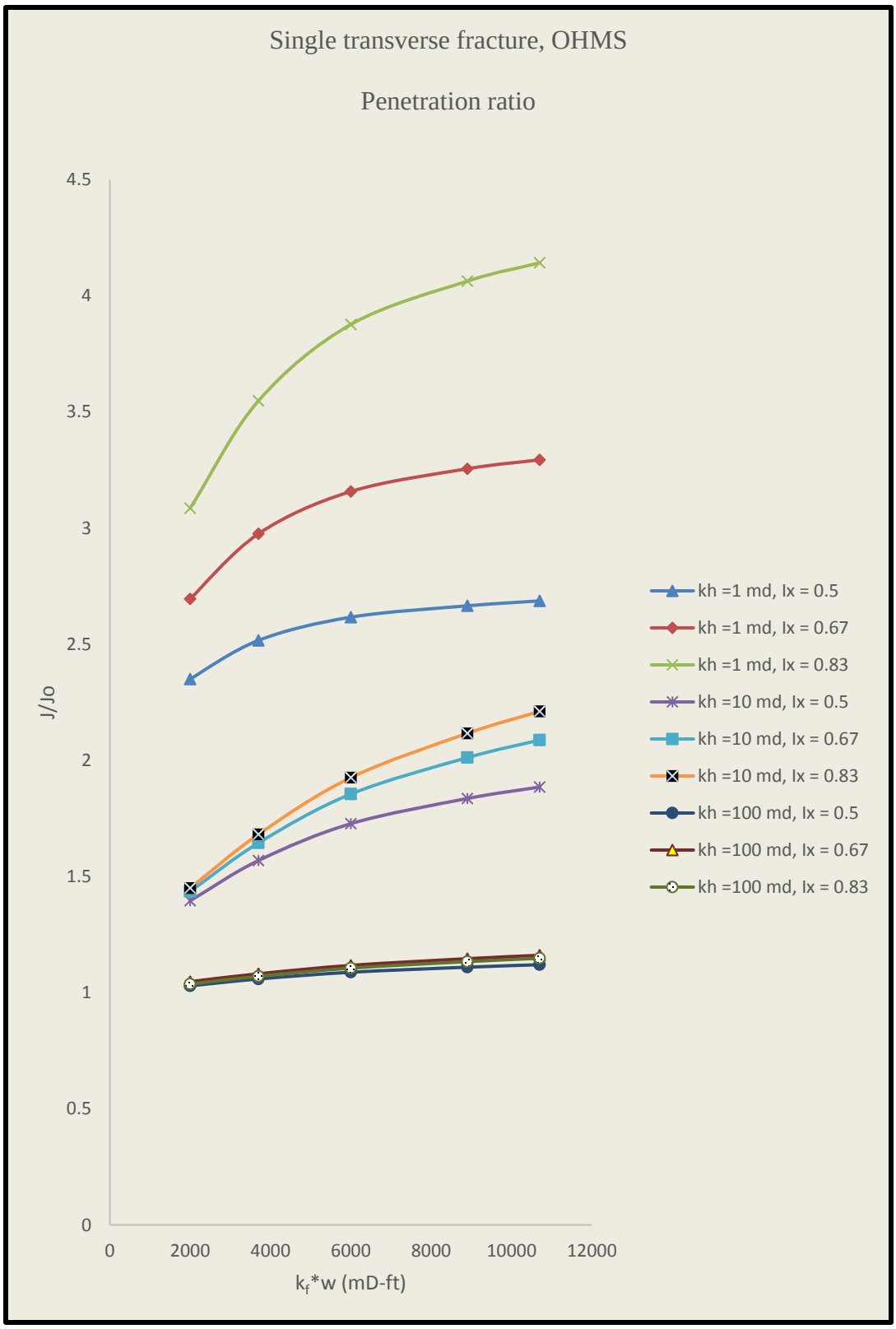

Figure 5.18. Results: Penetration ratio effect: Single transverse fracture; OHMS

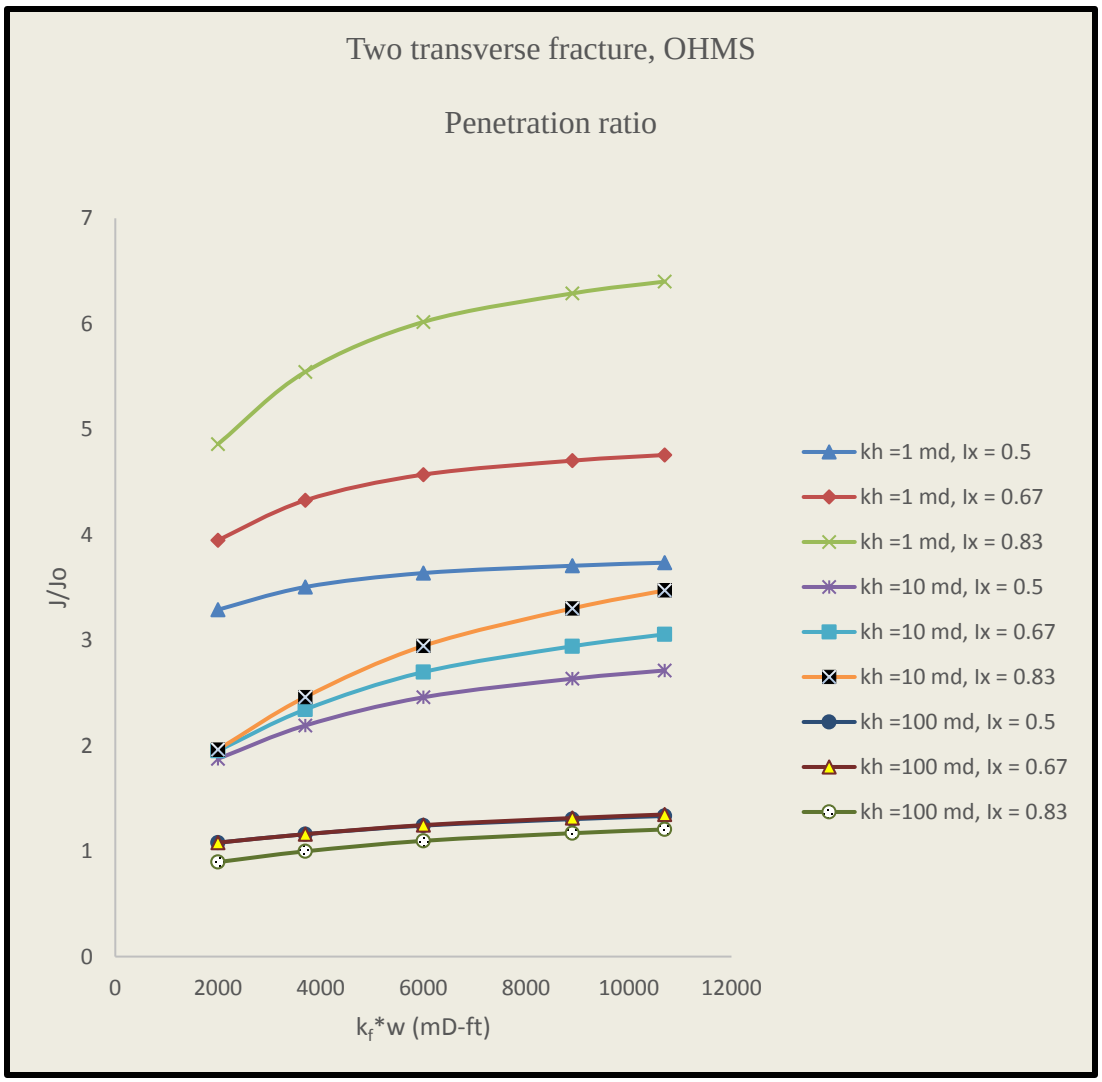

Figure 5.19. Results: Penetration ratio effect: Two transverse fracture; OHMS

Both Figure 5.18 and 5.19 show the same trend. For a 1 mD reservoir, there is a significant increase in production by changing the half-length (x_f) and for a 10 mD reservoir, there is a slight growth in production. In the case of a 100 mD reservoir, increasing the half-length (x_f) doesn't have any effect on production and in fact, can have an adverse impact on production as is seen in the two transverse fracture case.

5.2.3. Effect of Vertical to Horizontal Permeability (k_v/k_h) Ratio. The parametric study to investigate the effect of vertical to horizontal permeability (k_v/k_h) ratio on natural gas production was completed and the results are presented in this

section. Figure 5.20, 5.21 and 5.22 exhibits the results for wells completed with P-n-P completions for reservoir permeability (k_h) of 1 mD, 10 mD, and 100 mD sequentially. Only transverse fractures are shown.

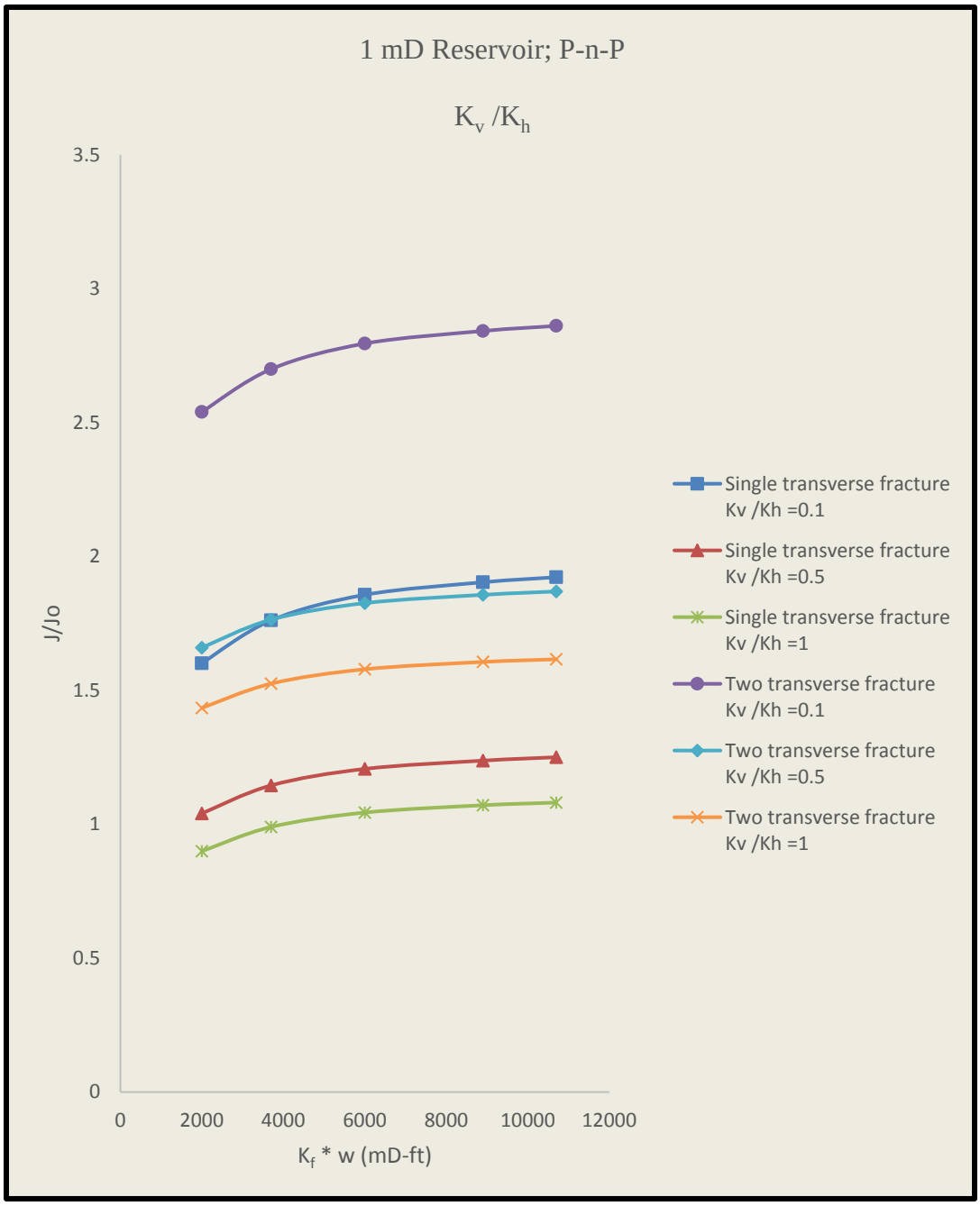

Figure 5.20. Results: k_v/k_h ratio effect: P-n-P; Transverse fractures-1 mD

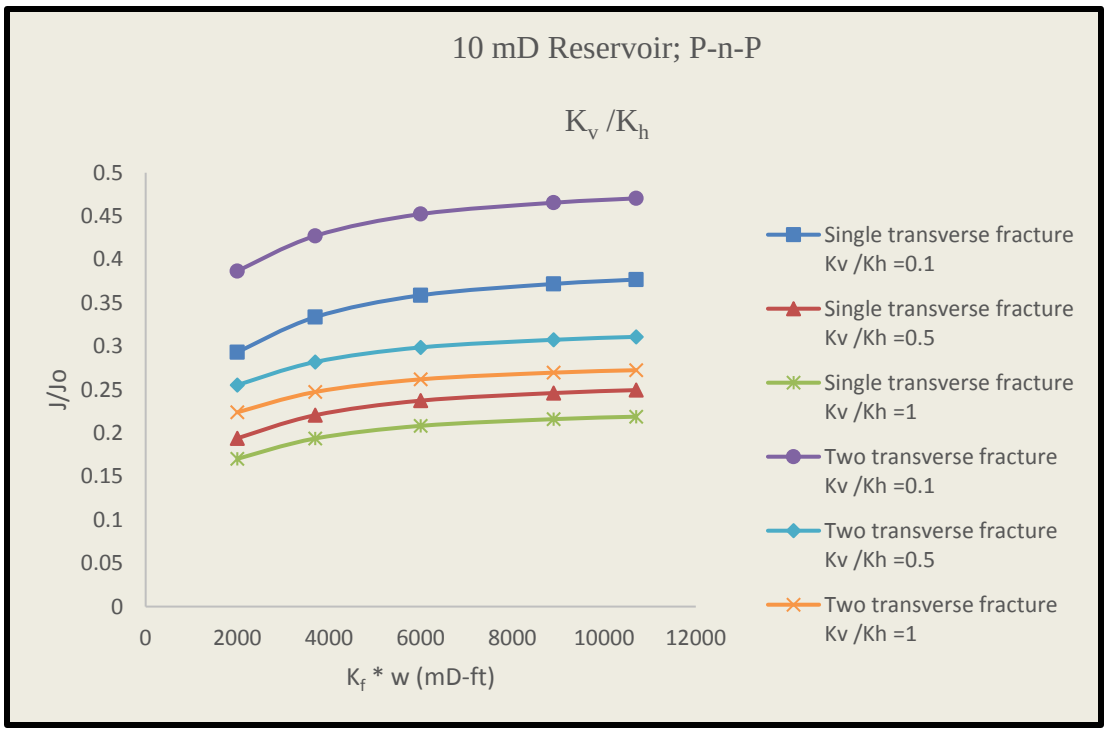

Figure 5.21. Results: k_v/k_h ratio effect: P-n-P; Transverse fractures-10 mD

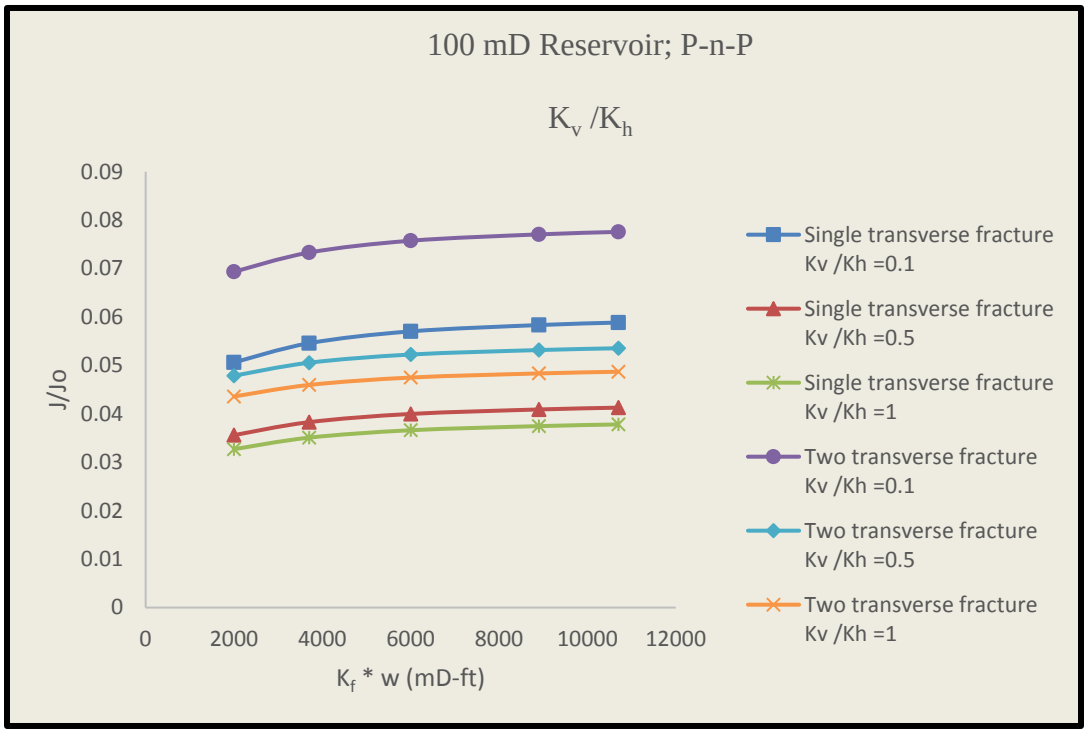

Figure 5.22. Results: k_v/k_h ratio effect: P-n-P; Transverse fractures-100 mD

Figure 5.20, 5.21 and 5.22 displays the same trend, and the folds of increase (FOI) decreases with bigger k_v/k_h ratio.

Figure 5.23, 5.24 and 5.25 shows the results for transverse fracture wells with OHMS completions for reservoir permeability (k_h) of 1 mD, 10 mD, and 100 mD respectively.

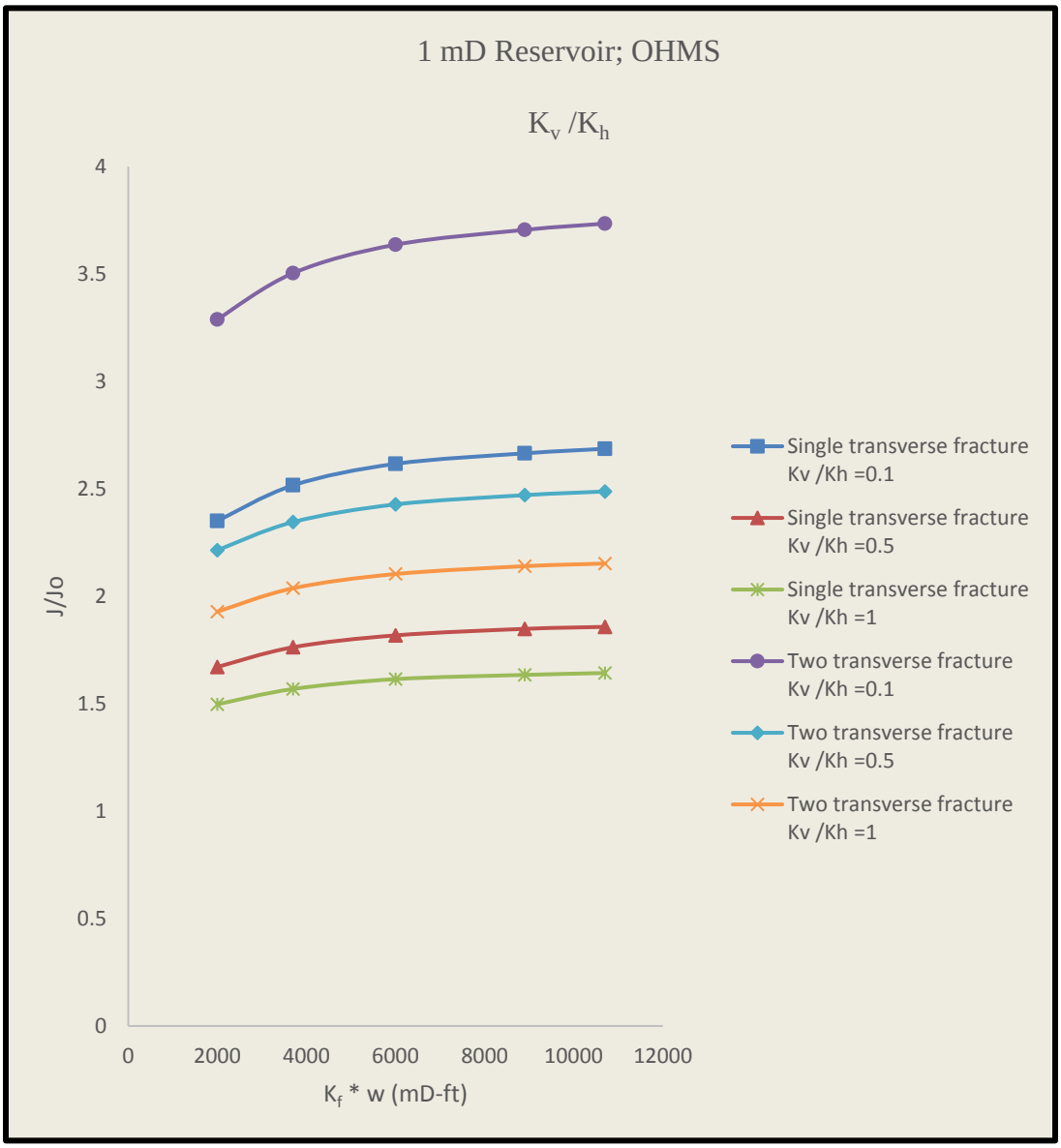

Figure 5.23. Results: k_v/k_h ratio effect: OHMS; Transverse fractures-1 mD

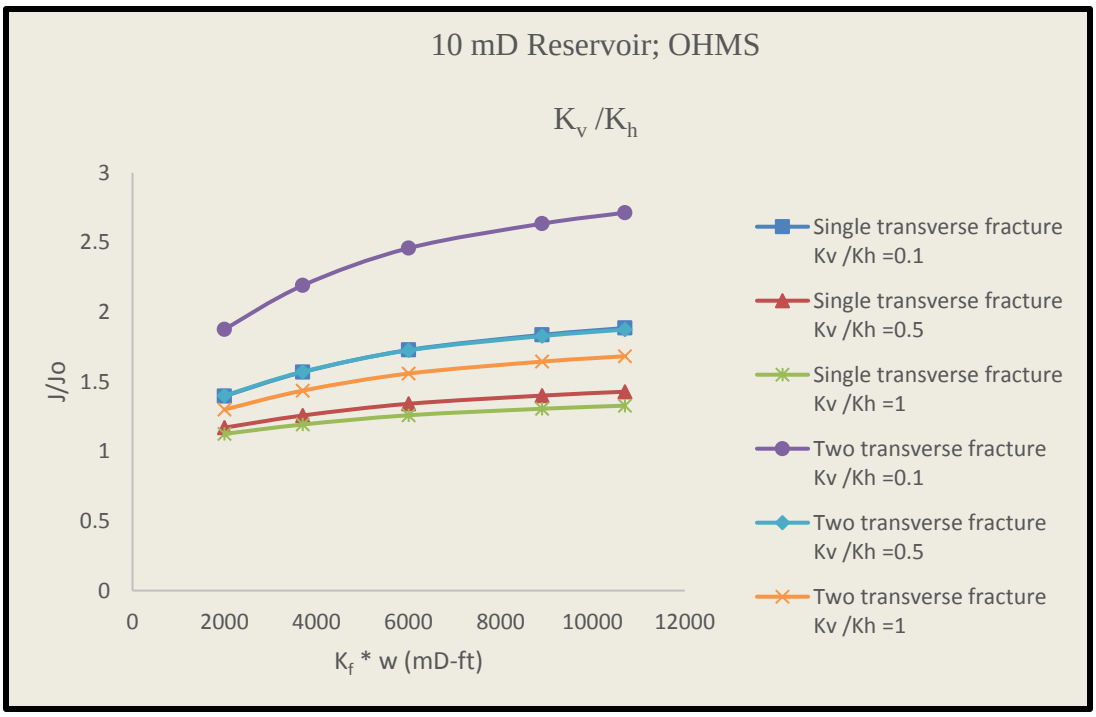

Figure 5.24. Result: k_v/k_h ratio effect: OHMS; Transverse fractures-10 mD

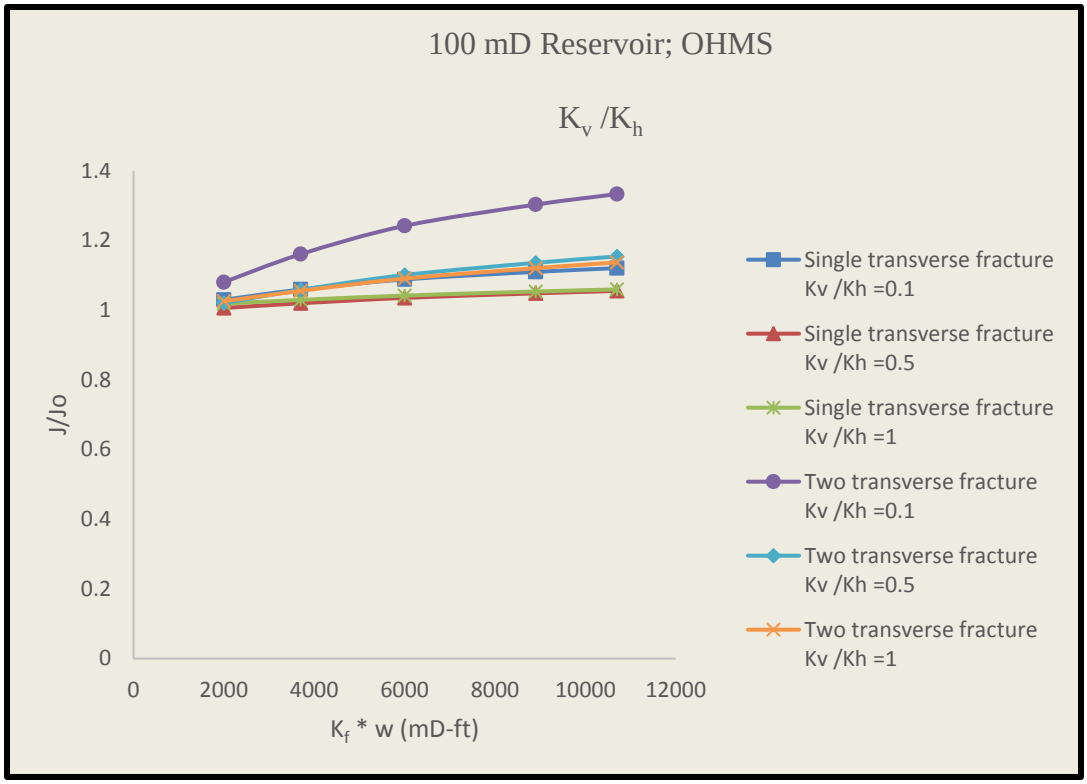

Figure 5.25. Results: k_v/k_h ratio effect: OHMS; Transverse fractures-100mD

Figure 5.23, 5.24 and 5.25 have the same trend. Natural gas production decreases with higher k_v/k_h ratio. In Figure 5.25, there is no significant reduction in the natural gas production for single and two transverse fractures for k_v/k_h ratios of 0.5 and 0.1.

Figure 5.26, 5.27 and 5.28 shows the results for longitudinal fracture in wells completed with P-n-P completions for reservoir permeability (k_h) of 1 mD, 10 mD, and 100 mD respectively. The folds of increase (FOI) decreases with increasing k_v/k_h ratio and the curves in all the three plots have a similar pattern.

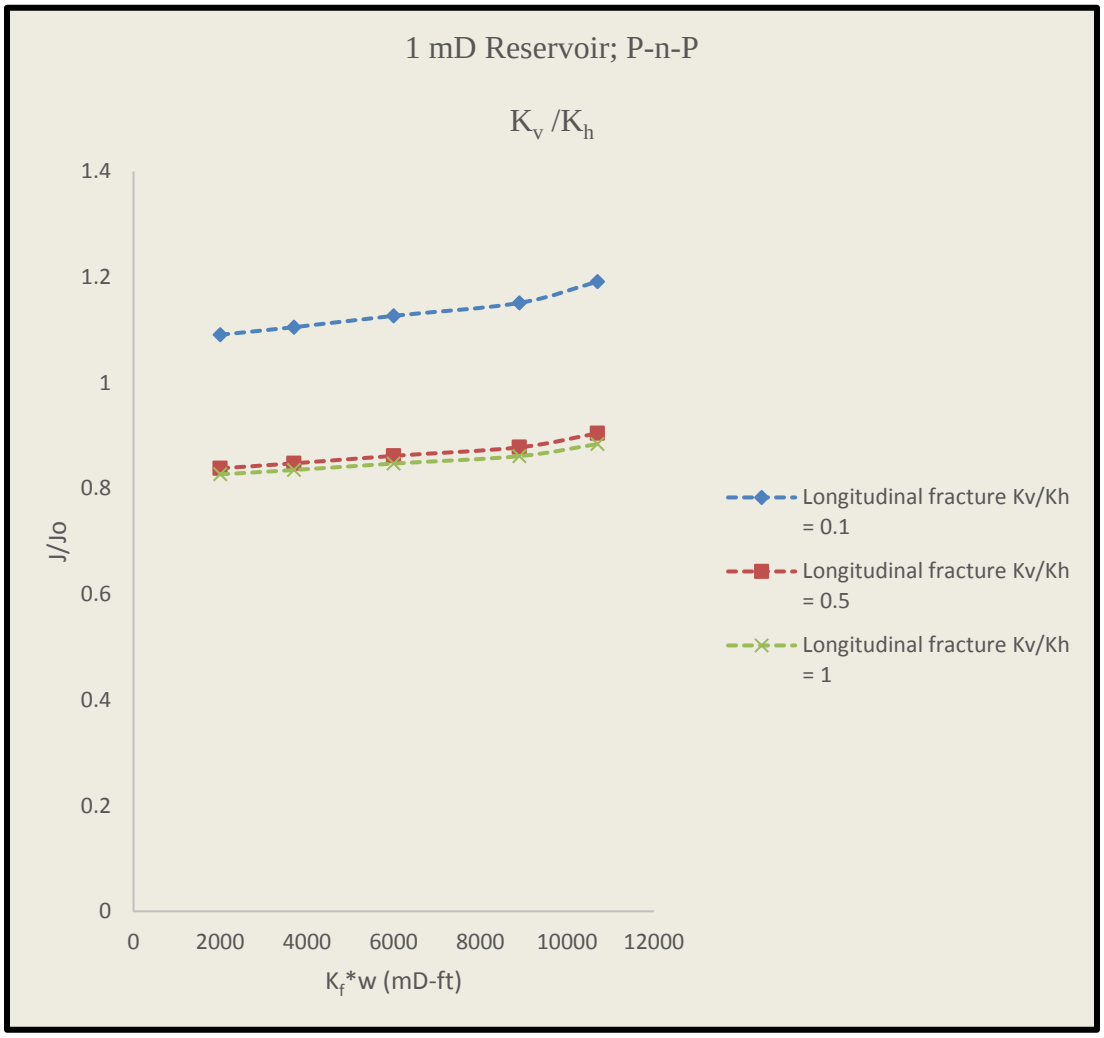

Figure 5.26. Results: k_v/k_h ratio effect: P-n-P; Longitudinal fracture-1mD

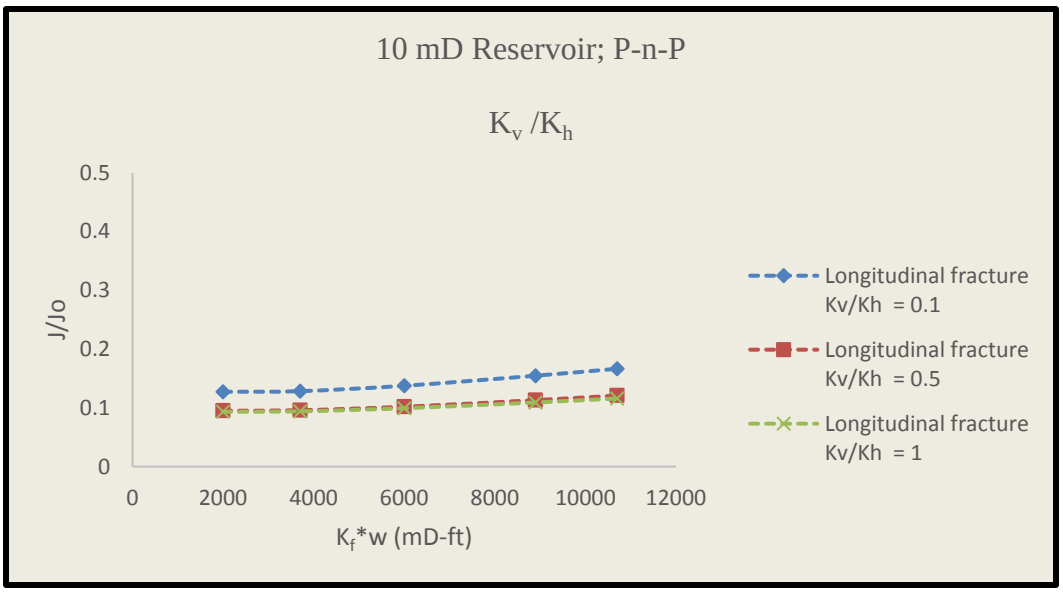

Figure 5.27. Results: k_v/k_h ratio effect: P-n-P; Longitudinal fracture-10mD

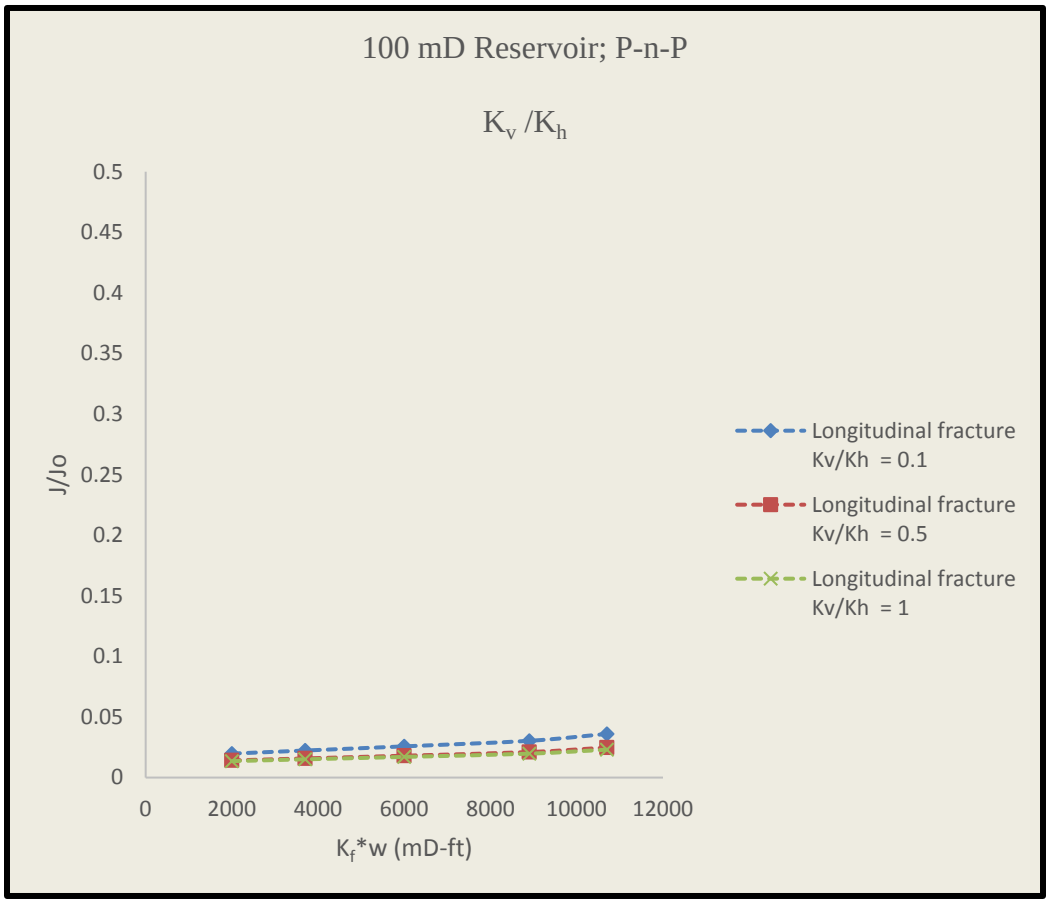

Figure 5.28. Results: k_v/k_h ratio effect: P-n-P; Longitudinal fracture-100mD

Figure 5.29, 5.30 and 5.31 displays the effect of k_v/k_h ratio on natural gas production in longitudinally fractured wells with OHMS completions. Reservoir permeability of 1 mD, 10 mD, and 100 mD are considered. In all the three plots, the folds of increase (FOI) decreases with higher k_v/k_h ratio.

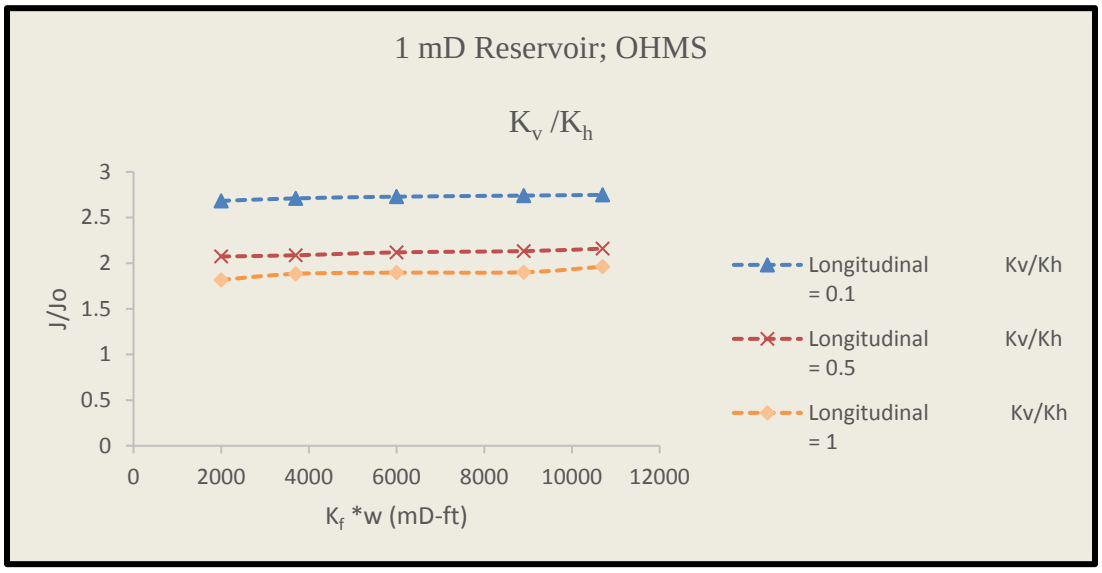

Figure 5.29. Results: k_v/k_h ratio effect: OHMS; Longitudinal fracture-1mD

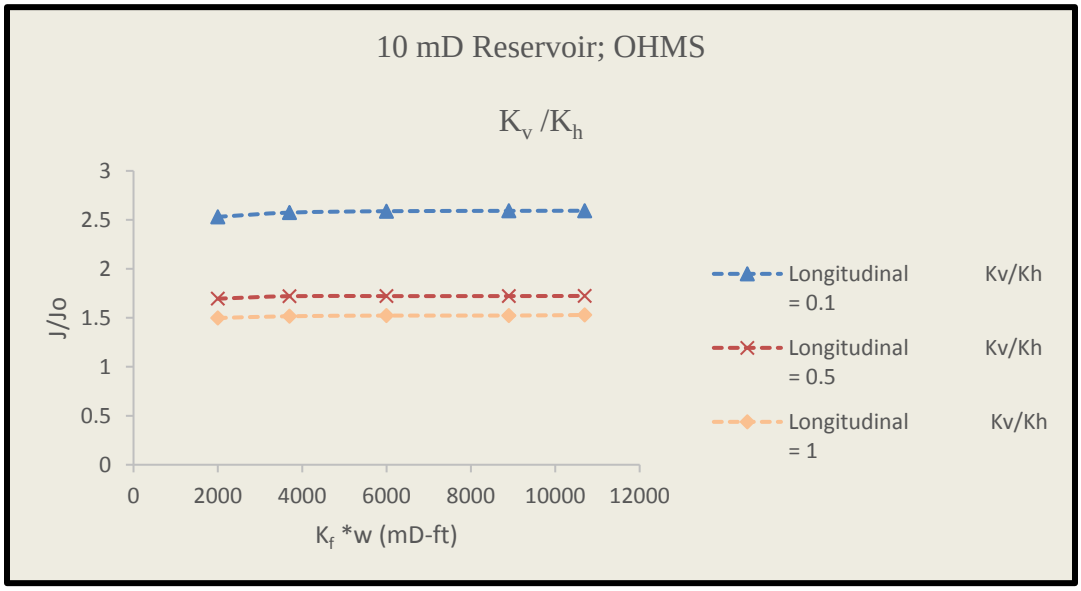

Figure 5.30. Results: k_v/k_h ratio effect: OHMS; Longitudinal fracture-10mD

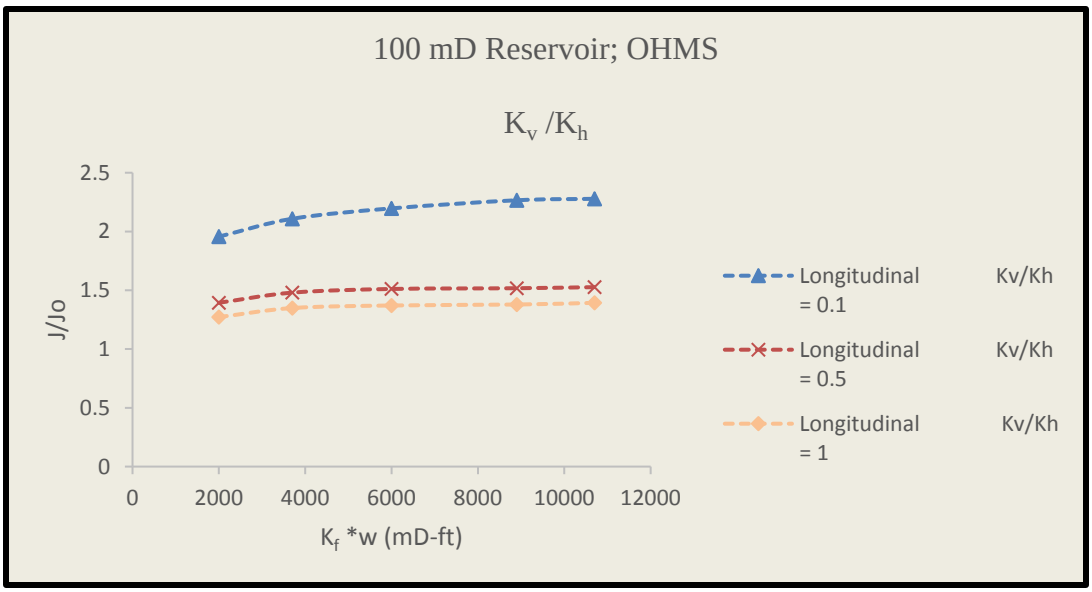

Figure 5.31. Results: k_v/k_h ratio effect: OHMS; Longitudinal fracture-100mD

The results from parametric studies showed that wells completed with OHMS completions out produced the wells with P-n-P completions in all the cases.

6. SUMMARY OF RESULTS AND CONCLUSIONS

This section discusses the simulation results from the base case and parametric studies. In the base case, the performance of transverse and longitudinally fractured wells with both OHMS and P-n-P completions are compared for reservoir permeability values of 1 mD, 10 mD, and 100 mD. The results from the simulations concluded that longitudinally fractured wells outperformed transverse fractured wells in OHMS completions above a certain reservoir permeability, and also the type of completion employed plays a vital role in choosing between transverse and longitudinal fractures.

6.1. BASE CASE RESULT SUMMARY: OHMS COMPLETIONS

In 1 mD reservoirs with OHMS completions, two transverse fractures outperformed longitudinal fracture whereas the performance of single transverse fracture is slightly lesser than the longitudinal fracture. When permeability increases to 10 mD reservoir, the performance of two transverse fracture is slightly higher than longitudinal fracture, but only for high fracture conductivity (C_f). When permeability increases to 100 mD, longitudinal fractures always outperform transverse fractures. The CFD analysis indicates longitudinal fractures outperformed transverse fractures by almost 100% in 100 mD reservoirs. In the case of 1 mD reservoir, multiple longitudinal fractures might perform better than transverse fractures but cannot be proved here due to the very small length of horizontal wellbore considered.

These results are in agreement with the results of Economides et al., (2010), Yang et al., (2015) and Kassim et al., (2016).

6.2. BASE CASE RESULT SUMMARY: P-n-P COMPLETIONS

For all reservoir permeability values considered in this study, transverse fracture performance in wells completed with P-n-P completions outperform longitudinal fractured P-n-P completions. Hence, results of this study suggest avoiding the application of longitudinal fractures in P-n-P completions. These results support the work of Yang et al., (2015).

6.3. BASE CASE RESULT SUMMARY: OHMS VS P-n-P COMPLETIONS

From the plots in Section 5.1, it can be inferred that OHMS completions have production increase when compared to unstimulated horizontal well, with increasing fracture conductivity. In P-n-P completions, folds of increase (FOI) are almost zero for reservoir permeabilities (k_h) of 10 mD and 100 mD. High rate water packs are preferred for cased hole completions in high permeability gas reservoirs (Welling, 1998).

Fracturing in cased hole completions is usually done in stages with many perforation clusters for each fracture stage. Due to modeling limitations, two perforations with 180° phasing are used in this study. This can be a reason for the very low folds of increase (FOI) in P-n-P completions in this work.

OHMS completions perform better than P-n-P completions in both transverse and longitudinally fractured horizontal wells. Open hole completions have a larger contact area with the reservoir since the entire horizontal wellbore is not cased and cemented, and the fractures are directly connected to the wellbore. In the case of P-n-P completions, fractures are linked to the wellbore through perforations, and if the perforations are poor connections or introduce tortuosity, then gas flow is affected.

Pressure and velocity contour analysis using CFD-Post provide a visualization of the gas production in OHMS and P-n-P completions. Figure 6.1 shows the pressure contour in the symmetry plane and a mid-section plane in an OHMS completion. A mid-section plane is created in CFD-Post to display the contour effectively. Figure 6.2 shows the pressure contour in the fracture outlets of an OHMS model. From Figure 6.1 and 6.2, it is clear that there is a pressure drop near the fracture outlets.

Figure 6.3 shows the velocity contour at the symmetry plane and fracture outlets, and there is an increase in velocity near the fracture outlets.

Figure 6.4 and 6.5 shows the pressure and velocity contour of P-n-P completion. Figure 6.4 displays that there is a pressure drop near both the outlets and the pressure is comparatively higher at the area where perforations meet the fracture. From Figure 6.5, it is evident that velocity at the outlets are higher compared to the velocity at the area where fracture meets perforations. If the perforations were of a much smaller size, the velocity at the contact area between fractures and perforations would have been very high.

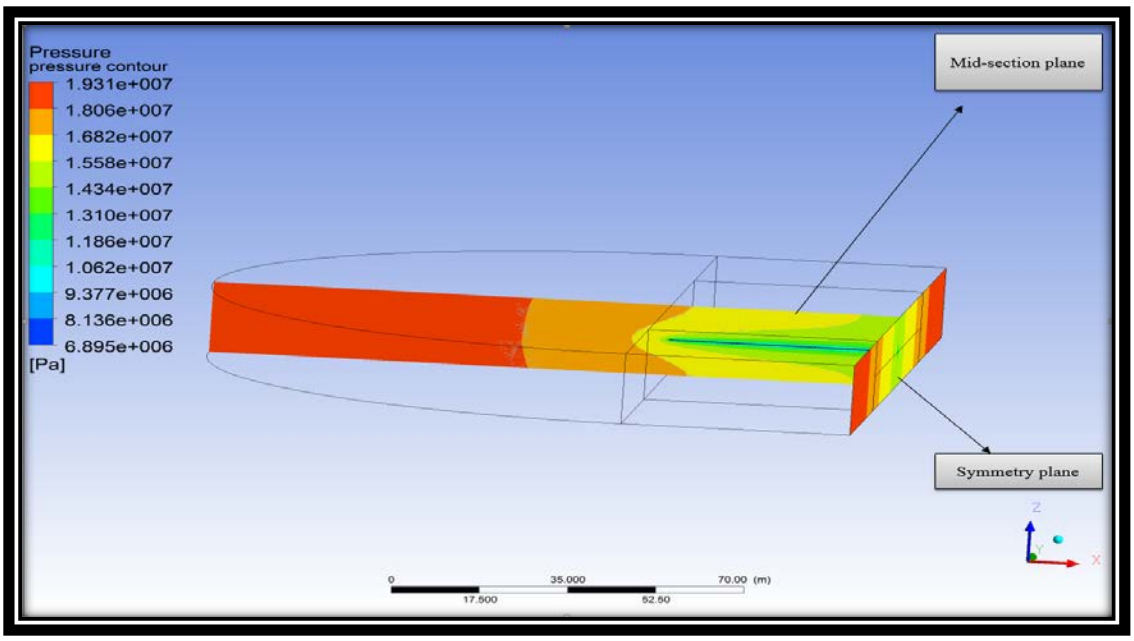

Figure 6.1. Pressure contour of symmetry plane in OHMS completion

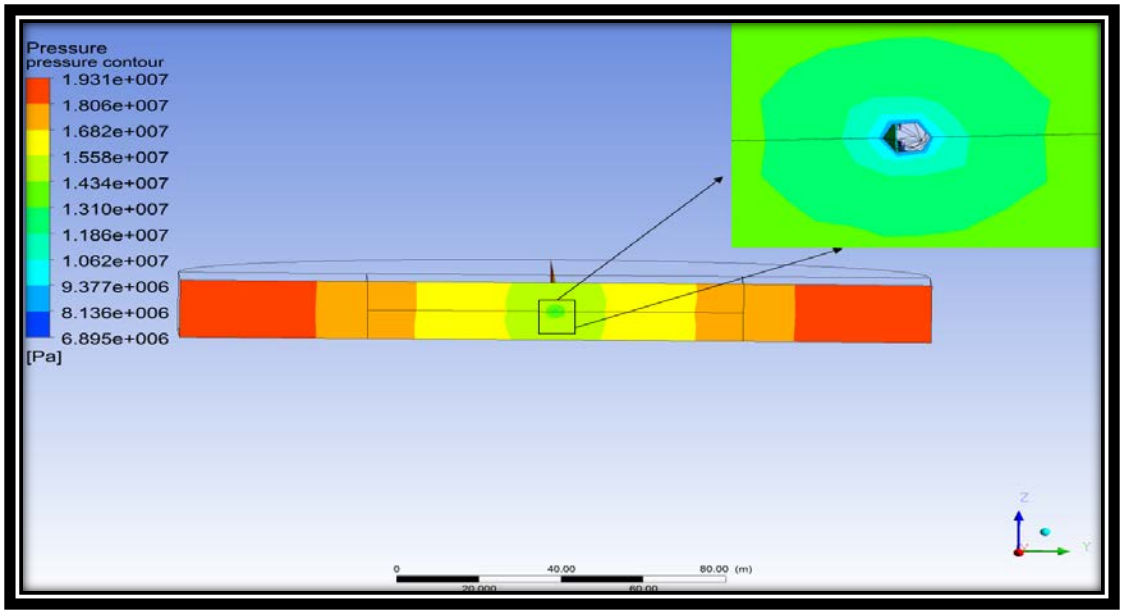

Figure 6.2. Pressure contour of fracture outlets in OHMS completion

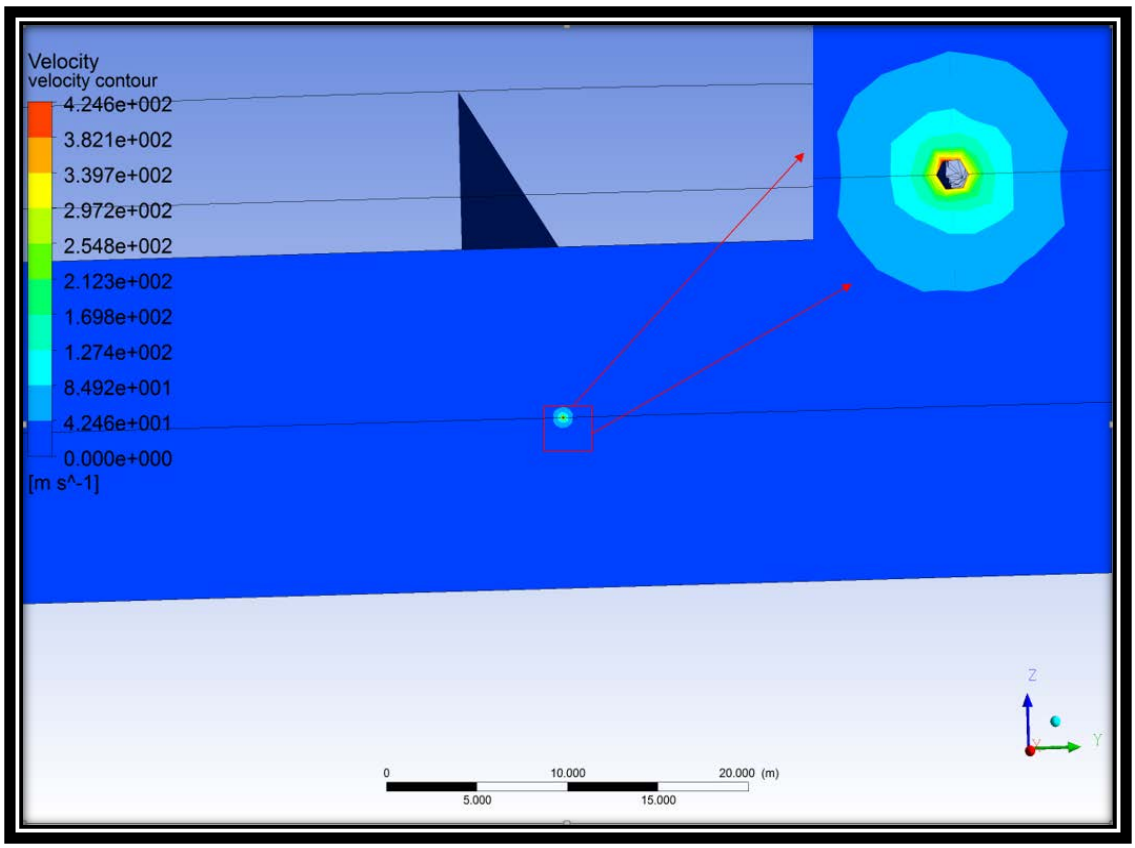

Figure 6.3. Velocity contour in OHMS completion

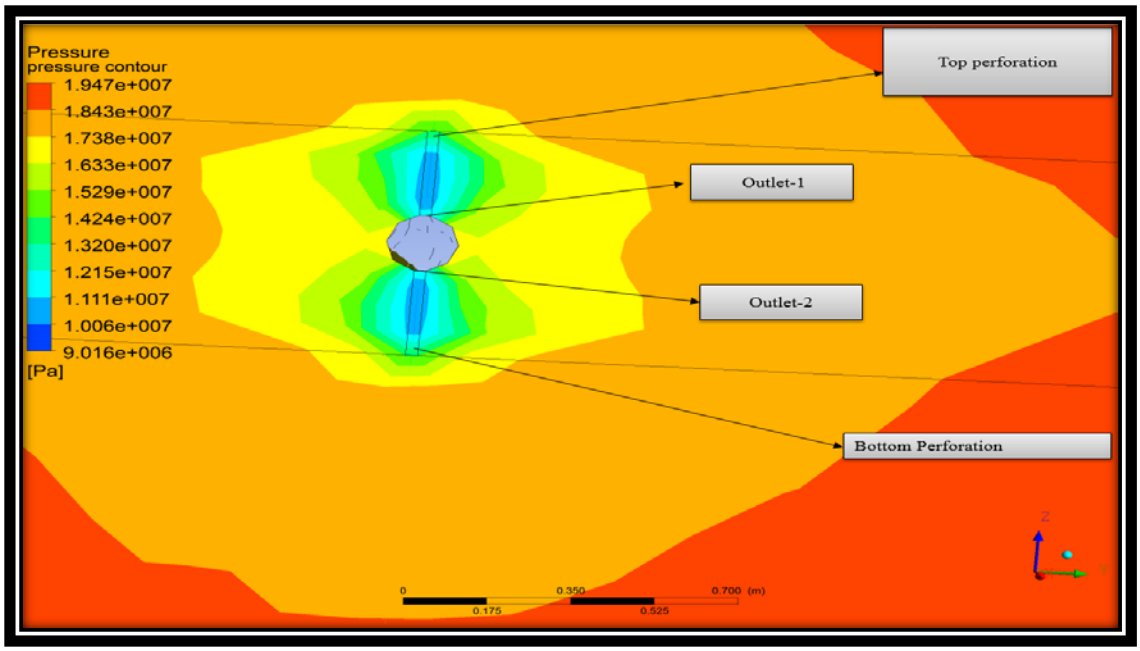

Figure 6.4. Pressure contour in P-n-P completion

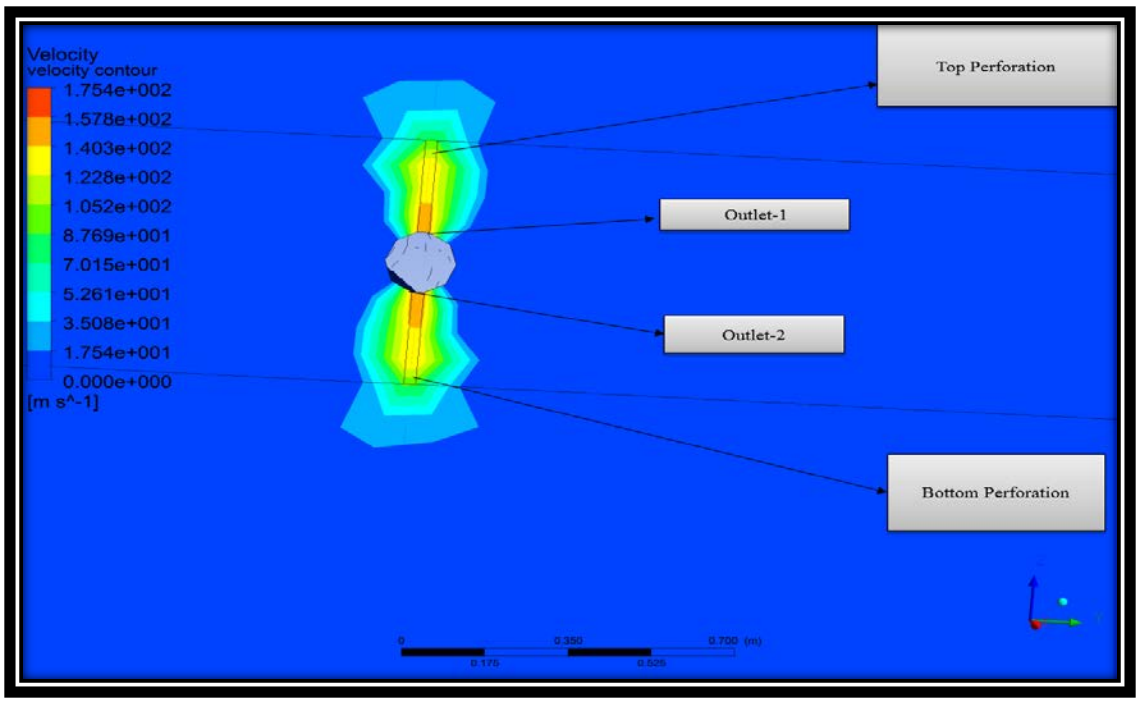

Figure 6.5. Velocity contour in P-n-P completion

6.4. PARAMETRIC STUDY SUMMARY

6.4.1. Fracture Width. Work done by Prat's in 1961 (Economides et al., 1994) addresses the requirement for good fracture permeability and fracture width in moderate to high permeability reservoirs and the results from the fracture width analysis matches with Prat's work. For reservoir permeability of 1 mD, P-n-P completions showed an increase in folds of increase (FOI) when fracture widths of 0.2 inch and 0.3 inches were used. These resulting values may be high. For reservoir permeability of 10 mD and 100 mD, the P-n-P completion results are in agreement with Prat's work. In the case of OHMS completions, for reservoir permeability of 1 mD, there is a small increase in natural gas production with an increase in fracture width. For 10 mD and 100 mD reservoirs, there is a significant increase in production with the increase in fracture width.

Except for the results of P-n-P completions in 1 mD reservoir, all other results matched with Prat's work and longitudinal fractures are better than transverse fractures in a 100 mD reservoir.

6.4.2. Penetration Ratio. Only transverse fracture models are analyzed to study the effect of penetration ratio. In a 1 mD reservoir, there is a considerable increase in production with an increase in fracture half length (x_f). For reservoirs with a permeability of 10 mD and 100 mD, increase in half length (x_f) didn't have a substantial effect on production. The effect of penetration ratio is same for both P-n-P and OHMS completions. Economides et al., (1994) in his book states that as reservoir permeability increases the need for fracture half length (x_f) is less significant and the results of the simulation support this.

6.4.3. Vertical to Horizontal Permeability Ratio. The results from k_v/k_h ratio study on wells completed with both P-n-P and OHMS completions for reservoir permeability values of 1 mD, 10 mD, and 100 mD shows the same trend. Folds of increase (FOI) decreases with increasing k_v/k_h ratio. All the three fracture models show the same pattern in results. The reservoir in this study is a thick reservoir with a net pay of 60 ft. The effect of vertical permeability (k_v) is significant only in thick reservoirs, and that is the reason for the decrease in natural gas production in this study. In thin reservoirs ($h< 50$ ft.), the decline in production will be minimal with the increase in k_v/k_h ratio.

In transverse fractures, gas flow into the fracture vertically and vertical permeability has a big effect on production. From the plots, it is clear that there is an increase in production of gas, but there is a corresponding increase in production from the unstimulated well which leads to decrease in folds of increase (FOI).

In the case of longitudinal fractures, horizontal permeability impacts the gas production. Longitudinal fracture with OHMS completions performs much better than transverse fractures in a 100 mD reservoir with the increase of k_v/k_h ratio.

Anisotropic permeability is important in horizontal wells since flow occurs in both the vertical and horizontal planes. The variation in permeability in different planes or directions is known as anisotropic permeability.

6.5. COMPARISON WITH AUGUSTINE'S WORK

Simulations performed in this study were compared with the results in terms of "relative conductivity" as shown in Augustine's plot in Section 1.1. Both P-n-P and

OHMS completions for transverse fractures are considered. In Augustine's plot, k_v/k_h value was assumed to be 0.01 and the reservoir height was taken as 100 ft. Figure 6.6 shows the comparison of simulation results with Augustine's work for both completions, after digitizing Augustine's plot at the range of reservoir permeability values considered for this study.

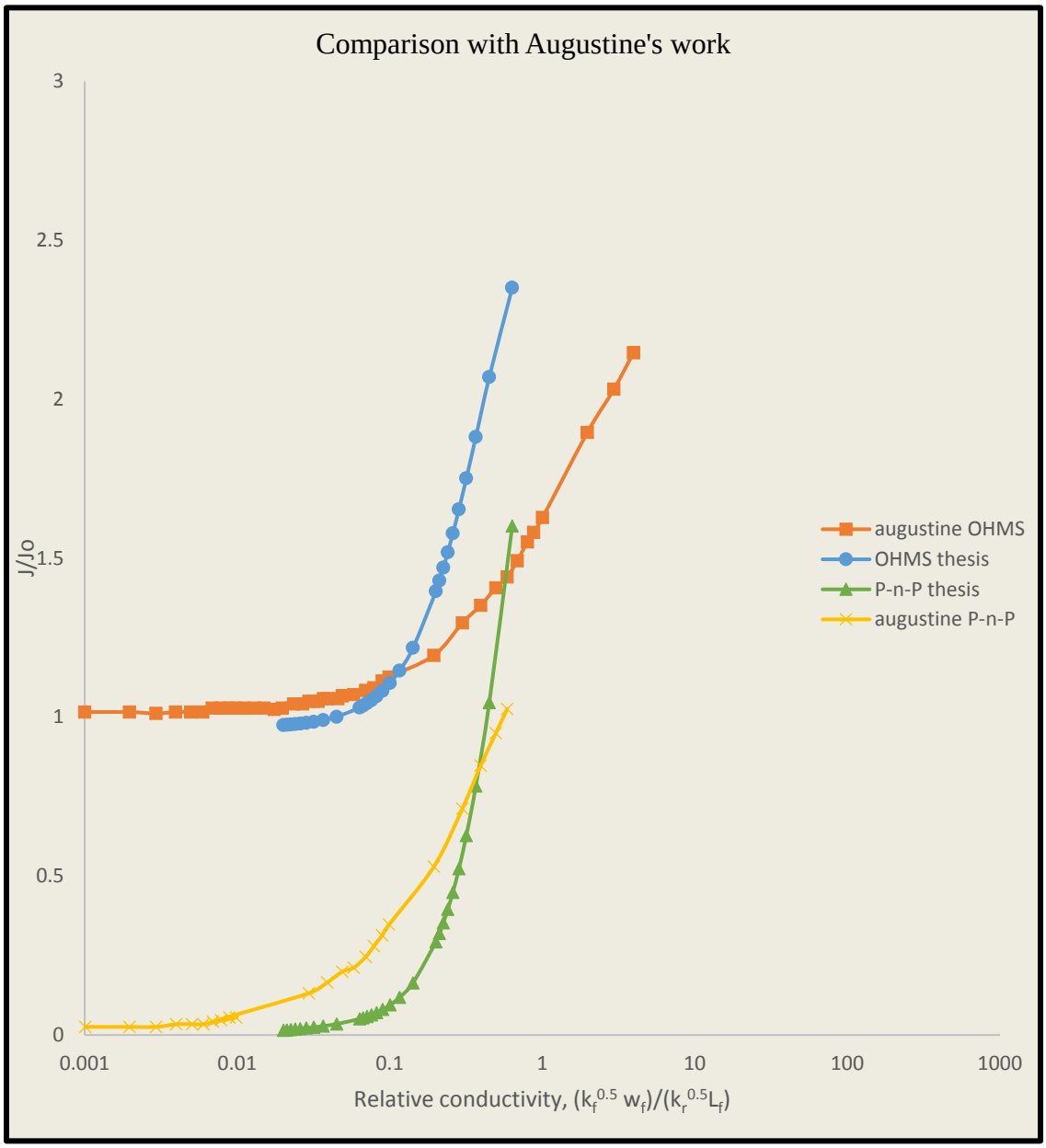

Figure 6.6. Comparison with Augustine's work

Figure 6.6 shows the same trend in curves. The slight variation in productivity index is due to the different parameters considered for the simulation. The simulation was carried out using k_v/k_h value of 0.1 and the reservoir thickness was 60 ft. Reservoir permeabilities ranging from 1 mD to 1000 mD was used. Fracture permeability was assumed to be 120000 mD. It is apparent from the figure that OHMS completions have better performance than P-n-P completions in high-permeability reservoirs, and the results are in agreement with Augustine's work.

Figure 6.7 shows the simulation results for fracture permeability (kf) of 120000 mD and 570000 mD for both completions, plotted in terms of relative conductivity defined by Augustine, using the same parameters as in Figure 6.6.

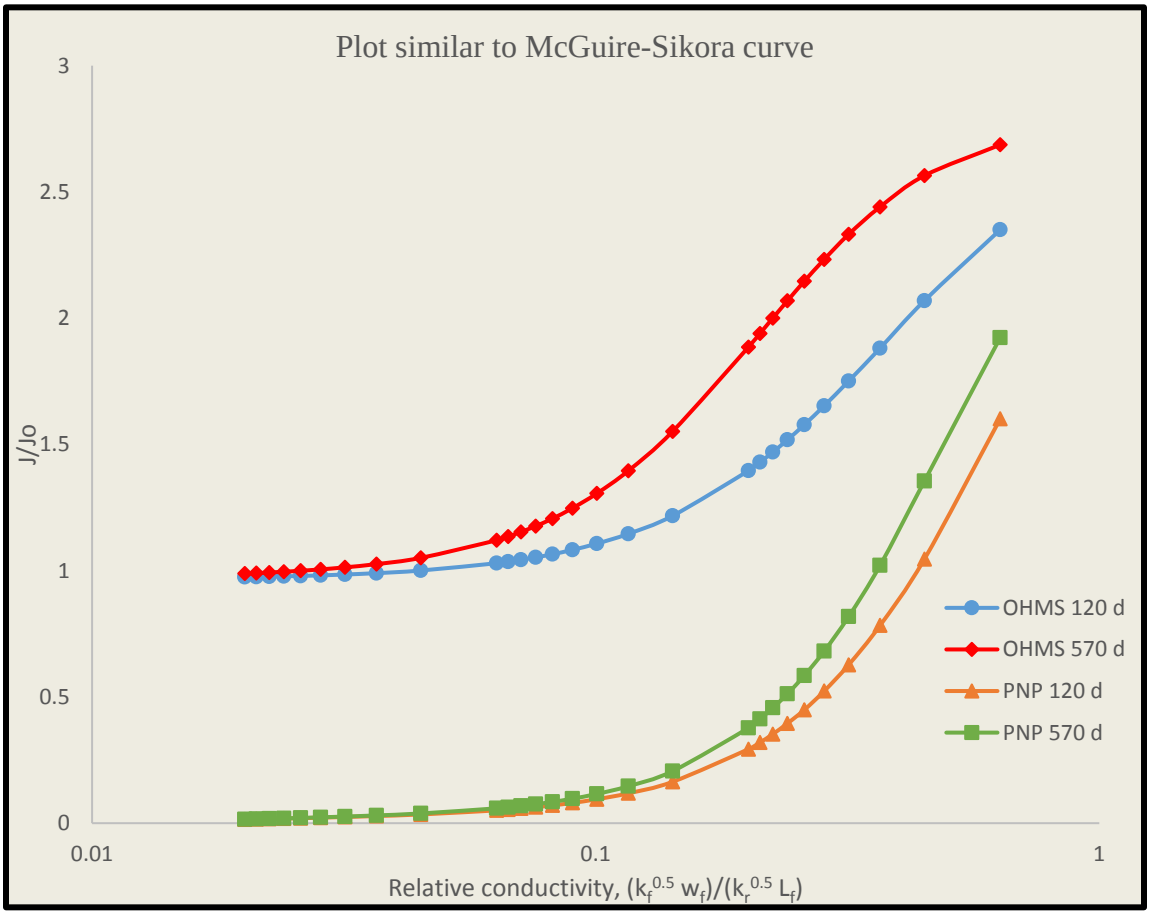

Figure 6.7. Results presented as McGuire-Sikora curve

The curve patterns are comparable to Mcguire-Sikora curves. From Figure 6.7 it is clear that for high permeability reservoirs, productivity index values almost becomes equal for different fracture permeability (k_f) values. Folds of increase (FOI) is almost less than one for open hole completions and in the case of cased hole completions folds of increase (FOI) almost becomes zero. Thus, increasing the fracture permeability in high permeability reservoirs doesn't improve natural gas production.

6.6. CONCLUSIONS

A three-dimensional computational fluid dynamics model using ANSYS FLUENT 15.0 was developed to analyze the performance of transverse fractures with longitudinal fractures in high-permeability gas reservoirs. The CFD model was validated with the horizontal well equations developed by Joshi (1988). Production comparison was made including P-n-P and OHMS completions. The following are the conclusions of this work.

- Longitudinal fractures with OHMS completions outperformed transverse fractures in gas reservoirs with permeability $\geq$ 10 mD.
- The length of the wellbore (300 ft.) was a barrier in modeling multiple longitudinal/transverse fractures. The actual production performance in high-permeability gas reservoirs may be different in the case of multiple fractures and should be investigated
- For horizontal wells with any fracture model, P-n-P completions do not outperform an OHMS completion. The results are in agreement with the historical studies and most gas well field studies.
- The performance of high-permeability gas reservoirs with both completions was in agreement with Augustine's 2-D work. The folds of increase (FOI) for P-n-P completions was almost zero.
- Using actual field information in demonstrating a gas flow will give more precise results than the results obtained from this work.

7. FUTURE WORK

The following are suggestions regarding the future work related to this study.

Actual field data should be used to model real well geometry, PVT data and production should be used to make the modeling effort more realistic. Production scenarios and constraints might be more complicated than the conditions assumed in this work.

ANSYS FLUENT software comprises of extensive physical modeling abilities. Hence, this research can be developed further by including the different types of completion equipment and by considering the actual length of the wellbore in the simulation model.

P-n-P completions should be modeled by considering the fracturing stages and the perforation clusters in each stage. Multiple transverse and longitudinal fractures can be incorporated into the model by considering the real length of the wellbore. This gives an opportunity to study about fracture interference effects and optimum spacing between fractures which helps in designing a perfect fracture treatment.

Production comparison between P-n-P and OHMS completions are made assuming flow from the fractures created. Production from natural fractures is not considered in this study. A model can be created which accounts for production from natural fractures and also heat transfer effects on production can be examined by enabling the heat transfer option in FLUENT.

BIBLIOGRAPHY

Ahmad Haidari, CFD image: <http://www.ansys-blog.com/wp-content/uploads/2015/04/OTC2015.png>.

Algadi, O. A., L. Castro, R. Mittal, and B. Hughes, 2015, Comparison of Single-Entry Coiled Tubing-Activated Frac Sleeves vs . Multi-Cluster Plug-and-Perf Completion in the Permian and Anadarko Basin : A Case Study: SPE 174943.

Anderson, J. D., 1995, Computational Fluid Dynamics: THE BASICS WITH APPLICATIONS.

ANSYS, Inc., 2013, "ANSYS FLUENT Theory Guide," Release 15.0

ANSYS, Inc., 2013, "ANSYS Meshing User's Guide," Release 15.0

ANSYS, Inc., 2013, "DesignModeler User Guide," Release 15.0

ANSYS, Inc., 2013, "ANSYS FLUENT User's Guide," Release 15.0

Augustine, J. R., 2011, Openhole versus Cemented Completions for Horizontal Wells with Transverse Fractures : an Analytical Comparison (REVISED): SPE 142279.

Bagci, S., J. Kowan, B. Hughes, R. Development, and G. Way, 2016, Hydraulic Fracture Modeling and Well Performance Analysis in CTD Wells Completed in Tight Sands: SPE 180473.

Bellarby, J., 2009, Well Completion Design.

Bocaneala, B., C. Barrett, B. Holland, M. E. Langford, and C. Energy, 2015, The Evolution of Completion Practices and Reservoir Stimulation Techniques in the North Sea: SPE 175443.

Britt, L. K., 1985, Optimized Oilwell Fracturing of Moderate-Permeability Reservoirs: SPE 14371.

Burton, W. A., 2013, Unconventional Completions : Which one is Right for Your Application ? SPE 166431.

Byrne, M., M. A. Jimenez, E. A. Rojas, and E. Castillo, 2013, Computational Fluid Dynamics for Reservoir and Well Fluid Flow Performance Modelling: SPE 144130.

Casero, A., L. Tealdi, R. L. Ceccarelli, A. Ciuca, G. Pace, B. Malone, and J. Athans, 2009, Multiple Transverse Fracturing in Horizontal Open Hole Allows Development of a Low-Permeability Reservoir in the Foukanda Field, Offshore Congo: SPE 119140.

Cholet, H., 2000, Well production practical book.

Demarchos, a S., M. J. E. Consultants, M. M. Porcu, M. J. Economides, and U. Houston, 2006, Transversely Multi f ractured Horizontal Wells : A Recipe for Success: SPE 102262.

Economides, M. J., M. Yang, and a N. Martin, 2010, Fracturing Horizontal Transverse, Horizontal Longitudinal and Vertical Wells: Criteria for Decision: SPE 137328.

Economides, M. J., and T. Martin, 2007, Modern Fracturing - Enhancing Natural Gas Production.

Elphick, J. J., R. P. Marcinew, and B. Brady, 1993, Effective Fracture Stimulation in High-Permeability Formations: SPE 25380.

Esionwu, C., A. Marker, and M. Claus, 2014, Further Aerodynamics and Propulsion and Computational Techniques: CFD Solution Methodology.

Hunt, J. L., and M. Azari, 1996, Fracturing Horizontal Wells In Gas Reservoirs: SPE 35260.

Ikoku, C. U., 1992, Natural Gas Production Engineering.

J.E. Brown, Dowell Sclumberger, and M.J. Economides, M. U. L., 1992, An Analysis of Hydraulically Fractured Horizontal Wells: SPE 24322.

Jimenez, M.-A., and J. C. Chavez, 2009, Understanding the Near-wellbore Phenomena for Hydraulically Fractured wells: A Comprehensive Inflow Performance Numerical Model: SPE 122361.

Kassim, R. S., L. K. Britt, N. S. I. Fracturing, and S. Dunn-, 2016, Multiphase Flow Performance Comparison of Multiple Fractured Transverse Horizontal Wells vs longitudinal Wells in Tight and Unconventional Reservoirs with Stress Dependent Permeability: SPE 181813.

Kennedy, R. L., W. N. Knecht, D. T. Georgi, and B. Hughes, 2012, Comparisons and Contrasts of Shale Gas and Tight Gas Developments, North American Experience and Trends: SPE 160855.

King, G. E., 2012, Hydraulic Fracturing 101: What Every Representative, Environmentalist, Regulator, Reporter, Investor, University Researcher, Neighbor and Engineer Should Know About Estimating Frac Risk and Improving Frac Performance in Unconventional Gas and Oil Wells: SPE 152596.

Kullman, J., 2011, The Complicated World of Proppant Selection.

Lolon, E. P., A. Texas, S. T. Chipperfield, S. I. E, and D. A. Mcvay, 2004, The Significance of Non-Darcy and Multiphase Flow Effects in High-Rate, Frac-Pack Gas Completions: SPE 90530.

Magalhaes, F., D. Zhu, S. Amini, and P. Valko, 2007, Optimization of Fractured-Well Performance of Horizontal Gas Wells: SPE 108779.

Malalasekera, H. K. V. and W., 2007, An Introduction to Computational Fluid Dynamics: THE FINITE VOLUME METHOD

Michael Economides, Ronald Oligney, P. V., 2002, Unified Fracture Design

Mukherjee, H., and M. Economides, 1991, A Parametric Comparison of Horizontal and Vertical Well Performance: SPE 18303.

Ozkan, E., M. Brown, R. Raghavan, and H. Kazemi, 2011, Comparison of Fractured-Horizontal-Well Performance in Tight Sand and Shale Reservoirs: SPE 121290.

Peng, D.-Y., and D. B. Robinson, 1976, A New Two-Constant Equation of State: Industrial & Engineering Chemistry Fundamentals.

Phelan, K., H. Adefashe, and A. Casero, 2013, Open Hole Multi-Stage Completion System in Unconventional Plays: Efficiency Effectiveness and Economic: SPE 164009.

Pretechnologies, CFD image: <http://www.pretechnologies.com/sectors/oil-and-gas/subsea-processing>.

Rahim, Z., A. Al-kanaan, H. Al-anazi, S. Aramco, R. Kayumov, and Z. Al-jalal, 2015, Comparing Effectiveness Between Cemented Plug and Perf and Open Hole Ball Drop Completion Assemblies to Ensure Optimal Multistage Fracturing Treatment and Well Performance — Field Examples: SPE 177511.

Reimer, J., M. Ng, B. Dusterhoft, P. Pony, and B. Birkelo, 2015, Comparing Openhole Packer Systems with Cemented Liner Completions in the Northern Montney Gas Resource Play : Results From Microseismic Monitoring and Production: SPE 174955.

Rivenbark, M., and J. Appleton, 2013, Cemented Versus Open Hole Completions: What is Best for Your Well? SPE 163946.

Sickle, S. Van, J. Galloway, C. Mcclellan, C. E. Llc, D. Snyder, P. Plus, and E. Services, 2015, Economic and Operational Analysis of Systematically Deploying New: SPE 176984.

Smith, M. B., and R. R. Hannah, 1996, High-permeability fracturing: The evolution of a technology: Journal of Petroleum Technology.

Smith, M., A. Bale, and L. Britt, 2004, An investigation of Non-Darcy flow effects on hydraulic fractured oil and gas well performance: SPE 90864.

Snyder, D., and Seale, R.A., 2011, Optimisation of completions in unconventional reservoirs for higher ultimate recovery: SPE 142729.

Snyder, D., 2012, Comparison of Production Results from Open Hole and Cemented Multistage Completions in the Marcellus Shale: SPE 155095.

Sofialidis, D., 2013, Express Introductory Training in ANSYS Fluent Boundary Conditions & Solver Settings Boundary Conditions & Introduction to ANSYS Fluent.

Soliman, M. Y., M. Azari, J. L. Hunt, and C. C. Chen, 1996, Design and analysis of fractured horizontal wells in gas reservoirs: SPE 35343.

Soliman, M. Y., and P. Boonen, 1997, Review of Fractured Horizontal Wells Technology: SPE 36289.

Soliman, M. Y., R. Pongratz, M. Rylance, and M. Smith, 2006, Fracture Treatment Optimization for horizontal well Completions: SPE 102616.

Srinivasan, K., J. Krishnamurthy, R. Williams, P. Dharwadkar, and T. Izykowski, 2016, Eight-Plus Years of Hydraulic Fracturing in the Williston Basin : What Have We Learned ? SPE 179156.

Sun, D., B. Li, M. Gladkikh, R. Satti, and R. Evans, 2011, Computational Fluid Dynamics Software and a Semi-Analytical Model: SPE 143663.

Theppornprapakorn, V., and S. Dunn-norman, 2014, A CFD Validation of Historical Production Studies Comparing Plug- and-Perf to Openhole Sleeve Completion Methods in Horizontal Multi-stage Fractured Wells: SPE 1886725.

Thompson, D., K. Rispler, S. Stadnyk, O. Hoch, and B. McDaniel, 2009, Operators Evaluate Various Stimulation Methods for Multizone Stimulation of Horizontals in North East British Columbia: SPE 119620.

Tianyiu Liu, Texas A&M University, Matteo Marongiu-Porcu, Economides Consultants, Christine Ehlig Economides, Texas A&M University, and Michael J. Economides, U. of H., 2012, A Study of Transversely vs Longitudinally Farctured Horizontal Wells in a Moderate-Permeability Gas Reservoir: SPE 163317.

Valko, P., and M. J. Economides, 1996, Performance of fractured horizontal wells in high-permeability reservoirs: SPE 31149.

Villegas, M. E., and R. a. Wattenbarger, 1996, Performance of longitudinally fractured horizontal wells in high-permeability anisotropic formations: SPE 36453.

Vincent, M. C., C. M. Pearson, and J. Kullman, 2000, Non-Darcy and multiphase flow in propped fractures: case studies illustrate the dramatic effect on well productivity: SPE 54630.

W.J. McGuire, V. J. S., 1960, The Effect of Vertical Fractures on Well Productivity: SPE 1618-G.

Wang, X., and M. Economides, 2009, Advanced Natural Gas Engineering.

Wei, Y., and M. Economides, 2005, Transverse Hydraulic Fractures From a Horizontal Well: SPE 94671.

Welling, R. W. F., and S. Deepwater, 1998, Conventional High Rate Well Completions : Limitations of Frac & Pack , High Rate Water Pack and Open Hole Gravel Pack Completions: SPE 39475.

Wilson, B., D. Lui, J. Kim, M. Oil, M. Kenyon, and M. Mccaffrey, 2011, Comparative Study of Multistage Cemented Liner and Openhole System Completion Technologies in the Montney Resource Play: SPE 149437.

Wutherich, K. D., and K. J. Walker, 2012, Designing Completions in Horizontal Shale Gas Wells - Perforation Strategies: SPE 155485.

Yang, F., L. K. Britt, N. S. I. Fracturing, and S. Dunn-norman, 2015, The Effect of Well Azimuth or Don ’ t Let Your Landman Plan Your Well Path ! SPE 173331.

VITA

Hrithu Vasudevan was born in Kerala, India. He received his bachelor's degree in Mechanical Engineering from Mahatma Gandhi University, Kerala, India in 2010. He joined Corrtech International Pvt. Ltd., India in November 2010 – May 2011 as a Trainee Mechanical Engineer. His duties there included conducting field inspections, carrying out welder qualification and procedure qualification tests. Hrithu joined Dodsal E and C Pte. Ltd., UAE, as a Junior Mechanical Engineer in January 2012 – May 2013. He was assigned to supervise the fabrication and erection of piping and equipment, coordinating with clients, procuring materials for work and performing hydro tests.

In January 2014, Hrithu commenced his graduate studies in Petroleum Engineering at Missouri University of Science and Technology under Dr. Shari Dunn-Norman. During his time as a Master's Student, he held positions of Graduate Research Assistant and Graduate Teaching Assistant in the Department. He received a Master of Science degree in Petroleum Engineering from Missouri University of Science and Technology in December 2016.